12-13-2021

Structural and Mechanistic Investigation of D-Arginine Dehydrogenase and L-Arginine Dehydrogenase from Pseudomonas Aeruginosa

Archana Iyer
Georgia State University

STRUCTURAL AND MECHANISTIC INVESTIGATION OF D-ARGININE DEHYDROGENASE AND L-ARGININE DEHYDROGENASE FROM PSEUDOMONAS AERUGINOSA

by

ARCHANA IYER

Under the Direction of Giovanni Gadda, PhD

ABSTRACT

Pseudomonas aeruginosa has a two-enzyme D-arginine conversion system that enables it to utilize D-arginine as a nutrient. The coupled-enzyme system consists of D-arginine dehydrogenase (*Pa*DADH) and L-arginine dehydrogenase (*Pa*LADH). *Pa*DADH has been characterized structurally and mechanistically and established as an FAD-dependent enzyme that catalyzes the oxidation of D-arginine to iminoarginine, which can be non-enzymatically hydrolyzed to ketoarginine and ammonia.

A tyrosine 249 to phenylalanine variant of *Pa*DADH (*Pa*DADH-Y249F) was expressed and purified as a mixture of two cofactors, one protein population with regular FAD and one with a green-colored modified FAD. The chemically modified green FAD was investigated through various spectroscopic techniques. The yellow and green protein fractions were investigated structurally to uncover any clues about the modification. Molecular Dynamics and QM/MM were

also performed with the wild-type and the variant enzymes to investigate the contribution of protein dynamics and flavin electronics into making the 6-hydroxylation reaction possible in the variant enzyme.

*Pa*DADH-Y249F was also expressed and crystallized in the presence of D-arginine. The structure of this incubated enzyme was similar in overall topology to the wild-type enzyme, except for ambiguous electron density around the N5 and C6 atoms of the isoalloxazine moiety. The FAD modified at the N5 position was present in the variant enzyme and the green modified FAD. The presence of two modified flavin cofactors in a single crystal structure is unusual. The second modified FAD was characterized via accurate mass analysis and investigated spectroscopically.

While a lot is known about *Pa*DADH, *Pa*LADH has yet to be characterized kinetically. *Pa*LADH is the second enzyme in the coupled-enzyme D-arginine conversion system and catalyzes the reaction of ketoarginine and ammonia to L-arginine using NAD(P)H. *Pa*LADH can also catalyze the reverse reaction converting L-arginine to ketoarginine and ammonia using $NAD(P)^+$ and was characterized using a stopped-flow spectrophotometer. The forward reaction of *Pa*LADH was investigated as the product of the coupled-enzyme reaction by providing the nicotinamide substrate and D-arginine for *Pa*DADH, with *Pa*LADH also being present in the same reaction mix. We also hypothesize that *Pa*LADH and *Pa*DADH might form a protein complex for converting D-arginine to L-arginine, and the complex was probed using analytical ultracentrifugation and size-exclusion chromatography.

INDEX WORDS: D-amino acids, *Pseudomonas aeruginosa*, Flavins, Modified flavins, D-arginine dehydrogenase, L-arginine dehydrogenase.

STRUCTURAL AND MECHANISTIC INVESTIGATION OF D-ARGININE DEHYDROGENASE AND L-ARGININE DEHYDROGENASE FROM PSEUDOMONAS AERUGINOSA

by

ARCHANA IYER

A Dissertation Submitted in Partial Fulfillment of the Requirements for the Degree of

Doctor of Philosophy

in the College of Arts and Sciences

Georgia State University

2021

STRUCTURAL AND MECHANISTIC INVESTIGATION OF D-ARGININE DEHYDROGENASE AND L-ARGININE DEHYDROGENASE FROM PSEUDOMONAS AERUGINOSA

by

ARCHANA IYER

Committee Chair: Giovanni Gadda

Committee: Donald Hamelberg

Irene T. Weber

Electronic Version Approved:

Office of Graduate Studies

College of Arts and Sciences

Georgia State University

December 2021

DEDICATION

To my brother Vivek Iyer

ACKNOWLEDGEMENTS

I want to first and foremost thank my advisor Dr. Giovanni Gadda under whose direction and supervision all the work presented in this dissertation was completed. I also wish to thank my committee members Dr. Donald Hamelberg and Dr. Irene T. Weber, for their questions, guidance, suggestions, and collaborations throughout my graduate career at GSU. The various projects presented here would not be possible without the collaborative efforts and thoughtful suggestions provided by Dr. Markus Germann, Dr. Johnson Agniswamy, Dr. Samer Gozem, Dr. Siming Wang, Dr. Dabney Dixon, Dr. Alex Spring-Connell, Dr. Orozco-Yoelvis-Gonzalez, Mohamed Momin, Dr. Paulo Zaragoza, and Dr. Judith Klinman. I also wish to thank Kessey Jill Cham, Kedayne King, Will Thacker, and Will Lovett in the Chemistry department.

I would like to sincerely thank Daniel Ouedraogo and Dr. Renata Reis, who provided me with valuable mentorship and friendship and helped me navigate several complicated techniques and concepts. I would also like to thank the previous and current members of the Gadda lab, Dr. Swathi Gannavaram, Dr. Dan Su, Dr. Jacob Ball, Benjamin Dratch, Joanna Quaye, Maria Vodovoz, Elias Flores, and Mehrin Moni, who have provided helpful discussions and suggestions during our weekly lab meetings.

Last but not least, I am indebted to my friends Christopher Aguillon, Jessica Siemer, my partner Ravi Tripathi and my parents for their unwavering support during challenging times and have helped me learn, grow and develop resilience.

TABLE OF CONTENTS

ACKNOWLEDGEMENTS V

LIST OF TABLES XII

LIST OF FIGURES XIII

LIST OF EQUATIONS XVII

LIST OF SCHEMES XVIII

LIST OF ABBREVIATIONS XIX

1 INTRODUCTION 1

1.1 Role of D-amino acids 1

1.1.1 A brief history of chirality 1

1.1.2 D-amino acids in nature 2

1.1.3 D-amino acid metabolism 4

1.1.4 Arginine metabolism in P. aeruginosa 6

1.1.5 D-amino acid and metabolism in Pseudomonas 7

1.1.6 Role of the coupled-enzyme system in PAO1 (PaDADH and PaLADH) 9

1.2 FLAVINS AND FLAVIN-DEPENDENT ENZYMES 10

1.3 SPECIFIC AIMS 13

1.4 REFERENCES 16

2 AMINE OXIDATION BY D-ARGININE DEHYDROGENASE IN PSEUDOMONAS AERUGINOSA 24

2.1 ABSTRACT 24

2.2 INTRODUCTION 24

2.3 D-AMINO ACIDS AND THEIR METABOLISM 26

2.4 STRUCTURAL FEATURES OF *Pa*DADH 28

2.4.1 Overall fold of PaDADH 28

2.4.2 FAD-binding site 28

2.4.3 Substrate binding-domain 30

2.4.4 Structural comparison of PaDADH with pDAAO 30

2.5 SUBSTRATE SPECIFICITY OF *Pa*DADH 32

2.5.1 E87 dictates substrate specificity 33

2.5.2 A hydrophobic cage and a flexible loop extends substrate scope 34

2.5.3 Substrate specificity comparison to D-amino acid oxidases 35

2.6 STEADY-STATE KINETIC MECHANISM OF *Pa*DADH 35

2.6.1 Product release 36

2.6.2 Substrate inhibition via a dead-end complex 37

2.7 CATALYTIC MECHANISM 37

2.7.1 Mechanism CN bond cleavage 37

2.7.2 Restricted proton transfer 39

2.8 ROLE OF LOOP L1 DYNAMICS IN *Pa*DADH 41

2.8.1 S45/A46 switch and the Y53 gate 42

2.8.2 Dynamics of loop L1 in substrate capture and catalysis 43

2.9 OPEN QUESTIONS 45

2.10 REFERENCES 48

3 A SINGLE POINT MUTATION IN D-ARGININE DEHYDROGENASE UNLOCKS A TRANSIENT CONFORMATIONAL STATE RESULTING IN ALTERED COFACTOR REACTIVITY 56

3.1 ABSTRACT 56

3.2 INTRODUCTION 57

3.3 EXPERIMENTAL PROCEDURES 59

3.3.1 Materials. 59

3.3.2 Enzyme Preparation. 60

3.3.3 Flavin Extraction and MS-ESI Analysis. 60

3.3.4 6-OH-FAD pK_a Determination. 61

3.3.5 Lack of Reduction of the Y249F-g Enzyme with D-Arginine 61

3.3.6 NMR Analysis. 62

3.3.7 Conversion of FAD to 6-OH-FAD in the Y249F-y Enzyme. 62

3.3.8 ^{18}O-Incorporation into 6-OH-FAD. 62

3.3.9 Enzyme Crystallization. 63

3.3.10 X-Ray Data Collection and Processing. 64

3.3.11 Structure Solution and Refinement. 64

3.3.12 Molecular Dynamics Simulations..... 64

3.3.13 Molecular Dynamics Simulations with O_2 Molecules. 66

3.3.14 Principal Component Analysis. 66

3.3.15 Hybrid Quantum Mechanical/Molecular Mechanical (QM/MM) Calculations. 66

3.4 RESULTS 71

3.4.1 UV-Visible Absorbance of the Y249F-y and Y249F-g Enzymes. 71

3.4.2 MS-ESI Analysis of 6-OH-FAD. 71

3.4.3 Determination of the pK_a Value of 6-OH-FAD. 72

3.5 Lack of Activity of Y249F-g Enzyme. 72

3.5.1 NMR Analyses of 6-OH-FAD. 73

3.5.1 Conversion of FAD to 6-OH-FAD in the Y249F-y Enzyme. 74

3.5.1 Proposed Mechanism for the Formation of 6-OH-FAD. 75

3.5.2 X-Ray Crystal Structures of the Y249F-g and Y249F-y Enzymes..... 78

3.5.1 MD Simulations. 79

3.5.2 O_2 localization in the active site. 79

3.5.3 Hybrid QM/MM Electron Spin Density Flavin Computations. 80

3.6 DISCUSSION 84

3.7 CONCLUSION..... 87

3.8 ACKNOWLEDGEMENTS..... 88

3.9 REFERENCES..... 91

4 DISCOVERY OF A NEW FLAVIN N5-ADDUCT IN A TYROSINE TO PHENYLALANINE VARIANT OF D-ARGININE DEHYDROGENASE 103

4.1 ABSTRACT 103

4.2 INTRODUCTION 104

4.3 MATERIALS AND METHODS 106

4.3.1 Materials. 106

4.3.2 Expression and purification 106

4.3.3 Crystallization conditions 106

4.3.4 MS-ESI (-) analysis conditions 107

4.3.5 X-ray data collection and processing 107

4.3.6 Structure solution and refinement 108

4.3.7 UV-Visible absorption spectra 108

4.4 RESULTS 108

4.5 DISCUSSION 116

4.6 REFERENCES 123

5 CHARACTERIZATION OF A COUPLED-ENZYME D-ARGININE CONVERSION SYSTEM FROM PSEUDOMONAS AERUGINOSA 131

5.1 ABSTRACT 131

5.2 INTRODUCTION 132

5.3 MATERIALS AND METHODS 134

5.3.1 Materials *134*

5.3.2 Expression and Purification *134*

5.3.3 Enzymatic Assay *135*

5.3.4 Sedimentation velocity analytical ultracentrifugation *136*

5.3.5 Size-exclusion chromatography *137*

5.3.6 Kinetics *137*

5.3.7 Coupled-enzyme assay *137*

5.3.8 Data analysis *138*

5.3.9 Homology Modeling *138*

5.4 RESULTS **139**

5.5 DISCUSSION **144**

5.6 REFERENCES **148**

6 GENERAL DISCUSSION AND CONCLUSIONS **152**

LIST OF TABLES

Table 2.1 Crystal structures of *Pa*DADH deposited in PDB. 46

Table 2.2 Steady-State Kinetic Parameters for *Pa*DADH**.** 47

Table 3.1. Data collection and refinement statistics for X-ray crystal structures. 89

Table 3.2. QM/MM spin density calculations for flavin C6 atom. 90

Table 4.1. Data collection and refinement statistics..... 122

Table 5.1. Purification table for Ni-NTA purification of 6x His-tagged PaLADH. 136

Table 5.2. Steady-State kinetic parameters for PaLADH. 139

Table 5.3. Kinetic parameters for the coupled-enzyme assay. 141

LIST OF FIGURES

Figure 1.1 Enantiomers of glyceraldehyde. 2

Figure 1.2. D- and L-Amino acids. 2

Figure 1.3. The 3-D structure of DAAO monomer with iminotryptophan. 6

Figure 1.4. Three of the four arginine catabolic pathways in P.aeruginosa. I Arginine deiminase pathway, II arginine succinyltransferase pathway and III Arginine decarboxylase pathway. 8

Figure 1.5. Structure of FMN and FAD. 10

Figure 1.6. The versatility of flavin-dependent enzymes 12

Figure 2.1 Overall structure and active site of PaDADH in complex with iminoarginine. 29

Figure 2.2 Comparison of the three-dimensional structures of pDAAO (light-blue, PDB ID 1DDO) with PaDADH (gray, PDB ID 3NYE). Panel A represents the overall structure of the two enzymes and Panel B represents the active sites of the enzymes. For clarity, Y53 from PaDADH was omitted. Iminoacid C atoms in PaDADH are in green, iminotryptophan C atoms in pDAAO are in magenta and FAD moiety C atoms are in yellow and orange in PaDADH and pDAAO, respectively. 31

Figure 2.3 Overlay of the crystal structures of *Pa*DADH in complex with iminoarginine and iminohistidine. *Pa*DADH residues line the interior of the substrate binding pocket. (Some residues were omitted for clarity). Iminoarginine and iminohistidine bind in two distinct conformations. The surface of the substrate-binding pocket is in blue and the surface of the FAD-binding site is in white. Iminoarginine C atoms are in green, iminohistidine C atoms are in blue, FAD C atoms are in yellow, and side chain C atoms are in grey. The arrow indicates the entrance to the active site. 34

Figure 2.4 *Pa*DADH loop L1 with the S45, A46 and H48 residues. The isoalloxazine moiety of the FAD is in yellow, and the iminoarginine product is in green. Loop L1 is in magenta with H48 interacting with the iminoarginine product through two water molecules. 41

Figure 2.5 Open-closed conformations of loop L1. 42

Figure 2.6. Probability distribution of the S45A, A46G variant enzymes and the wild-type.All-atoms molecular dynamics simulations were carried out over 1.1 μs with 0.1 μs as equilibration time[58]. S45A variant is colored in blue, A46G variant in read and the wild-type in black. The inset represents the flavin fluorescence of the variants and the wild-type enzyme. 44

Figure 3.1. The division of $FADH^-$ into QM (shaded atoms) and MM atoms. The frontier valency is saturated by a hydrogen link atom (LA). 68

Figure 3.2. Spectroscopic characterization of the green flavin. 72

Figure 3.3. Spectroscopic characterization of the green flavin. 73

Figure 3.4. ^{1}H-NMR and HSQC spectra of the modified flavin. 76

Figure 3.5. Conversion of FAD to 6-OH-FAD in the Y249F-y enzyme. 77

Figure 3.6. The overall structure of the Y249F-g and Y249F-y enzymes. 81

Figure 3.7. The active sites of the Y249F-y and Y249F-g enzymes. 82

Figure 3.8. Conformational flexibility of active site in the Y249F-y variant. 83

Figure 3.9. Side-chain flexibility for R222 and R305..... 84

Figure 4.1. 2Fo-Fc electron density map (contoured at 1.2σ) for the two modified cofactors in the active site of PaDADH-Y249F. The left panel shows the additional density on the flavin C6 atom, i.e., 6-hydroxy-FAD (green). The right panel is in a different orientation

and shows the protruding density from the flavin N5 atom, i.e., N5-(4-guanidino-oxobutyl)-FAD (orange). 110

Figure 4.2. A) The overall structure of the PaDADH-Y249F (blue). The 6-OH -FAD is shown with green carbons, and the N5-(4-guanidino-oxobutyl)-FAD in orange carbons. B) The geometry of the two modified flavin cofactors observed in the active site of PaDADH-Y249F, showing the angle defined by the flavin C4a-N5-C5a atoms being co-planar in the 6-OH-FAD and bent in the N5-(4-guanidino-oxobutyl)-FAD. 113

Figure 4.3. Structural overlay of the PaDADH-Y249F (blue) with the N5-(4-guanidino-oxobutyl)-FAD (orange) and the PaDADH-WT (gray) with the N5-(4-methyl-2-pentanone)-FAD (yellow) and 6-OH-FAD shown (green)..... 114

Figure 4.4. A) The active site of PaDADH-Y249F(blue), where residue E87 interacts with the guanidium group of the N5-(4-guanidino-oxobutyl)-FAD (orange). B) The active site of PaDADH-WT (green) shows residue E87 with the guanidinium group of the oxidized product iminoarginine (pink). C) Overlay of the active sites of PaDADH-Y249F (blue) and PaDADH-WT (green). 114

Figure 4.5. UV-Visible absorption spectra of the PaDADH-Y249F. Oxidized enzyme (black) was treated with 15 mM D-arginine to obtain the spectra of the reduced enzyme (orange). Over 8 days of incubation, the reduced enzyme was slowly reoxidized along with an extra feature appearing around 360 nm (red). (Inset) The difference spectra of the enzyme incubated over 8 days and the initial oxidized enzyme with 16% of the oxidized enzyme added back to the spectra (green) to account for the incomplete formation of an N5-acyl adduct. 116

Figure 5.1. Lineweaver−Burk plot for the reverse reaction of PaLADH with NAD^+ and L-arginine as substrates. Data were fit to eq 5.2..... 140

Figure 5.2. Sedimentation velocity analytical ultracentrifugation velocity data for PaLADH and the complex of PaDADH and PaLADH. 143

Figure 5.3. Homology model of PaLADH generated by the comparative modeling module of Robetta server using the experimentally determined structure of alanine dehydrogenase (PDB: 1omo). 144

Figure 5.4. Multiple pathways for arginine metabolism in P. aeruginosa. 147

LIST OF EQUATIONS

Equation 3.1 61

Equation 5.1 138

Equation 5.2 138

LIST OF SCHEMES

Scheme 1.1. Scheme for the two-enzyme system for D-arginine conversion in P. aeruginosa. Adapted from Reference 38 14

Scheme 2.1 D-Arginine racemization with the two-enzyme racemic system in *Pseudomonas aeruginosa. Pa*LADH *is* Pseudomonas aeruginosa *L-arginine dehydrogenase.*..... 27

Scheme 2.2 Steady-State Kinetic Mechanism of *Pa*DADH. *Pa*DADH$_{ox}$, oxidized D-arginine dehydrogenase; S, amino acid substrate; *Pa*DADH$_{red}$, reduced D-arginine dehydrogenase; P, iminoacid product; PMS, phenazine methosulfate. k_5 and k_{11} are shown as irreversible because products are assumed to be close to zero during the determination of the initial rates of reaction; k_4 is shown although it is close to zero based on stopped-flow data.[45]. 38

Scheme 2.3 Hydride transfer mechanism in *Pa*DADH. B^- is a catalytic base, currently presumed to be a solvent molecule..... 39

Scheme 2.4 Reductive half-reaction of PaDADH accounting for a slow proton equilibrium in the Michaelis complex. S is the D-amino acid substrate. P is the iminoacid product. 40

Scheme 4.1. The versatility of the reduced flavin in *Pa*DADH-Y249F. 117

Scheme 4.2. Proposed mechanism for the formation of 6-OH-FAD in *Pa*DADH-Y249F..... 118

Scheme 5.1. Scheme for the conversion of D-arginine to L-arginine using the two-enzyme system of PaDADH and PaLADH..... 133

Scheme 5.2. Schematics for the coupled-enzyme assay..... 141

LIST OF ABBREVIATIONS

FAD: Flavin adenine dinucleotide

FMN: Flavin mononucleotide

UV: Ultraviolet

NMR: Nuclear magnetic resonance

MS: Mass spectrometry

*Pa*DADH: *Pseudomonas aeruginosa* D-arginine dehydrogenase

*Pa*LADH: *Pseudomonas aeruginosa* L-arginine dehydrogenase

PMS: Phenazine methosulfate

1 INTRODUCTION

1.1 Role of D-amino acids

1.1.1 A brief history of chirality

Louis Pasteur's investigation of alcoholic fermentation led him to discover molecular chirality and enantiomers.[1-3] A century after, numerous studies have investigated D-amino acids and the unassuming role they play in nature.[1, 4-9] Pasteur was studying fermentation-based alcohol productions and would investigate issues that local manufacturers would bring forth. [1] During one of his investigations of fermented grape juice, he extracted (+) tartaric acid or dextro-tartaric acid from tartar obtained from the fermentation containers.[1] Pasteur also extracted a racemic mixture from tartar the (-) tartaric acid, referred to as "left tartaric acid".[1] On crystallizing the racemic acid mixture, he observed an enantiomorphous sodium ammonium crystal, which did not display optical rotation and had different crystal morphology and dubbed it (±) tartaric acid.[1] The difference in optical properties, when not much was known about the molecular structure or atomic bonding, led Pasteur to recognize the existence of molecular chirality and postulate that chirality was a result of the tetrahedral arrangement of atoms in a molecule.[1-3] After his pioneering discovery of enantioselective fermentation of (±) tartaric acid by microorganisms, he decided to switch fields to study fermentation and microbiology, ultimately leading him to make significant developments like vaccinations and pasteurization.

During the 1800s, Jacobus van't Hoff and J.A. Le Bel independently developed the concept of the asymmetric carbon atom as Emil Fischer was finishing his doctorate.[10] Fischer would apply the asymmetrical carbon concept to work out the correct configuration of aldohexoses using a two-dimensional representation called Fischer projections.[10] The D- and L- assignments for amino acids were based on a proposal in 1906 by a Russian-American chemist Rosanoff based on the

location of the α-amino group relative to D-glyceraldehyde using Fischer projections commonly used for optical isomers (**Figure 1.1**). [11]

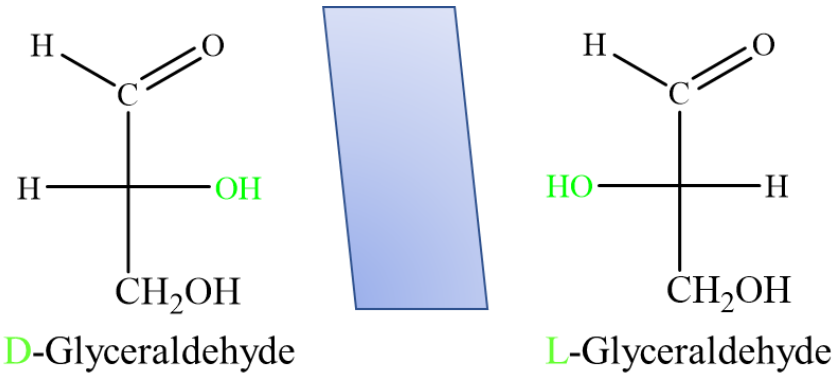

Figure 1.1 Enantiomers of glyceraldehyde.

1.1.2 D-amino acids in nature

Amino acids are a fundamental component of enzymes, antibodies, hormones, receptors, signaling peptides, and other essential molecules in living organisms.[4-9, 12-14] All standard amino acids except one have at least one asymmetric carbon and can exist as D- and L-amino acid forms (**Figure 1.2**). [12] While L-amino acids are more prevalent and are known as proteinogenic as they are susceptible to being translated into peptides and proteins, D-amino acids also play important roles. [5-9, 12-14] The role of D-amino acids was mainly thought of as non-functional and an unnatural occurrence. However, studies confirmed the presence of D-amino acids in soil, bacterial cell walls, and even human tissue.

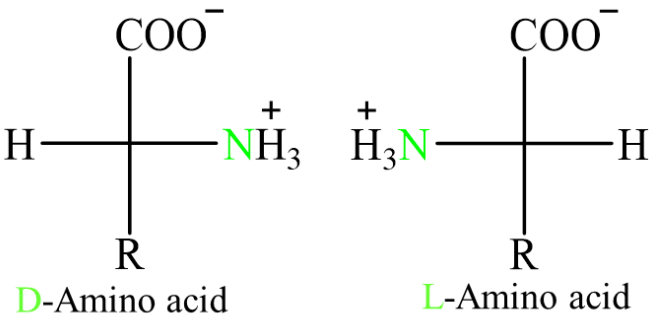

Figure 1.2. D- and L-Amino acids.

D-amino acids are found in free form in various food products, soil, plants, higher organism, as well as microorganisms like bacteria.[4-9, 12-19] Various factors like temperature, treatments with alkali or acids, ionizing radiation have propelled the presence of D-amino acids in free-form or as part of peptides or proteins found in food products, soil and water.[6, 12, 14]

D-amino acids have been found in peptides or proteins isolated from various tissues like the aorta, brain, and even eye lens in humans. [5] Studies on αA-crystallin isolated from human eye lens from aged subjects revealed the presence of D-aspartate residues.[5, 20] The conversion from the L- to D- form of aspartate was believed to be a result of racemization during the aging process, evidenced by the lack of the D- form in the αA-crystallin isolated from younger subjects.[5, 20] D-aspartate was also found in human teeth enamel, and the presence was thought to occur due to the aging process as well, as the older tooth enamel samples showed an increase in the presence of D-aspartate.[21] D-aspartate also plays an active role in endocrine functions in higher mammals by regulating the secretion of several hormones like testosterone, oxytocin, and melanin. [4, 6, 8, 18]

Apart from D-aspartate, a range of D-amino acids like D-serine, D-alanine and D-cysteine are also found in humans and other mammals.[8, 17, 18] D-serine also functions as a neuromodulator and co-agonist in the central nervous system, along with D-aspartate and D-alanine to regulate the function of N-Methyl-D-aspartate (NMDA) receptors.[5, 8, 17] D-serine also can be found in endocrine organs, albeit with an elusive functional relevance.[17] D-alanine, apart from being localized to the brain, is also found in pituitary glands, adrenal glands, and pancreas in mammals.[17, 18] D-leucine, D-proline, and D-glutamate are other D-amino acids that are also localized to rodent brains, with evidence of D-leucine and D-proline also being found in pituitary and pineal glands.[5, 8, 17] Aberrant levels of these D-amino acids can have a strong association with diseases like Schizophrenia, Parkinson's, Huntington’s, chronic pain, epilepsy and amyotrophic lateral

sclerosis.[4, 8, 17] Determination of the concentrations of D-amino acids in various tissues will be helpful as a diagnostic tool, as well as a form of therapy for relevant diseases. The advent of enantiomeric separation techniques has been advantageous to new biochemical studies of D-amino acids and has propelled applications of D-amino acids in medicine and the biotechnology industry.[22]

Different plant species also harbor free D-amino acids, and the abundance of D-amino acids in plants is indicative of their role in plant physiology.[6, 7, 14, 19, 23] Plants can uptake D-amino acids directly through the soil, as established in *Arabidopsis thaliana*.[16] Some D-amino acids have been shown to act as toxins for plants and growth inhibitors.[16] By contrast, D-isoleucine and D-valine were also demonstrated to promote seedling growth.[24] D-alanine has been reported not only to act as a stress signal in duckweed seedlings but also as a building block of moss chloroplasts.[7, 25]

One of the major sources of D-amino acids are microorganisms and their products.[4-7, 14] The peptidoglycan cell wall layers in bacteria commonly utilize D-amino acids like D-alanine and D-glutamate, which can enhance or decrease their resistance to certain antibiotics.[12, 14, 18] The amino sugar components of the cell wall are cross-linked by branched polypeptide chains that contain D-amino acids.[12], Penicillin, amongst other antibiotics, inhibits this cross-linking reaction between an L-glycine residue and a D-alanine residue, thereby preventing the incorporation of D-alanine into the cell wall.[12] A large number of synthetic peptide antibiotics and the natural gramicidin contain D-amino acids and have found these peptides effective against *Clostridium botulinum*.[12]

1.1.3 D-amino acid metabolism

Bacterial enzymes can synthesize D-amino acids like D-alanine and D-glutamate by amino acid racemases (PLP-dependent or independent) or enzymes that catalyze the amination of specific

α-ketoacids.[15] However, the diversity of D-amino acids extracted from bacteria and their surrounding soil is indicative that bacteria have more mechanisms to synthesize or racemize the other D-amino acids. [9, 15] Plants take up D-amino acids by roots from the soil utilizing various transporter proteins like Lysine-Histidine Transporter (LHT1) or the broad-range Amino acid permease (AAP1). The enzyme D-Ala-D-Ala ligase was functionally characterized only in *Physcomitrella patens*, even though the dipeptide D-Ala-D-Ala has been detected in a wide variety of grasses and tobacco.[7] Alanine racemase is another enzyme whose function has only been characterized in *Chlamydomonasreinhardtii* and alfalfa, but orthologs have been identified in a wide variety of plant life.[7]

D-amino acid dehydrogenases were first identified in *Pseudomonas fluorescens* and are catabolic enzymes that oxidize D-amino acids. [26] The D-amino acid dehydrogenases are flavin-dependent dehydrogenases as they do not use molecular oxygen and were reoxidized using methylene blue and dichloroindophenol as artificial electron acceptors.[26, 27] The most well established and characterized enzyme that facilitates the catabolism of D-amino acids are D-amino acid oxidases (DAAO).[8, 23, 27-29] DAAO was first reported by Krebs in 1935 as a flavin-dependent enzyme that catalyzed the oxidative deamination of D-amino acids in pig kidney, and liver samples.[30]Almost all eukaryotes including fungi, fish, amphibians and higher mammals depend on DAAO to regulate D-amino acid levels. [27] Perhaps the most critical function of the peroxisomal DAAO is to maintain appropriate levels of D-serine in humans to maintain the activation of NMDA receptors.[4, 8, 17, 27] All DAAO enzymes share some standard structural features, although with some key differences in their catalytic efficiency and kinetic mechanisms. All DAAOs exist as a homodimer, with two domains: an FAD binding domain and a substrate binding domain. The FAD binding domain is buried deep inside the protein and adopts an elongated conformation

(**Figure 1.3**). [23, 27]In *Pseudomonas aeruginosa*, a D-glutamate dehydrogenase, with a high sequence homology to D-alanine dehydrogenase was established in *Pseudomonas aeruginosa*.

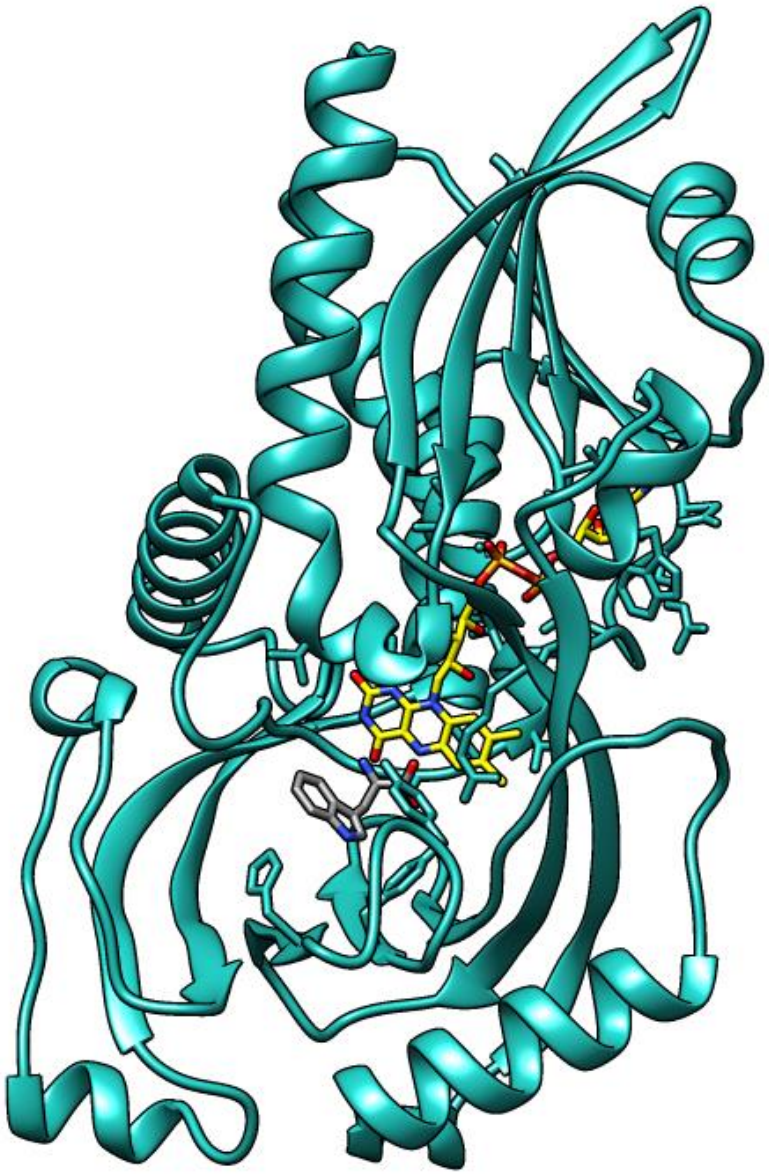

Figure 1.3. The 3-D structure of DAAO monomer with iminotryptophan.
DAAO from pig kidney(Teal ribbon) is shown here in complex with the non-covalently bound FAD (yellow sticks) and Iminotryptophan (grey sticks) (PDB: 1DDO).

1.1.4 Arginine metabolism in P. aeruginosa

Arginine is one of the most versatile amino acids in terms of function, like acting as a precursor for synthesizing nitric oxide, creatine, urea, proline, glutamate, and other polyamines,

functioning as a precursor protein building block. [31, 32] *Pseudomonas aeruginosa* PA01 has at least four catabolic pathways for arginine.[33] The first pathway is called the arginine deiminase pathway and utilizes ATP to convert L-arginine to L-ornithine and can be induced by L-arginine (Figure 1.4). Aerobic L-arginine degradation is accomplished by the arginine succinyltransferase pathway, where succinylated L-arginine is converted to L-glutamate and succinate (Figure 1.4). The arginine decarboxylase pathway produces putrescine, a precursor for spermidine, and permits the bacteria to grow on agmatine and putrescine (Figure 1.4). The arginine transaminase pathway kicks in when the arginine succinyltransferase pathway is blocked and allows for bacterial growth on L-arginine. [34]

1.1.5 D-amino acid and metabolism in Pseudomonas

Pseudomonas aeruginosa PAO1 can utilize D-alanine, D-glutamate, D-glutamine, and D-arginine as the sole carbon and nitrogen sources.[34-36] The *dadRAX* operon in *P. aeruginosa* codes for DadR, a transcriptional regulator, DadA, a D-alanine dehydrogenase, and DadX, an amino acid racemase, is responsible for D-alanine metabolism and regulation.[36] The *dadRAX* was discovered in *P. aeruginosa* during an investigation of the bacteria's utilization of arginine and putrescine and was found to be highly conserved in *Pseudomonas*.[36] DadX, a product of *dadRAX*, is an alanine racemase that catalyzes the racemization of L-alanine to D-alanine, and the DadA catalyzes the oxidative deamination of D-alanine to pyruvate using FAD as a cofactor and an unknown electron acceptor.[36] DadA not only catalyzes the oxidation of D-alanine but has broad substrate specificity and can also oxidize all other D-amino acids, except D-glutamate and D-glutamine. [36]

Figure 1.4. Three of the four arginine catabolic pathways in *P.aeruginosa*. I Arginine deiminase pathway, II arginine succinyltransferase pathway and III Arginine decarboxylase pathway.[1]

The *dguR-dguABC* operon discovered in *P. aeruginosa* by DNA microarray experiments was established to be essential for D-glutamate catabolism.[35] DguA is another member of the FAD-dependent amino acid dehydrogenase family in PAO1.[35] DguA was proposed to be a D-glutamate dehydrogenase based on the sequence homology to the DadA, an alanine dehydrogenase.[35] The activity of DguA was tested against a lot of D-amino acids, and it displayed the highest activity

[1] *Image reproduced from Reference 24 with permission from the Copyright Clearance Center.*

with D-glutamate, D-proline, and D-glutamine, with no activity towards D-aspartate and D-asparagine amongst others. [35]

1.1.6 Role of the coupled-enzyme system in PAO1 (PaDADH and PaLADH)

Multiple catabolic pathways for arginine add to the redundancies of arginine metabolism in *P. aeruginosa* and ensure arginine utilization. *dauBAR* is another operon, similar to the *dadXAR*, and *dguR-dguABC* operons have been reported to be essential for D-arginine utilization in *P. aeruginosa*.[34, 37] The expression of the *dauBAR* operon is regulated by two transcriptional regulators, DauR, which acts as a repressor, and ArgR, which functions as an activator.[34]

The other products of the *dauBAR* operon are DauA, an FAD-dependent D-arginine dehydrogenase (*Pa*DADH), and DauB or L-arginine dehydrogenase (*Pa*LADH), both of which function as a coupled-enzyme D-arginine conversion system.[34, 37] From previous studies, it was known that PAO1 could utilize D-alanine, D-glutamate, D-glutamine and D-arginine as the sole carbon and nitrogen sources.[34-36] Mutants with *dauA* and *dauB* knocked out lost the ability to utilize D-arginine as a source of carbon, and nitrogen.[34, 37] *Pa*DADH or DauA is a true dehydrogenase with broad substrate specificity with the highest activity displayed with D-arginine and D-lysine and no activity for D-glutamate and D-aspartate, highlighting its preference for cationic side chains.[34, 38] *Pa*DADH catalyzes the oxidation of D-arginine into iminoarginine, which could be hydrolyzed to form 2-ketoarginine and ammonia using) using an artificial electron acceptor like phenazine methosulfate (PMS). DauB or *Pa*LADH is the second enzyme in this cascade and can catalyze a NAD(P)H-dependent reaction to convert 2-ketoarginine and ammonia to L-arginine.[37]

The *Pa*DADH-*Pa*LADH system is essential for converting D-arginine to L-arginine, as L-arginine is the only form that the other metabolic pathways can further metabolize in PAO1.[37] The

coupled-enzyme system enables the bacteria to survive on D-arginine and prevents any potential adverse side-effects that free D-arginine might have in the bacteria.

1.2 FLAVINS AND FLAVIN-DEPENDENT ENZYMES

Flavins are a class of yellow-colored cofactors with the basic structure of 7,8-dimethyl-10-alkylisoalloxazine. Riboflavin or vitamin B2 acts as a precursor and can be modified to form the versatile enzyme cofactors flavin mononucleotide (FMN) and flavin adenine dinucleotide(FAD)(Figure 1.5).

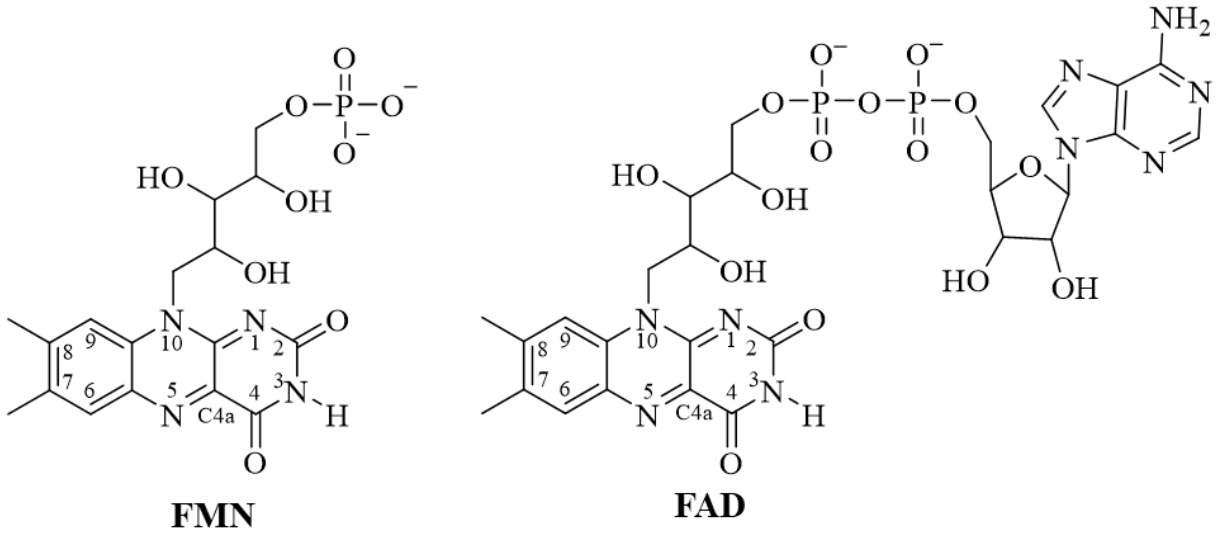

Figure 1.5. Structure of FMN and FAD.

The two cofactors, FMN and FAD, form an essential component of many flavin-dependent enzymes and can be bound in a non-covalent manner or covalently via the 6- or 8- positions on the isoalloxazine. [39]The "Old yellow enzyme" was the first flavin-dependent enzyme discovered by Warburg and during studies of biological oxidations in yeast, and since then, multiple flavoenzymes have been purified and characterized. [40, 41] Flavoenzymes perform a wide range of functions in the cell, like DNA repair, apoptosis, cell growth, and detoxification, amongst many others (Figure 1.6).[42, 43]

The versatility of the flavin cofactor is due to the reactive center, the isoalloxazine ring. The isoalloxazine ring is formed by the fusion of xylene, pyrazine, and pyrimidine rings.[43] The aromatic conjugated system confers chemical versatility to the flavin to carry out transfers of one or two electrons, nucleophilic or electrophilic reactions, and acid/base catalysis.[43, 44] In free solution (pH 7.0), the redox potential for oxidized flavin/two-electron reduced flavin pair is -207 mV, 314 mV for the oxidized flavin/one-electron reduced flavin pair, and -124 mV for the one-electron reduced flavin/two-electron reduced flavin pair, making the flavin cofactors a good candidate for redox reactions.[39] The spectroscopic properties and reactivity of flavins are greatly affected when functional groups like methyl, hydroxyl, cyano, thiol, or amino, or halogens like bromide or chloride, are introduced onto the isoalloxazine ring, i.e., 9-OH-flavin and 6-OH-flavins appear green in their unprotonated form.[45-57] Synthetic, modified flavins have been long used to probe chemical mechanisms and investigate protein environments surrounding the flavin cofactor in flavoenzymes.[46, 52] The 6-OH group is the most common naturally occurring modification for flavins. However, this modified flavin has mainly been ignored due to its lack of activity in glycolate oxidase and electron-transferring flavoprotein.[47, 51, 58-60] The surrounding amino acid residues can significantly modulate the versatility of the flavin in the active site of an enzyme.[39]

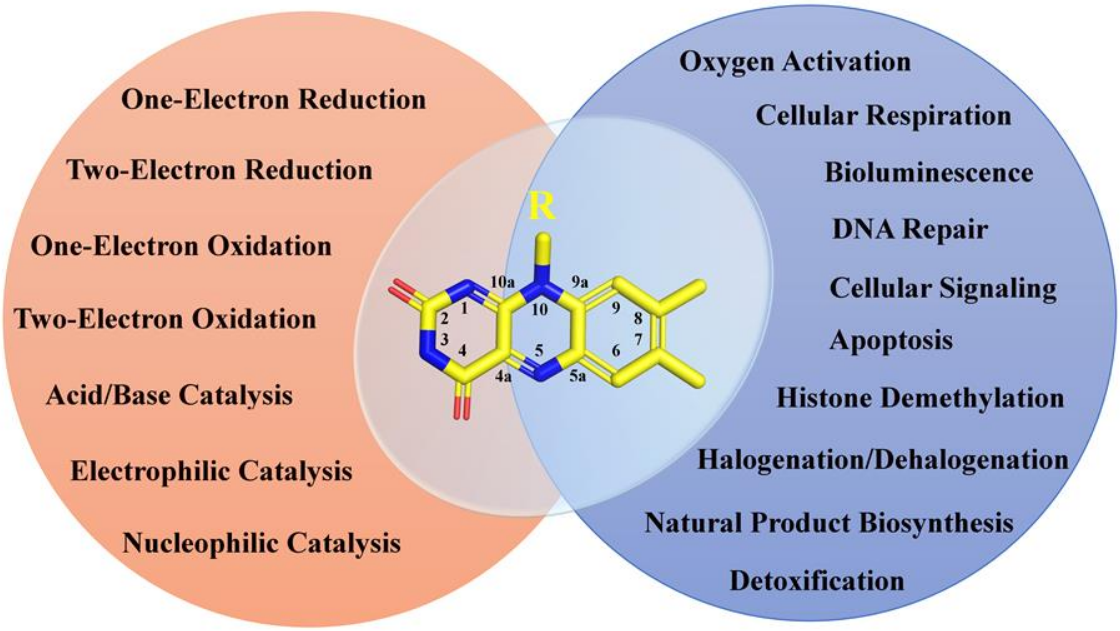

Figure 1.6. The versatility of flavin-dependent enzymes.

1.3 SPECIFIC AIMS

- **Investigation of the mechanism of formation of 6-OH-FAD in Y249F variant of *Pa*DADH**

*Pa*DADH is a true dehydrogenase, as it does not react with molecular oxygen during turnover to reoxidize the reduced flavin, and an artificial electron acceptor was used to characterize *Pa*DADH kinetically.[61] In the crystal structure of the wild-type *Pa*DADH (PDB code: 3NYE, 1.30 Å resolution), the hydroxyl O atom of Tyr249 was observed to be 3.0 Å from the carboxylate group of the iminoarginine product of the reaction bound, and 4.6 Å and 3.6 Å from the N5 and C6 atoms of the Isoalloxazine cofactor, respectively in the active site of the enzyme. At the time, tyrosine 249 seemed to be a viable candidate to serve as a catalytic base, which had not yet been identified for *Pa*DADH.[38] Purification of the Y249F variant of *Pa*DADH in which tyrosine 249 is replaced with phenylalanine yielded two distinct protein fractions: one with enzymatically active FAD and a green fraction with an unreactive modified FAD. The green fraction contained a modified form of flavin with significantly different spectroscopic properties. A previous graduate student established the green flavin as an FAD cofactor hydroxylated at the 6 positions by analysis using NMR, mass spectrometry, and UV−visible absorption spectroscopy.[12]

The current study aims to investigate the origin of the oxygen in the 6-OH-FAD found in the Y249F variant of PaDADH by ^{18}O isotope incorporation and investigate the effect of the mutation on the microenvironment surrounding the flavin using X-ray crystallography and Molecular Dynamics (MD). The conversion of FAD to 6-OH-FAD in the active site of Y249F *Pa*DADH seems to be substrate-assisted, like what was seen for the C30A variant of Trimethylamine Dehydrogenase (TMADH) from *Methylophilus methylotrophus*. TMADH was incubated with the substrate in $^{18}O_2$ and $H_2{}^{18}O$, and MS-ESI experiments determined the incorporation of ^{18}O. [62] Similarly, for the Y249F variant of *Pa*DADH, the enzyme fraction with

FAD would be incubated with D-alanine in the presence of $^{18}O_2$ and then analyzed via MS-ESI to investigate the incorporation of ^{18}O from molecular oxygen rather than water, owing to the rich oxidative chemistry of molecular oxygen. This study will provide further insights into the unconventional roles of residues in modulating the reactivity of versatile cofactors like flavins.

- **Kinetic Characterization of *Pa*LADH**

*Pa*DADH is part of a two-enzyme system with *P. aeruginosa* L-arginine dehydrogenase (*Pa*LADH). Together, they catalyze the conversion of D-arginine to L-arginine.[33, 63] *Pa*LADH catalyzes the conversion of 2-ketoarginine and ammonia into D-arginine, oxidizing NAD(P)H in the process. *Pa*LADH can also generate L-arginine from 2-ketoarginine and ammonia driven by NADH or NADPH, as shown in Scheme 1.1. This two-enzyme D-arginine conversion system has enabled *Pseudomonas aeruginosa* to gain an edge over other bacteria, enabling it to survive solely on D-arginine as a nitrogen and carbon source. [33, 64]

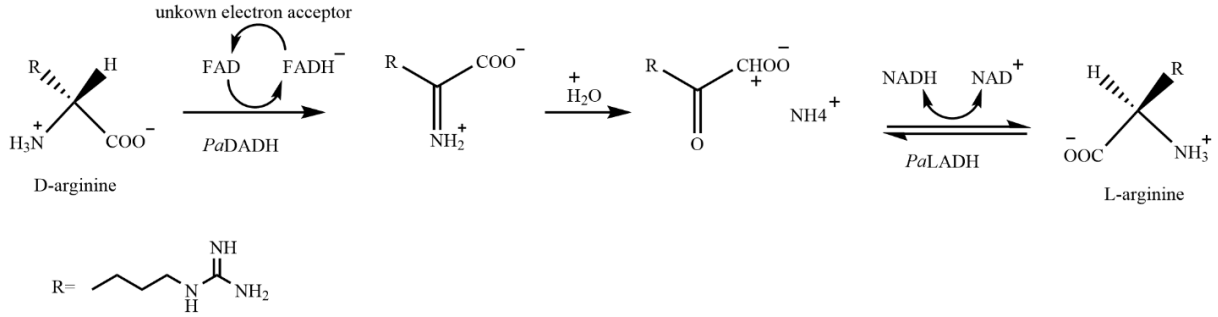

Scheme 1.1. Scheme for the two-enzyme system for D-arginine conversion in *P. aeruginosa*. Adapted from Reference 38

*Pa*LADH activity will be assayed by testing the enzyme against one of the products of *Pa*DADH; 2-ketoarginine and NAD(P)H by observing the NAD(P)H consumption at 340 nm using a stopped-flow spectrophotometer. The reverse reaction for *Pa*LADH would lead to oxidation of L-arginine to ketoarginine and ammonia, generating NAD(P)H in the process, and will be monitored with varying concentrations of NADP+ and L-arginine. The kinetic

characterization of *Pa*LADH will provide insights into its role in the novel two-enzyme D-arginine conversion system.

- **Determine if *Pa*LADH and *Pa*DADH form an active complex.**

*Pa*DADH and *Pa*LADH are part of a two-enzyme system in *P. aeruginosa* and catalyze the conversion of D-arginine to L-arginine. [33, 63] PaDADH and PaLADH may interact to form a protein-protein complex to streamline the D-arginine conversion reaction. The other advantage of this two-enzyme arginine conversion process in *P. aeruginosa* is that D-arginine can be converted to L-arginine to prevent the utilization during translation and incorporation into newly translated proteins. Crystallization trials will be carried out to co-crystallize purified *Pa*LADH and *Pa*DADH and subject to X-ray diffraction. Other techniques like sedimentation velocity analytical ultracentrifugation (AUC) will also be used to elucidate the protein-protein interaction between *Pa*LADH and *Pa*DADH.

This two-enzyme D-arginine conversion system has enabled *P. aeruginosa* to gain an edge over other bacteria, enabling it to survive solely on D-arginine as a nitrogen and carbon source.[33, 64] *P. aeruginosa* is an opportunistic pathogen that colonizes the lungs of almost 80% of cystic fibrosis (CF) patients. [65] It has been found that the lungs of CF patients have an excess of free amino acids.[66] The excess of free amino acids in CF lungs provides conditions for this bacterium to mutate and develop auxotrophic strains, which have a selective advantage over other bacteria and other strains of *P. aeruginosa*.[66] The investigation of these unique systems will expand the knowledge on *P. aeruginosa* colonization mechanisms in CF, which are crucial to developing new therapeutics. This study will provide insights into a novel D-arginine conversion system that utilizes two enzymes instead of the conventional one-enzyme racemase system.

1.4 REFERENCES

[1] Gal, J. (2008) The discovery of biological enantioselectivity: Louis Pasteur and the fermentation of tartaric acid, 1857--a review and analysis 150 yr later, *Chirality 20*, 5-19.

[2] Pasteur, L. (1848) Memoires sur la relation qui peut exister entre la forme crystalline et al composition chimique, et sur la cause de la polarization rotatoire, *Compt. rend. 26*, 535-538.

[3] Pasteur, L. (1848) Sur les relations qui peuvent exister entre la forme crystalline, la composition chimique et le sens de la polarization rotatoire, *Annales Chimie Phys. 24*, 442-459.

[4] Bastings, J., van Eijk, H. M., Olde Damink, S. W., and Rensen, S. S. (2019) d-amino Acids in Health and Disease: A Focus on Cancer, *Nutrients 11*.

[5] Fujii, N. (2002) D-amino acids in living higher organisms, *Orig Life Evol Biosph 32*, 103-127.

[6] Grishin, D. V., Zhdanov, D. D., Pokrovskaya, M. V., and Sokolov, N. N. (2020) D-amino acids in nature, agriculture and biomedicine, *All Life 13*, 11-22.

[7] Kolukisaoglu, U. (2020) D-amino Acids in Plants: Sources, Metabolism, and Functions, *Int J Mol Sci 21*.

[8] Fuchs, S. A., Berger, R., Klomp, L. W., and de Koning, T. J. (2005) D-amino acids in the central nervous system in health and disease, *Mol Genet Metab 85*, 168-180.

[9] Cava, F., Lam, H., de Pedro, M. A., and Waldor, M. K. (2011) Emerging knowledge of regulatory roles of D-amino acids in bacteria, *Cell Mol Life Sci 68*, 817-831.

[10] Magner, J. A. (2004) Emil Fischer (1852–1919): The Stereochemical Nature of Sugars, *The Endocrinologist 14*.

[11] Rosanoff, M. A. (1906) ON FISCHER'S CLASSIFICATION OF STEREO-ISOMERS.1, *Journal of the American Chemical Society 28*, 114-121.

[12] Friedman, M. (1999) Chemistry, nutrition, and microbiology of D-amino acids, *J Agric Food Chem 47*, 3457-3479.

[13] Towse, C. L., Hopping, G., Vulovic, I., and Daggett, V. (2014) Nature versus design: the conformational propensities of D-amino acids and the importance of side chain chirality, *Protein Eng Des Sel 27*, 447-455.

[14] Vranova, V., Zahradnickova, H., Janous, D., Skene, K. R., Matharu, A. S., Rejsek, K., and Formanek, P. (2012) The significance of D-amino acids in soil, fate and utilization by microbes and plants: review and identification of knowledge gaps, *Plant and Soil 354*, 21-39.

[15] Radkov, A. D., and Moe, L. A. (2014) Bacterial synthesis of D-amino acids, *Appl Microbiol Biotechnol 98*, 5363-5374.

[16] Forsum, O., Svennerstam, H., Ganeteg, U., and Nasholm, T. (2008) Capacities and constraints of amino acid utilization in Arabidopsis, *New Phytol 179*, 1058-1069.

[17] Kiriyama, Y., and Nochi, H. (2016) D-Amino Acids in the Nervous and Endocrine Systems, *Scientifica (Cairo) 2016*, 6494621.

[18] Sasabe, J., and Suzuki, M. (2019) Distinctive Roles of D-Amino Acids in the Homochiral World: Chirality of Amino Acids Modulates Mammalian Physiology and Pathology, *Keio J Med 68*, 1-16.

[19] Gordes, D., Kolukisaoglu, U., and Thurow, K. (2011) Uptake and conversion of D-amino acids in Arabidopsis thaliana, *Amino Acids 40*, 553-563.

[20] Fujii, N., Satoh, K., Harada, K., and Ishibashi, Y. (1994) Simultaneous stereoinversion and isomerization at specific aspartic acid residues in alpha A-crystallin from human lens, *J Biochem 116*, 663-669.

[21] Helfman, P. M., and Bada, J. L. (1975) Aspartic acid racemization in tooth enamel from living humans, *Proc Natl Acad Sci U S A 72*, 2891-2894.

[22] Keating, J. J., Bhattacharya, S., and Belfort, G. (2018) Separation of D, L-amino acids using ligand exchange membranes, *Journal of Membrane Science 555*, 30-37.

[23] Todone, F., Vanoni, M. A., Mozzarelli, A., Bolognesi, M., Coda, A., Curti, B., and Mattevi, A. (1997) Active site plasticity in D-amino acid oxidase: a crystallographic analysis, *Biochemistry 36*, 5853-5860.

[24] Erikson, O., Hertzberg, M., and Nasholm, T. (2004) A conditional marker gene allowing both positive and negative selection in plants, *Nat Biotechnol 22*, 455-458.

[25] Monselise, E. B., Levkovitz, A., and Kost, D. (2015) Ultraviolet radiation induces stress in etiolated Landoltia punctata, as evidenced by the presence of alanine, a universal stress signal: a (1)(5)N NMR study, *Plant Biol (Stuttg) 17 Suppl 1*, 101-107.

[26] Tsukada, K. (1966) D-amino acid dehydrogenases of Pseudomonas fluorescens, *J Biol Chem 241*, 4522-4528.

[27] Pollegioni, L., Piubelli, L., Sacchi, S., Pilone, M. S., and Molla, G. (2007) Physiological functions of D-amino acid oxidases: from yeast to humans, *Cell Mol Life Sci 64*, 1373-1394.

[28] Takahashi, S., Abe, K., and Kera, Y. (2015) Bacterial d-amino acid oxidases: Recent findings and future perspectives, *Bioengineered 6*, 237-241.

[29] Genchi, G. (2017) An overview on D-amino acids, *Amino Acids 49*, 1521-1533.

[30] Krebs, H. A. (1935) Metabolism of amino-acids: Deamination of amino-acids, *Biochem J 29*, 1620-1644.

[31] Morris, S. M., Jr. (2007) Arginine metabolism: boundaries of our knowledge, *J Nutr 137*, 1602S-1609S.

[32] Wu, G., and Morris, S. M., Jr. (1998) Arginine metabolism: nitric oxide and beyond, *Biochem J 336 (Pt 1)*, 1-17.

[33] Jann, A., Matsumoto, H., and Haas, D. (1988) The fourth arginine catabolic pathway of Pseudomonas aeruginosa, *J Gen Microbiol 134*, 1043-1053.

[34] Li, C., Yao, X., and Lu, C. D. (2010) Regulation of the dauBAR operon and characterization of D-amino acid dehydrogenase DauA in arginine and lysine catabolism of Pseudomonas aeruginosa PAO1, *Microbiology (Reading) 156*, 60-71.

[35] He, W., Li, G., Yang, C. K., and Lu, C. D. (2014) Functional characterization of the dguRABC locus for D-Glu and d-Gln utilization in Pseudomonas aeruginosa PAO1, *Microbiology (Reading) 160*, 2331-2340.

[36] He, W., Li, C., and Lu, C. D. (2011) Regulation and characterization of the dadRAX locus for D-amino acid catabolism in Pseudomonas aeruginosa PAO1, *J Bacteriol 193*, 2107-2115.

[37] Li, C., and Lu, C. D. (2009) Arginine racemization by coupled catabolic and anabolic dehydrogenases, *Proc Natl Acad Sci U S A 106*, 906-911.

[38] Fu, G., Yuan, H., Li, C., Lu, C. D., Gadda, G., and Weber, I. T. (2010) Conformational changes and substrate recognition in Pseudomonas aeruginosa D-arginine dehydrogenase, *Biochemistry 49*, 8535-8545.

[39] Fraaije, M. W., and Mattevi, A. (2000) Flavoenzymes: diverse catalysts with recurrent features, *Trends Biochem Sci 25*, 126-132.

[40] Williams, R. E., and Bruce, N. C. (2002) 'New uses for an Old Enzyme'--the Old Yellow Enzyme family of flavoenzymes, *Microbiology (Reading) 148*, 1607-1614.

[41] Stott, K., Saito, K., Thiele, D. J., and Massey, V. (1993) Old Yellow Enzyme. The discovery of multiple isozymes and a family of related proteins, *J Biol Chem 268*, 6097-6106.

[42] Joosten, V., and van Berkel, W. J. H. (2007) Flavoenzymes, *Current Opinion in Chemical Biology 11*, 195-202.

[43] van Berkel, W. J. H. Flavoenzymes, Chemistry of, In *Wiley Encyclopedia of Chemical Biology*, pp 0-0.

[44] Leys, D., and Scrutton, N. S. (2016) Sweating the assets of flavin cofactors: new insight of chemical versatility from knowledge of structure and mechanism, *Curr Opin Struct Biol 41*, 19-26.

[45] Claiborne, A., Massey, V., Fitzpatrick, P. F., and Schopfer, L. M. (1982) 2-Thioflavins as active site probes of flavoproteins, *The Journal of biological chemistry 257*, 174-182.

[46] Ghisla, S., and Massey, V. (1986) New flavins for old: artificial flavins as active site probes of flavoproteins, *Biochem J 239*, 1-12.

[47] Ghisla, S., Massey, V., and Yagi, K. (1986) Preparation and some properties of 6-substituted flavins as active site probes for flavin enzymes, *Biochemistry 25*, 3282-3289.

[48] Massey, V., Claiborne, A., Biemann, M., and Ghisla, S. (1984) 4-Thioflavins as active site probes of flavoproteins. General properties, *J Biol Chem 259*, 9667-9678.

[49] Massey, V., and Hemmerich, P. (1980) Active-site probes of flavoproteins, *Biochemical Society transactions 8*, 246-257.

[50] Schöllnhammer, G., and Hemmerich, P. (1974) Nucleophilic Addition at the Photoexcited Flavin Cation: Synthesis and Properties of 6- and 9-Hydroxy-Flavocoenzyme Chromophores, *European Journal of Biochemistry 44*, 561-577.

[51] Thorpe, C., and Massey, V. (1983) Flavin analogue studies of pig kidney general acyl-CoA dehydrogenase, *Biochemistry 22*, 2972-2978.

[52] Detmer, K., Schopfer, L. M., and Massey, V. (1984) Reactions of 1-deaza-FAD-substituted phenol hydroxylase and melilotate hydroxylase, *J Biol Chem 259*, 1532-1538.

[53] Edmondson, D. E., Kenney, W. C., and Singer, T. P. (1978) Synthesis and isolation of 8 alpha-substituted flavins and flavin peptides, *Methods Enzymol 53*, 449-465.

[54] Ghisla, S., and Mayhew, S. G. (1976) Identification and properties of 8-hydroxyflavin--adenine dinucleotide in electron-transferring flavoprotein from Peptostreptococcus elsdenii, *Eur J Biochem 63*, 373-390.

[55] Claiborne, A. (1986) Studies on the structure and mechanism of Streptococcus faecium L-alpha-glycerophosphate oxidase, *J Biol Chem 261*, 14398-14407.

[56] Massey, V., Ghisla, S., and Yagi, K. (1986) 6-Thiocyanatoflavins and 6-mercaptoflavins as active-site probes of flavoproteins, *Biochemistry 25*, 8103-8112.

[57] Schollnhammer, G., and Hemmerich, P. (1974) Nucleophilic addition at the photoexcited flavin cation: synthesis and properties of 6- and 9-hydroxy-flavocoenzyme chromophores, *Eur J Biochem 44*, 561-577.

[58] Igarashi, K., Verhagen, M. F., Samejima, M., Schulein, M., Eriksson, K. E., and Nishino, T. (1999) Cellobiose dehydrogenase from the fungi Phanerochaete chrysosporium and Humicola insolens. A flavohemoprotein from Humicola insolens contains 6-hydroxy-FAD as the dominant active cofactor, *J Biol Chem 274*, 3338-3344.

[59] Marshall, K. R., Gong, M., Wodke, L., Lamb, J. H., Jones, D. J., Farmer, P. B., Scrutton, N. S., and Munro, A. W. (2005) The human apoptosis-inducing protein AMID is an oxidoreductase with a modified flavin cofactor and DNA binding activity, *J Biol Chem 280*, 30735-30740.

[60] Whitfield, C. D., and Mayhew, S. G. (1974) Purification and properties of electron-transferring flavoprotein from Peptostreptococcus elsdenii, *J Biol Chem 249*, 2801-2810.

[61] Yuan, H., Fu, G., Brooks, P. T., Weber, I., and Gadda, G. (2010) Steady-state kinetic mechanism and reductive half-reaction of D-arginine dehydrogenase from Pseudomonas aeruginosa, *Biochemistry 49*, 9542-9550.

[62] Lu, X., Nikolic, D., Mitchell, D. J., van Breemen, R. B., Mersfelder, J. A., Hille, R., and Silverman, R. B. (2003) A mechanism for substrate-Induced formation of 6-hydroxyflavin mononucleotide catalyzed by C30A trimethylamine dehydrogenase, *Bioorg Med Chem Lett 13*, 4129-4132.

[63] Li, C., Yao, X., and Lu, C. D. (2010) Regulation of the dauBAR operon and characterization of D-amino acid dehydrogenase DauA in arginine and lysine catabolism of Pseudomonas aeruginosa PAO1, *Microbiology 156*, 60-71.

[64] Ouedraogo, D., Ball, J., Iyer, A., Reis, R. A. G., Vodovoz, M., and Gadda, G. (2017) Amine oxidation by d-arginine dehydrogenase in Pseudomonas aeruginosa, *Arch Biochem Biophys 632*, 192-201.

[65] Bhagirath, A. Y., Li, Y., Somayajula, D., Dadashi, M., Badr, S., and Duan, K. (2016) Cystic fibrosis lung environment and Pseudomonas aeruginosa infection, *BMC Pulm Med 16*, 174.

[66] Barth, A. L., and Pitt, T. L. (1996) The high amino-acid content of sputum from cystic fibrosis patients promotes growth of auxotrophic Pseudomonas aeruginosa, *J Med Microbiol 45*, 110-119.

2 AMINE OXIDATION BY D-ARGININE DEHYDROGENASE IN PSEUDOMONAS AERUGINOSA

(This chapter has been published verbatim in Ouedraogo D., Ball J., Iyer A., Reis R.A.G., Vodovoz M., and Gadda G. (2017) Arch Biochem Biophys, 632, 192-201; the author contributed to the introduction, D-amino acids, and their metabolism, open questions sections, all schemes, some figures in addition, to help with editing the final manuscript.)

2.1 ABSTRACT

D-Arginine dehydrogenase from Pseudomonas aeruginosa (*Pa*DADH) is a flavin-dependent oxidoreductase, which is part of a novel two-enzyme racemization system that functions to convert D-arginine to L- arginine. *Pa*DADH contains a noncovalently linked FAD that shows the highest activity with D-arginine. The enzyme exhibits broad substrate specificity towards D-amino acids, particularly with cationic and hydrophobic D-amino acids. Biochemical studies have established the structure and the mechanistic properties of the enzyme. The enzyme is a true dehydrogenase because it displays no reactivity towards molecular oxygen. As established through solvent and multiple kinetic isotope studies, *Pa*DADH catalyzes an asynchronous CH and NH bond cleavage via a hydride transfer mechanism. Steady-state kinetic studies with D-arginine and D-histidine are consistent with the enzyme following a ping-pong bi-bi mechanism. As shown by a combination of crystallography, kinetic and computational data, the shape and flexibility of loop L1 in the active site of *Pa*DADH are important for substrate capture and broad substrate specificity

2.2 INTRODUCTION

In 1848 Louis Pasteur made the groundbreaking discovery of molecular chirality[1]. Pasteur was also among the first to observe enantioselectivity in a biochemical process, which is now a well-established concept[1-3]. Numerous investigations were launched concerning D-amino acids and their roles in nature[4, 5]. Later in 1935, Hans Krebs discovered D-amino acid oxidase (DAAO)

through the observation that D-amino acids undergo selective deamination by homogenates derived from pig kidney[6].

D-amino acid oxidase is a ubiquitous flavin-dependent enzyme found in various species of bacteria, fungi, and mammals, and remains the most extensively studied enzyme that oxidizes D-amino acids, with more than 30 structures deposited in the Protein Data Bank[7]. D-amino acid oxidase from pig kidney (pDAAO) remains the most studied orthologue of the D-amino acid oxidase structural family, which also contains D-amino acid oxidases from other organisms, sarcosine oxidases, glycine oxidase and dimethylglycine oxidase[8-11].The enzyme has become a model for stereospecific flavin-dependent oxidoreductases that oxidize D-amino acids into their corresponding iminoacids. Flavin-dependent enzymes that oxidize D-amino acids also include D-glutamate oxidase, D-amino acid dehydrogenase, and D-arginine dehydrogenase, among others[12-16].

The function of DAAO in microorganisms is to utilize D-amino acids as a nutrient source, although the functions of the enzyme in eukaryotes is still under investigation[8, 17]. Mammalian DAAO has been reported to function in maintaining critical concentrations of D-serine that acts as a neuromodulator in mammals[18-20]. To gain an in-depth understanding of D-amino acid oxidizing enzymes, the readers are referred to recent reviews on DAAO and D-aspartate oxidase[7, 19, 21, 22].

*Pa*DADH is emerging as a paradigm for flavin-containing enzymes that oxidize positively charged D-amino acids and is an important complement to the D-amino acid oxidase, which catalyzes the oxidative deamination of small and hydrophobic substrates. The present review highlights the mechanistic and structural findings published over the past seven years on D-arginine dehydrogenase from *Pseudomonas aeruginosa* which is a member of the DAAO structural family. D-arginine dehydrogenase is an FAD-dependent enzyme that catalyzes the

oxidative deamination of D-amino acids to their respective iminoacids, which nonenzymatically hydrolyze to α-keto acids and ammonia[23, 24]. The enzyme plays a pivotal role in utilizing D-arginine as a primary source of carbon and nitrogen[16]. *Pa*DADH oxidizes the CN bond between the Cα atom and the amino group of the D-amino acid converting it to an iminoacid[25]. The enzyme does not display any reactivity towards molecular oxygen, which could potentially be a preventative mechanism to avoid production of harmful reactive oxygen species in host cells.

2.3 D-AMINO ACIDS AND THEIR METABOLISM

D-amino acids occur in free-form naturally in soil, plants, and are utilized by microorganisms commonly found in soil i.e., *P. aeruginosa*[26]. Racemization of amino acids depends on various abiotic factors like temperature, ionizing radiation, metal ions and pH, including several biotic factors like enzymes[4]. Environmental pressures and increased D-amino acid content in soil and waterways have forced bacteria to evolve in order to not only metabolize, but utilize and synthesize D-amino acids[4].

Higher organisms lack an extensive machinery in place to degrade D-amino acids**.** Indeed, high levels of D-isomers are not tolerated and have a toxic effect on plants and fungi growth[27, 28]. In humans, D-amino acids have specialized roles such as D-serine and D-aspartate which are agonists for N-methyl-D-aspartate receptors and D-aspartate is also associated with ageing in tissues[18, 29-32]. D-amino acids in most eukaryotes are racemized via a one-enzyme racemase, most of which are pyridoxal 5'-phosphate (PLP)-dependent[19, 32, 33].

In bacteria, however, several cases of the utilization of D-amino acids in peptidoglycan layers have been reported[34]. Bacteria, in most cases, have the required machinery in place to metabolize and utilize D-amino acids[34]. D-alanine and D-glutamate are among the D-amino acids that are most prevalent in bacteria, making alanine and glutamate racemases essential in

microorganisms[35]. Tsukada in 1966 demonstrated that *Pseudomonas fluorescens* had two distinct D-amino acid dehydrogenases expressed in cells treated with D-tryptophan[15]. Both enzymes use FAD as a cofactor and do not use molecular oxygen as an electron acceptor. One of the D-amino acid dehydrogenases specifically reacted with dichlorophenolindophenol as an electron acceptor, while the other with methylene blue and were named D-amino acid:2,6-dichloroindophenol oxidoreductase and D-amino acid :methylene blue oxidoreductase, respectively[15].

Haas and associates in 1988 provided evidence for an arginine racemase in *P. aeruginosa* by demonstrating utilization of D-arginine by arginine auxotrophs, yet they were not able to demonstrate arginine racemase activity *in vitro*[24]. Li and Lu in 2009 discovered a novel two-enzyme system that functions to convert D-arginine to L-arginine in *P. aeruginosa*. Further analysis of the two gene products revealed that the two-enzyme system is composed of an FAD-dependent D-arginine dehydrogenase and an NAD(P)H-dependent L-arginine dehydrogenase as described in Scheme 2.1[23]. The two enzymes are products of the dauBAR operon, which can be induced by D-arginine and D-lysine. The gene products DauA and DauB provide a unique coupled anabolic and catabolic system that enables *Pseudomonas aeruginosa* strain PAO1 to utilize D-arginine as the only source of carbon and nitrogen. Li and Lu also reported that the DauBAR operon is conserved among several other bacterial species[16, 23, 36].

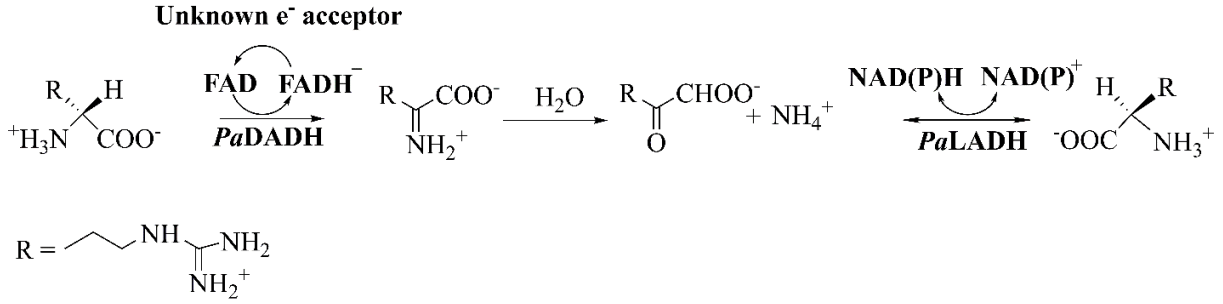

Scheme 2.1 D-Arginine racemization with the two-enzyme racemic system in *Pseudomonas aeruginosa. Pa*LADH *is* Pseudomonas aeruginosa *L-arginine dehydrogenase.*

2.4 STRUCTURAL FEATURES OF *Pa*DADH

2.4.1 Overall fold of PaDADH

The three-dimensional structure of *Pa*DADH was determined by X-ray crystallography at high resolution without added D-amino acids (~ 1.06 Å, PDB ID: 3NYC)[36]. However, extra density for a low occupancy iminoarginine was found in the active site. Ligand-free and bound forms were obtained, the latter of which was probably due to the product of the enzymatic reaction being trapped during the expression of the enzyme by *Escherichia. coli*.[36] The *Pa*DADH crystal structures were also determined for crystals grown in presence of D-arginine and D-histidine thereby yielding a *Pa*DADH/iminoarginine (PDB ID 3NYE)[36] and PaDADH/iminohistidine (PDB ID 3NYF)[36] complexes. Additionally, a covalent N5 flavin adduct was obtained at atomic-resolution in the enzyme co-crystallized with D-leucine instead of the expected iminoleucine (PDB ID 3SM8)[37]. Table 1 summarizes the crystal structures of *Pa*DADH available in the PDB. The four structures of hexahistidine-tagged *Pa*DADH are highly similar, with RMS deviations of less than 0.14 Å for 381 Cα atoms, and display a non-covalently bound FAD as the cofactor[36]. All 375 residues of *Pa*DADH were well defined in the electron density map and organized in two domains. The FAD-binding site is formed by a central six-stranded β-sheet surrounded by a three-stranded antiparallel β-sheet with two α-helices on one side and five α-helices on the other side (Figure 2.1A). The substrate binding site is composed of an eight-stranded β-sheet and two short antiparallel β-strands that constitute a sandwich surrounded by four α-helices and four loops (L1 to L4)[36] (Figure 2.1A).

2.4.2 FAD-binding site

The crystal structures of *Pa*DADH show a noncovalently bound FAD as the cofactor[36]. The flavin adopts an elongated conformation with the isoalloxazine moiety located at the interface

of the substrate-binding site and the FAD-binding site. The adenosine portion of the FAD moiety is buried deep within the FAD-binding site[36] (Figure 2.1A). The ribose ring moiety has hydrogen bond interactions with the main-chain of R33 and A171, water molecules and the side chain of E32. The pyrimidine portion of the isoalloxazine moiety interacts through hydrogen bonds with backbone atoms of the I335, Q336, H48 and a water molecule while the benzene portion forms van der Waals contacts with R44, R222, W301, G303 and R305 [36]. Crystallographic data of *Pa*DADH demonstrate that the isoalloxazine moiety of the FAD is in a non-planar conformation with a ring puckering angle of 15° along the N5 – N10 axis, defining two planes containing the benzene and pyrimidine moieties[36]. The bent conformation agrees with other flavin-dependent enzymes structures containing flavin in the reduced state[38, 39].

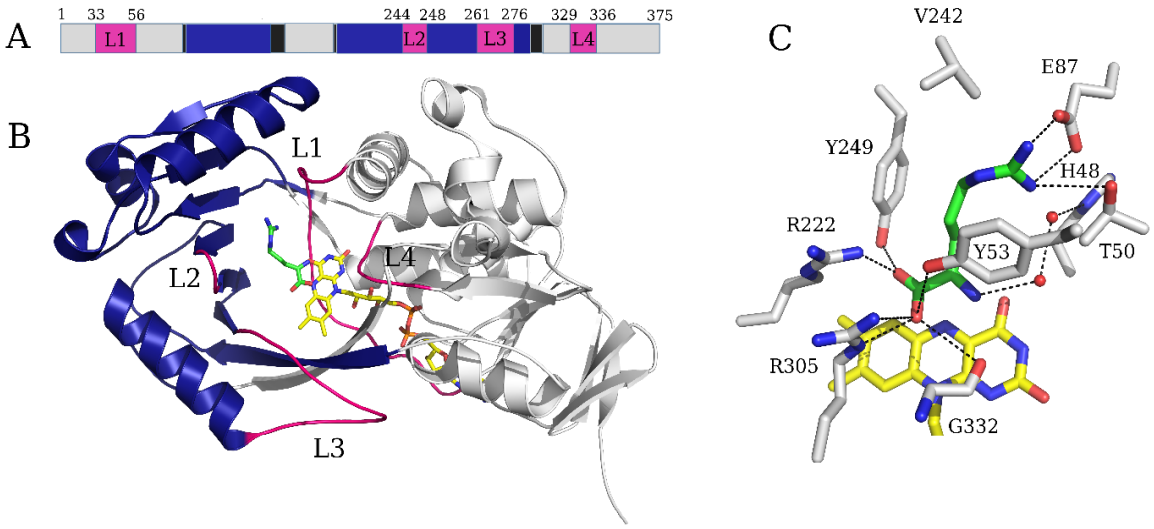

Figure 2.1 Overall structure and active site of *Pa*DADH in complex with iminoarginine.
(A) The *Pa*DADH structure is shown in cartoon diagram. C atoms are colored in gray for the FAD-binding site and in blue for the substrate-binding site. Iminoarginine and FAD stick representations are illustrated in green and yellow, respectively. Loops (L1 to L4) that contribute to the active site are highlighted in magenta. (B) Close-up view of the active site showing the substrate interactions of the active site residues and FAD with the iminoarginine product. Protein side chains are displayed in sticks.

2.4.3 Substrate binding-domain

The substrate-binding site of *Pa*DADH is formed by a small entrance that becomes wider at the bottom of the active site pocket and is about 10 Å deep when measured from the Cα atom of G54 to the FAD O2 atom[36]. The carboxylate group of the iminoarginine product occupies the same plane as the isoalloxazine moiety of the FAD, while its side chain is almost perpendicular to the FAD (Figure 2.1B)[36]. The side chain atoms of Y53, R222, Y249, R305, and the main-chain carbonyl of G332 form polar interactions with the iminoproduct carboxylate group (Figure 2.1B)[36]. The side chain of the iminoarginine product has van der Waals interactions with the side chain of V242, hydrogen bond interaction with T50 and Y53, and ionic interaction with E87 side chain[36] (Figure 2.1B). Two water molecules are located near the imino group of the product and form a hydrogen bond network extending to the side chain of H48[36]. The entrance of the active site is controlled by a flexible loop L1, which is formed by residues 33-56. The loop L1 has two different peptidyl regions including residues 45-47 and residues 50-56 adopting two conformations depending on whether the substrate is present or not in the active site[36].

2.4.4 Structural comparison of PaDADH with pDAAO

Previous crystallographic analysis showed that *Pa*DADH has a high three-dimensional structural similarity compared to pDAAO[36]. The crystal structures of *Pa*DADH (PDB ID 3NYE) and pDAAO (PDB ID 1DDO) were used for an in-depth comparison of the overall structure and the active site of the two enzymes[36, 40, 41]. pDAAO and *Pa*DADH share 17.2 % sequence identity with a RMS deviation value of 2.4 Å for 270 Cα atoms [36]. *Pa*DADH and pDAAO were chosen since both enzymes catalyze the same chemical reaction except that DAAO utilizes molecular oxygen as its electron acceptor. As shown in Figure 2.2A, the overall structure of *Pa*DADH is similar to pDAAO. The isoalloxazine moiety of the FAD is located at the interface between the

FAD-binding site and the substrate-binding site in both enzymes[36]. The main difference between the two structures is observed in the FAD-binding site as indicated in Figure 2.2A where three antiparallel β-sheets in *Pa*DADH are replaced by an α-helix in pDAAO[36]. The substrate binding-domain in both *Pa*DADH and pDAAO is characterized by the presence of a large β-sheet[36] (Figure 2.2A).

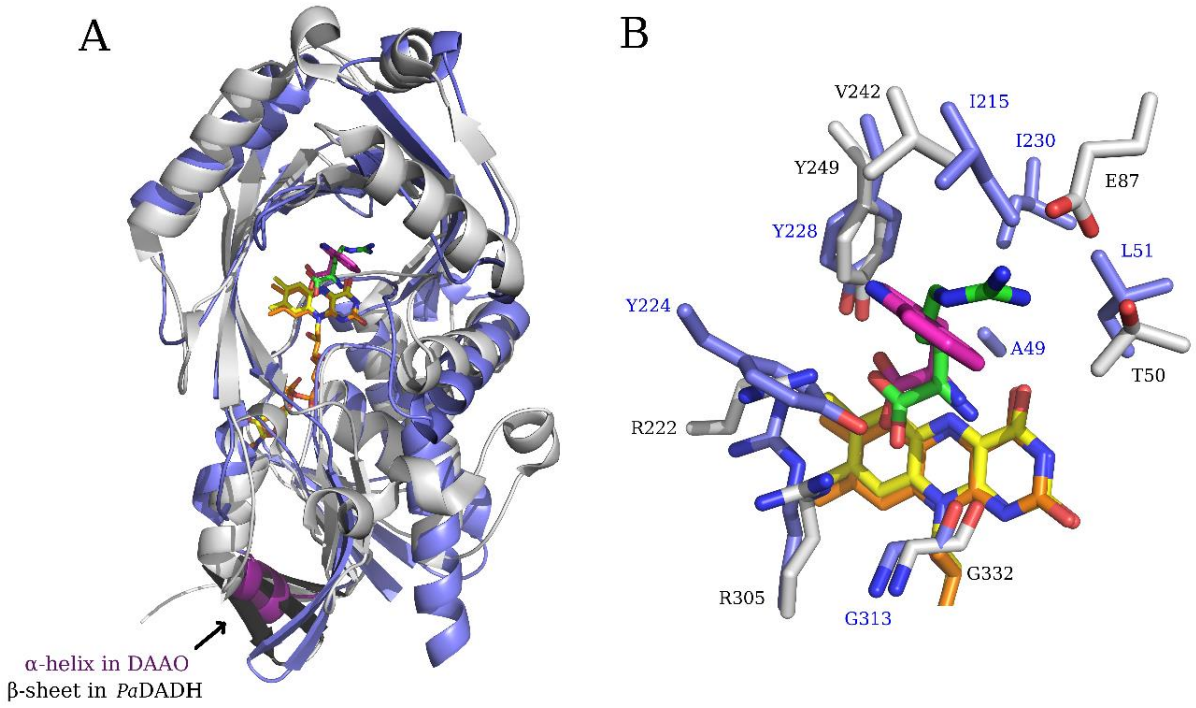

Figure 2.2 Comparison of the three-dimensional structures of pDAAO (light-blue, PDB ID 1DDO) with *Pa*DADH (gray, PDB ID 3NYE). Panel A represents the overall structure of the two enzymes and Panel B represents the active sites of the enzymes. For clarity, Y53 from *Pa*DADH was omitted. Iminoacid C atoms in *Pa*DADH are in green, iminotryptophan C atoms in pDAAO are in magenta and FAD moiety C atoms are in yellow and orange in *Pa*DADH and pDAAO, respectively.

The active site of *Pa*DADH in complex with iminoarginine and pDAAO in complex with imonotryptophan showed that the ligands in both enzymes bind at the *re* face of the isoalloxazine ring of the FAD moiety[36, 40] (Figure 2.2B). The carboxylate groups of the iminoproducts in both enzymes lie in planes that are parallel to the isoalloxazine moiety (Figure 2.2B). On the contrary, the side chains of the iminoproducts are quasi-perpendicular to the isoalloxazine moiety of the

FAD (Figure 2.2B). In pDAAO only the side chain of an arginine, R283, interacts with the iminoproduct carboxylate group whereas in *Pa*DADH two arginine residues, R222 and R305, participate in the interaction (Figure 2.2B)[36]. pDAAO has polar interactions with the iminotryptophan product formed by the side chain residues of Y224, Y228, and the main chain O atom of G313, which are similar to the interaction in *Pa*DADH formed by the side chains of Y53, Y249 and the main chain O atom of G332 (Figure 2.2B). The side chains of A49, L51, I215, I230 and Y224 in pDAAO form a hydrophobic cage that interacts with the iminotryptophan product. *Pa*DADH has a similar hydrophobic cage, but a key difference is the presence of E87 and T50 in *Pa*DADH in place of I230 and L51 in pDAAO, respectively[36, 40] (Figure 2.2B).

2.5 SUBSTRATE SPECIFICITY OF *Pa*DADH

*Pa*DADH exhibits broad substrate scope, being most active with large basic and hydrophobic substrates, and demonstrates the highest activity with D-arginine and D-lysine[42] (Table 2). *Pa*DADH is strictly stereospecific and L-amino acids are not substrates[36]. *Pa*DADH cannot oxidize the anionic amino acids aspartate and glutamate. The anionic amino acids are oxidized by specific D-aspartate and D-glutamate oxidases[12, 21]. The portion of the *Pa*DADH active site that binds the main chain follows intuition for the most part by providing a protein positive charge(s) from R222 and R305 to bind the carboxylate of the substrate, and hydrogen-bonds from Y53 and the main chain O atom of G332 to bind the amino group. The portion of the active site that binds the side chain of the substrate is fine-tuned to bind arginine with E87 positioned to form an electrostatic interaction at a distance of 2.5 Å with the guanidinium head-group of arginine (Figure 2.1B)[36]. The relatively large active site volume and the presence of a hydrophobic cage comprised of residues Y53, Y254, M240, and V242 grants *Pa*DADH the ability to oxidize large hydrophobic amino acids as well[43]. The large active site of *Pa*DADH and the lack

of a handle on glycine is likely the reason glycine cannot find an optimal configuration to be oxidized and smaller hydrophobic substrates are oxidized slowly by *Pa*DADH[36]. Based on crystallographic and computational evidence *Pa*DADH is proposed to be further modulated by a flexible loop to enhance the substrate scope by providing active site plasticity[36].

2.5.1 E87 dictates substrate specificity

D-Arginine and D-lysine are the best substrates for *Pa*DADH as determined by their large k_{cat}/K_m values in the 10^6 $M^{-1}s^{-1}$ range[36]. The kinetic parameter k_{cat}/K_m defines the ability of the enzyme for capturing the substrate to form the enzyme-substrate complex that proceeds to catalysis[44]. D-Arginine exhibits the largest k_{cat}/K_m value at pH 8.7 of 3.4 x 10^6 $M^{-1}s^{-1}$, about 7-fold higher than the next closest k_{cat}/K_m value with D-lysine[36]. The bi-dentate electrostatic interaction that arginine engages with E87 is likely more energetically favorable than the mono-dentate interaction involved with D-lysine and may account for the differences in kinetic parameters. Replacement of E87 with leucine resulted in a 20-fold decrease in the k_{cat}/K_m value with D-arginine, yet the value is still in the 10^5 $M^{-1}s^{-1}$ range, hence the contributions of the hydrophobic cage and other H-bonds to bind the D-arginine side-chain, such as T50 shown in Figure 2.3, is substantial[42].

The k_{cat}/K_m value with D-histidine as a substrate is considerably lower than with D-arginine and D-lysine simply because D-histidine cannot interact with E87[42]. In the crystal structure of the iminohistidine complex as shown in Figure 2.3, the iminohistidine product is present in two distinct conformations, one of which does not point towards E87 and may partially explain the 1000-fold lower k_{cat}/K_m values with D-histidine as compared to D-arginine[36]. Further evidence of a distinct binding behavior for D-histidine comes from the inverse solvent viscosity effect on the k_{cat}/K_m value. Such a solvent effect is not seen with D-arginine as a substrate[45].

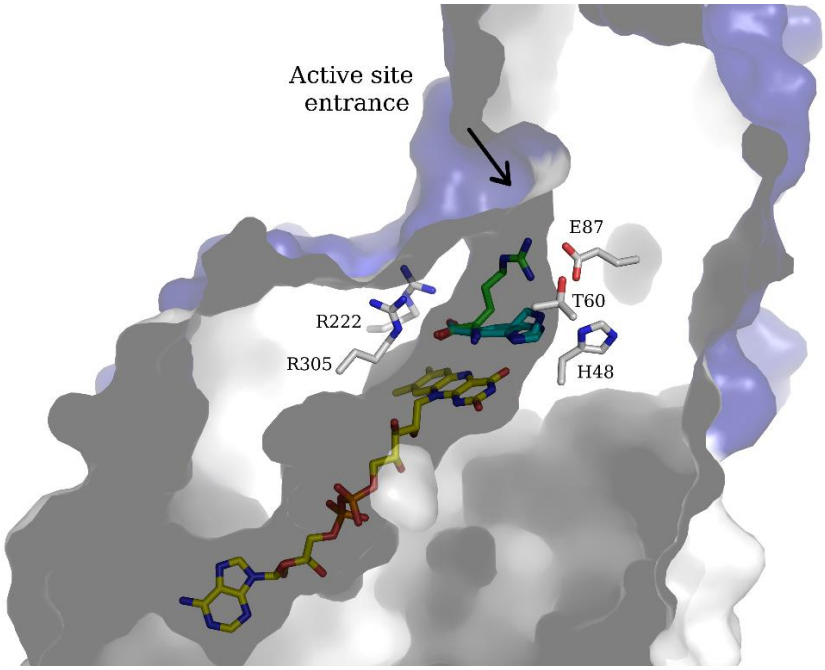

Figure 2.3 Overlay of the crystal structures of *Pa*DADH in complex with iminoarginine and iminohistidine. *Pa*DADH residues line the interior of the substrate binding pocket. (Some residues were omitted for clarity). Iminoarginine and iminohistidine bind in two distinct conformations. The surface of the substrate-binding pocket is in blue and the surface of the FAD-binding site is in white. Iminoarginine C atoms are in green, iminohistidine C atoms are in blue, FAD C atoms are in yellow, and side chain C atoms are in grey. The arrow indicates the entrance to the active site.

2.5.2 A hydrophobic cage and a flexible loop extends substrate scope

In addition to large k_{cat}/K_m values for amino acids substrates bearing positively charged side chains, *Pa*DADH can efficiently oxidize the bulky aromatic substrates tyrosine and phenylalanine, and the sulfur-containing methionine (Table 2.2)[36]. The ability of *Pa*DADH to accommodate hydrophobic amino acid substrates is rooted in the presence of a hydrophobic cage as mentioned above. The D-phenylalanine and D-tyrosine substrates most likely form π-π stacking interactions with either or both of Y53 and Y249[36]. D-Tyrosine can also potentially form hydrogen bonds with one or both Y53 and Y249 residues. D-Methionine is also a good substrate, making it likely that the sulfur of methionine engages in favorable sulfur-π interactions with the aromatic rings of Y53 and Y249[42, 46]. The flexible loop L1 of *Pa*DADH is present in two alternate conformations and is proposed to act as a gate to control substrate entry/exit and substrate

accommodation[36]. A similar loop is found in pDAAO composed of residues 216-228[40]. Loop L1 in *Pa*DADH may help lock small substrates in place by closing tightly, whereas in the case of large substrates like D-tyrosine and D-tryptophan the loop may protrude outward[36].

2.5.3 Substrate specificity comparison to D-amino acid oxidases

The specificity of *Pa*DADH for large and positively charged substrates is opposite to that of the *p*DAAO and human DAAO enzymes, which show a preference for smaller hydrophobic substrates i.e., D-alanine, and likewise possess small active site volumes of 160 and 220 $Å^3$, respectively[7]. The substrate specificity of the yeast enzymes, *Rg*DAAO and *Tv*DAAO, demonstrate a preference for amino acids bearing large and bulky hydrophobic side-chains such as valine, phenylalanine and tryptophan[47]. Naturally, the key factors that determine the specificity of each of the enzymes seem to lie within the interactions of the substrate side-chain with the active site residues and the relative sizes of the active site pockets.

2.6 STEADY-STATE KINETIC MECHANISM OF *Pa*DADH

The steady-state kinetic mechanism of *Pa*DADH is consistent with the minimal ping-pong bi-bi kinetic mechanism depicted in Scheme 2[45]. Evidence for a ping-pong mechanism stems from the occurrence of parallel lines in the double reciprocal plots of the enzymatic rates versus varied concentrations of D-arginine or D-histidine at different fixed concentrations of PMS as electron acceptor. The artificial electron acceptor PMS was utilized because the physiological oxidizing substrate has not been established. As shown in Scheme 2.2, the irreversible release of the iminoacid product (k_5) must occur before the second substrate, PMS, binds to enzyme (k_7)[45]. In agreement with a ping-pong mechanism, the binding of PMS was not significantly altered when either D-arginine or D-histidine was used as the reducing substrate, yielding a K_m of around 10 µM in both cases. Flavin reduction (k_3) was demonstrated to be irreversible with D-histidine as

substrate using rapid kinetics approaches[45]. The reoxidation of the flavin (k_9) is also presumed to be irreversible after examination of the reduction potentials of $PMS/PMSH_2 > FAD/FADH_2$, with values of +80 and -200 mV respectively[48]. However, it is worth noting that the reduction potentials could potentially be considerably different when buried within the enzyme environment.

2.6.1 Product release

The release of the iminoacid product (k_5) is partially rate determining for the overall turnover of the enzyme with D-arginine as substrate. Evidence for this conclusion comes from the effect of increasing solvent viscosity on the normalized rate constant for overall turnover when the enzyme is saturated with substrates[21.] Product release is the only diffusion-controlled step present in the proposed steady-state kinetic mechanism of *Pa*DADH[45]. The k_{cat} value for D-arginine exhibits a linear dependence on increasing viscosity yielding a positive slope of 0.14, consistent with product release being partially rate-determining[45]. Furthermore, the k_{red} value for D-arginine is not measurable using stopped-flow reaction techniques due to the reduction occurring within the dead-time of the instrument, consistent with an estimated value for flavin reduction $\geq 800\ s^{-1}$ [49]. Thus, another step other than product release may also be contributing to the overall rate of turnover with D-arginine but has yet to be elucidated. In the case of D-histidine, increasing solvent viscosity elicited no effect on k_{cat}, indicating product release was not limiting for turnover[45]. Comparison of the k_{red} value of 60 s^{-1} with D-histidine and its corresponding k_{cat} of 35 s^{-1} implies that flavin reduction is at least partially rate-limiting with D-histidine as substrate[45]. Yet this also implies there is another step that occurs during the overall catalytic turnover, such as an internal isomerization of the enzyme, that contributes to k_{cat} with D-histidine as well.

2.6.2 Substrate inhibition via a dead-end complex

At sufficiently high concentrations of D-arginine (> 0.5 mM) during steady-state turnover, substrate inhibition of *Pa*DADH occurs[45]. D-Arginine binds to the free reduced enzyme to form a dead-end complex *Pa*DADH$_{red}$-D-Arg as shown in Scheme 2.2. The accumulation of the dead-end complex leads to a lower overall rate of turnover. Substrate inhibition due to the formation of dead-end complexes between the reduced enzyme and substrate has been observed in other flavoproteins such as nitroalkane oxidase, flavocytochrome b2, thymidylate synthase, aldehyde oxidase, and cellobiose dehydrogenase[50-54].

2.7 CATALYTIC MECHANISM

2.7.1 Mechanism CN bond cleavage

The reductive-half reaction of *Pa*DADH was investigated to gain insight on the mechanism of CN bond cleavage. During flavin reduction with either D-leucine or D-histidine, C4a or flavin N5 adducts were not observed, which is consistent with a hydride transfer mechanism (Scheme 2.3). pH-Profiles and computational studies showed that the hydride transfer in *Pa*DADH is triggered by the abstraction of the substrate α-NH_3^+ group proton (Scheme 2.3). Moreover, substrate, solvent and multiple kinetic isotope effects studies on wild-type *Pa*DADH were consistent with the NH and CH bond cleavage of the substrate occurring asynchronously with irreversible flavin reduction. In order to investigate on the status of the base that abstracts the substrate α-NH_3^+ group proton (Scheme 2.3), Y53F and Y249F variant enzymes were generated through site-directed mutagenesis. Indeed, the crystal structure of *Pa*DADH shows that the hydroxyl groups of Y53 and Y249 residues are at a distance $\leq$ 4 Å from the substrate amino group consistent with the Y53 and Y249 residues to act as a base[25, 36]. The pH-profile studies on the reductive-half reaction of the Y53F and Y249F variant enzymes, and subsequent steady-state

kinetic studies on E87L and H48F enzymes, established that Y53, Y249, E87 or H48 residues were not the catalytic base that triggers the hydride transfer reaction to the enzyme-bound flavin[25, 42]. Thus, it was proposed that the α-NH_3^+ group of the substrate loses its proton to the solvent to trigger amine oxidation in *Pa*DADH[25, 42, 49].

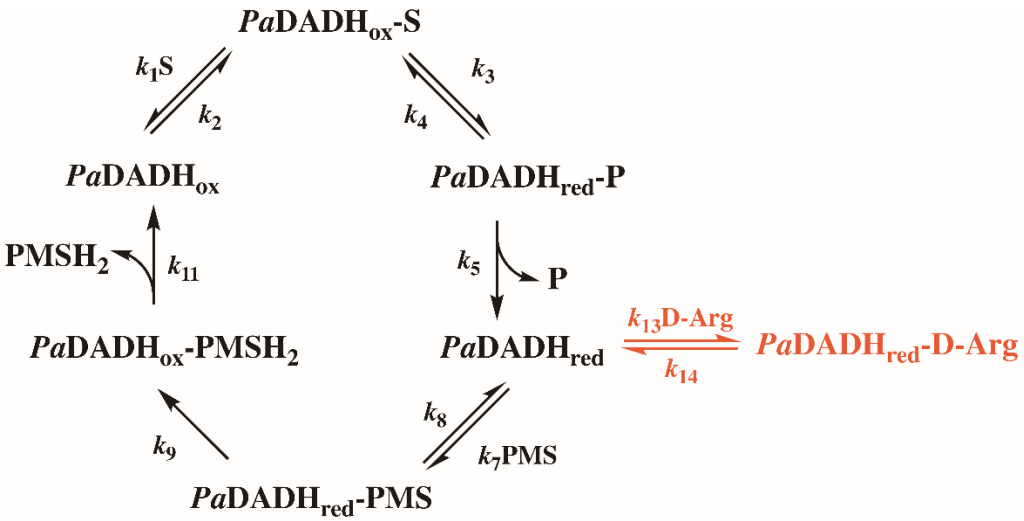

Scheme 2.2 Steady-State Kinetic Mechanism of *Pa*DADH. *Pa*$DADH_{ox}$, oxidized D-arginine dehydrogenase; S, amino acid substrate; *Pa*$DADH_{red}$, reduced D-arginine dehydrogenase; P, iminoacid product; PMS, phenazine methosulfate. k_5 and k_{11} are shown as irreversible because products are assumed to be close to zero during the determination of the initial rates of reaction; k_4 is shown although it is close to zero based on stopped-flow data.[45]

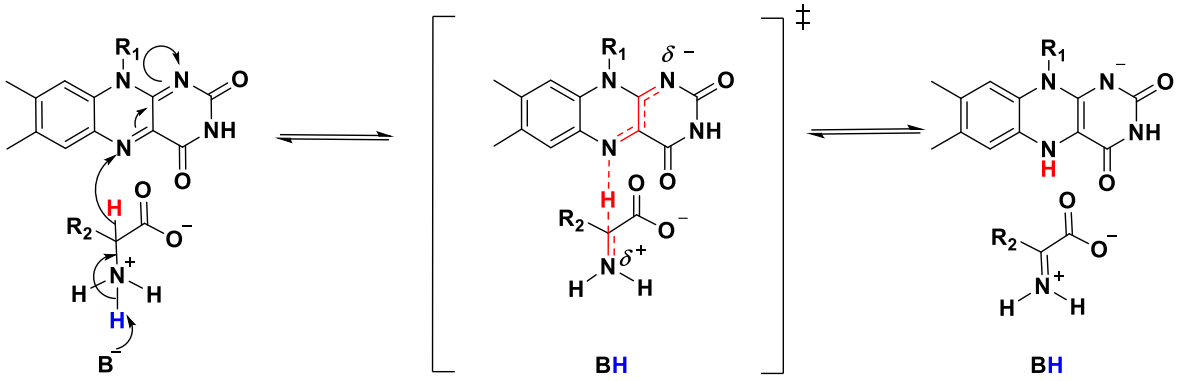

Scheme 2.3 Hydride transfer mechanism in *Pa*DADH. B^- is a catalytic base, currently presumed to be a solvent molecule.

Similar to the wild-type *Pa*DADH, no flavin intermediates were observed in the Y53F and Y249F variants consistent with a hydride transfer mechanism. On the contrary, flavin reduction was reversible in both the Y53F and Y249F variants. Moreover, the solvent and multiple kinetic isotope effect studies on the Y53F and Y249F variants demonstrated a synchronous CH and NH bond cleavage, consistent with a hydride transfer, and an alteration in the relative timing of the two bond cleavages as compared to the wild-type enzyme[25]. Based on this observation, it was concluded that the two tyrosine residues are involved in the stabilization of the transition state in *Pa*DADH to facilitate the hydride transfer from the substrate Cα to the N5 atom of the isoalloxazine moiety of the FAD[25].

2.7.2 Restricted proton transfer

The pH-profile studies on K_d value and computational studies indicate that *Pa*DADH prefers to bind the protonated form of the substrate (i.e., α-NH_3^+)[49]. As shown in Scheme 2.4, after formation of the ESH^+ complex the substrate then loses a proton to form the ES complex that proceeds to catalysis. A prominent hollow observed in the k_{cat} pH-profiles with D-lysine as a substrate with the wild-type *Pa*DADH provides evidence that the equilibration of the proton within

the enzyme-substrate complex (i.e., k_{16}/k_{15} in Scheme 2.4) is slower than other relevant kinetic steps (Scheme 2.4). [42] A hollowed pH-profile is usually observed with sticky substrates, which have a very high capacity to proceed to catalysis (i.e., k_3) after the formation of the enzyme-substrate complex.[55-57]

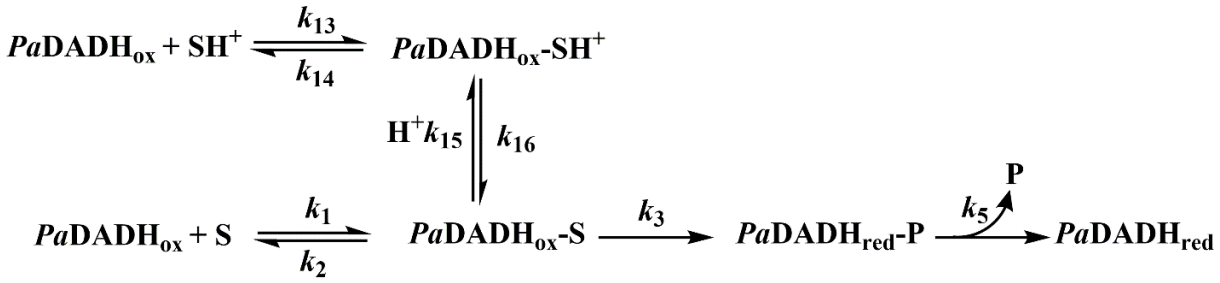

Scheme 2.4 Reductive half-reaction of *Pa*DADH accounting for a slow proton equilibrium in the Michaelis complex. S is the D-amino acid substrate. P is the iminoacid product.

The pH-profiles on the variant enzymes H48F and E87L provide further evidence that the hollow is related to a sub-optimal binding of the substrate in the active site of the enzyme[42]. The E87 residue stabilizes D-arginine by engaging in an ionic interaction with the substrate guanido group, thereby replacement of the E87 side chain to leucine impaired the optimal binding of the substrate, resulting in a slow proton release to the solvent[42]. It was shown that the hollowed pH-profile of the H48F variant, which is not in direct contact with the substrate, is possibly due to the disruption of the hydrogen-bond network between the water molecules, H48 residue and the amino group of the substrate (Figure 2.4)[36, 42]. The hydrogen-bond network is important to optimize substrate binding and to prevent a slow proton release from the enzyme-substrate complex[42] (Figure 2.4). As shown in the crystal structure, E87 has an ionic interaction with the substrate guanido group, while H48 interacts indirectly with the substrate via two water molecules (Figure 2.4).[36] Thus, it was concluded that both H48 and E87 residues participate in the optimal orientation

of the substrate to prevent a slow proton exchange between the ESH^+ complex and the solvent[42] (Figure 2.4).

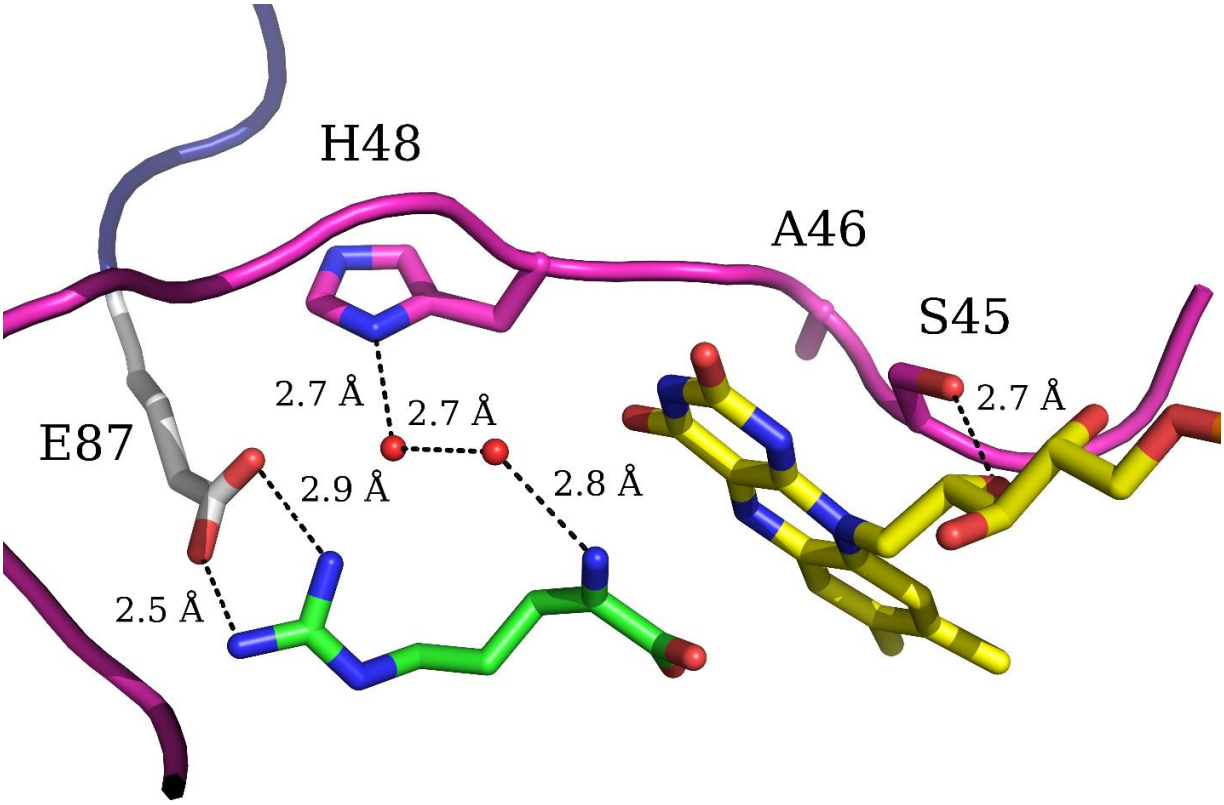

Figure 2.4 *Pa*DADH loop L1 with the S45, A46 and H48 residues. The isoalloxazine moiety of the FAD is in yellow, and the iminoarginine product is in green. Loop L1 is in magenta with H48 interacting with the iminoarginine product through two water molecules.

2.8 ROLE OF LOOP L1 DYNAMICS IN *Pa*DADH

The crystallographic data showed that *Pa*DADH has an active site loop L1 with two flexible segments that span the FAD-binding site and the substrate-binding site.[36] Loop L1 was also shown to occupy two distinct conformations corresponding to an open, competent substrate binding conformation, and a catalytically relevant, ligand-bound closed conformation[36] (Figure 2.5). Y53 in loop L1, located at the entrance of active site, was proposed to act as a gate to control the access to the active site.[36] In the FAD-binding site the side chains of S45 and A46 in loop L1,

which do not interact directly with the substrate, adopt two alternate conformations depending on whether the ligand is present in the active site or not (Figure 2.5).[36] Thus, the alternating conformations of S45 and A46, dubbed the S45/A46 switch, was also considered to participate in the catalytic function of *Pa*DADH.[36]

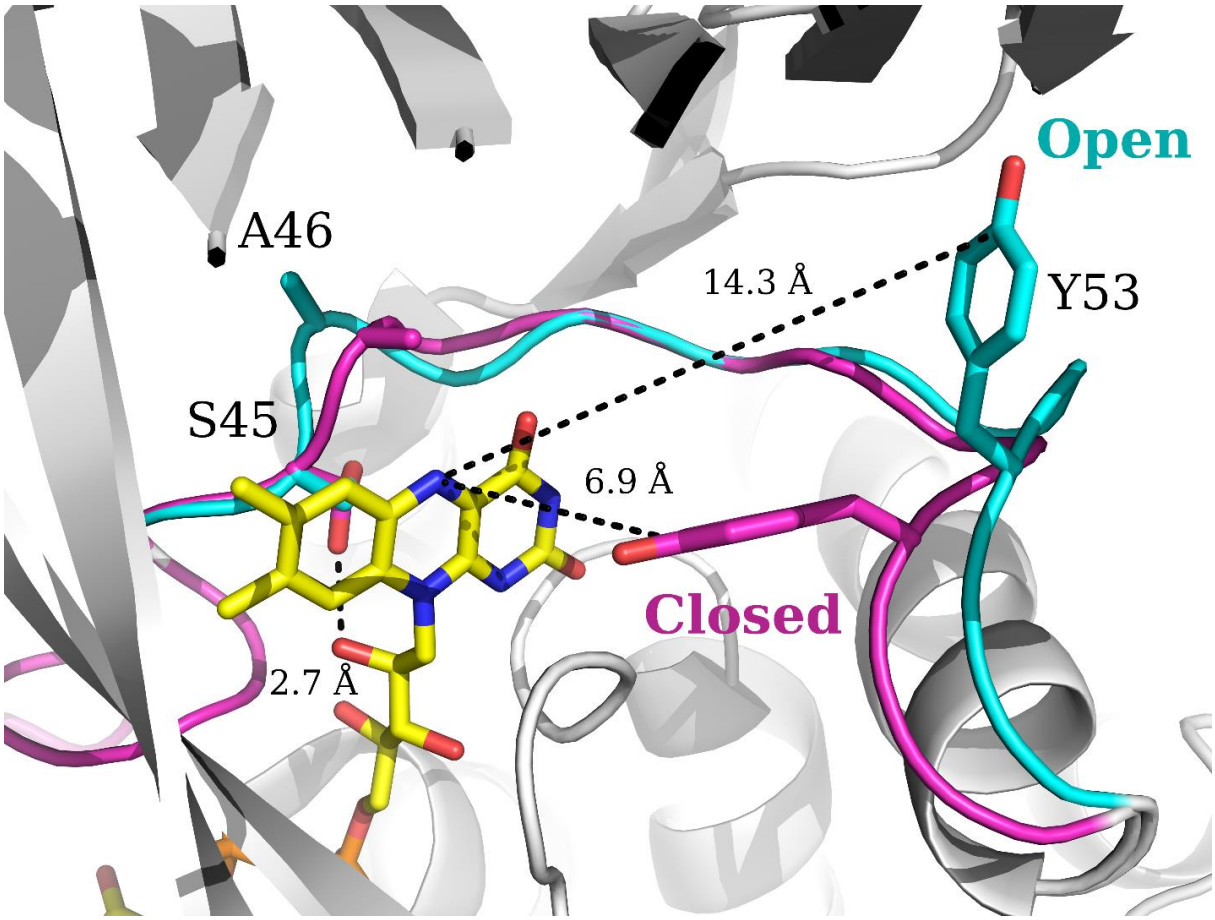

Figure 2.5 Open-closed conformations of loop L1.
The open conformation is shown in blue and the closed conformation in magenta. The C atoms in the isoalloxazine ring of the FAD are shown in yellow.

2.8.1 S45/A46 switch and the Y53 gate

In the open conformation, as shown by the crystal structure, both the side chains of S45 and A46 located at the FAD-binding site point away from the isoalloxazine moiety, while the side chain of Y53 points away from the active site pocket toward the bulk solvent (Figure 2.5).[36] In the closed conformation, the side chains of S45 and A46 move closer to the isoalloxazine moiety and

the side chain of Y53 gate swings back into the active site pocket to interact with the carboxylate group of the iminoarginine product.[36] The S45 and A46 were mutated individually to alanine and glycine, respectively, to investigate the dynamics of loop L1.[58] The molecular dynamics data indicate that in both S45A and A46G variants the Y53 gate has a higher probability to be in the open conformation as compared to the wild-type enzyme, where the gate has almost equal probability to be in the open and closed conformations during the simulation time.[58] Thus, it was concluded that the conformations of the S45/A46 switch and the Y53 gate are coupled.[58] Moreover, the intensity of the fluorescence spectroscopy showed a ~2-fold increase in the S45A and A46G variant enzymes compared to the wild-type when the flavin was excited at its lower energy peak in the enzyme bound-flavin.[58] The emission peak of the flavin fluorescence of the enzyme-bound flavin was red-shifted from 513 nm in the wild-type to 522 nm in both the variant enzymes (Figure 2.6). It was concluded that the active site in the S45A and the A46G variants is more exposed to the solvent due to the higher probability of the Y53 gate to stay in the open conformation with respect to wild-type *Pa*DADH (Figure 2.6).[58]

2.8.2 Dynamics of loop L1 in substrate capture and catalysis

The dynamics of loop L1 participate in the optimal orientation of the enzyme-substrate complex, as evidenced by molecular dynamics simulations and steady-state kinetic approaches.[58] The pH-independent k_{cat}/K_m values were lowered by 12-fold in the S45A and A46G variants compared to the wild-type.[42, 58] Based on the decreased k_{cat}/K_m values observed in the S45A and A46G variants, it was proposed that the likelihood of substrate capture in the variants is impaired due to the higher probability of the Y53 gate to be in the open conformation as compared to the wild-type enzyme.[58] A hollow was observed in the k_{cat} pH-profiles for both the S45A and A46G variants, consistent with a restricted proton transfer from the enzyme-substrate complex to the

solvent.[58] To gain insights on the effect of loop L1 dynamics on the rate of flavin reduction, the reductive half-reaction of both variants was investigated. No conclusions could be drawn on the impact of the mutations on the rate of flavin reduction because both variants could not be saturated with the slow substrate D-leucine, preventing a direct measurement of the rate constant for flavin reduction.[58]

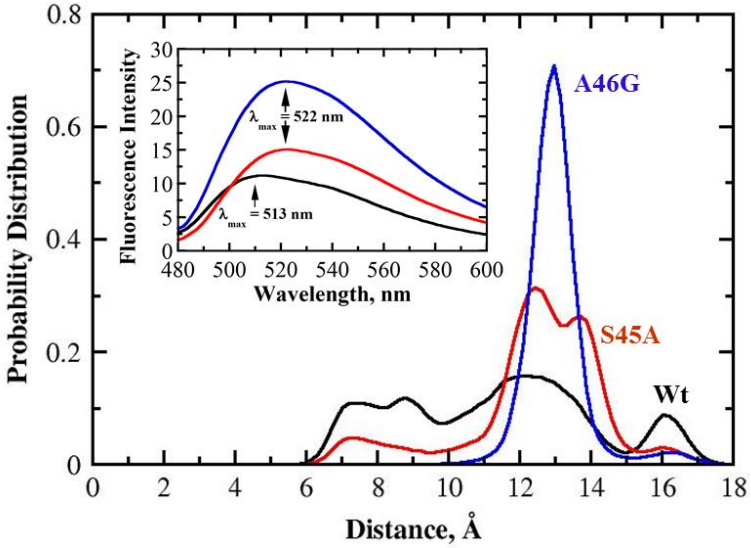

Figure 2.6. Probability distribution of the S45A, A46G variant enzymes and the wild-type.All-atoms molecular dynamics simulations were carried out over 1.1 μs with 0.1 μs as equilibration time[58]. S45A variant is colored in blue, A46G variant in read and the wild-type in black. The inset represents the flavin fluorescence of the variants and the wild-type enzyme.

The movement of side chain residues in mobile loops has been shown to participate in the catalytic function of several enzymes.[59] In *Rg*DAAO, Y238 was proposed to act as a gate that may control substrate entrance and product exit from the active site, and the corresponding residue in pDAAO, Y224, was proposed to contribute to the active site plasticity responsible for the binding of various substrates.[40, 60] Y215 in lactate oxidase and E89 in phosphoenolpyruvate carboxykinase, which are not in direct contact with the substrate, help to optimize substrate binding.[61, 62] Residues on flexible loop portions located at the entrance of enzymes not only act as gates but have been shown to shield the active site from the solvent upon binding of the substrate.[59, 63-65]

2.9 OPEN QUESTIONS

The mechanistic and structural features of *Pa*DADH have been established. However, several open questions remain. The physiological electron acceptor of the enzyme has yet to be identified. *In vitro,* PMS has been used as an artificial electron acceptor. Based on the abundance of quinones in nature and their participation in many electron transport systems, quinones could possibly act as potential physiological electron acceptors of the enzyme. Engineering a *Pa*DADH that is capable or reacting with oxygen could be useful in exploiting the enzyme function in industrial use to separate racemic mixtures. Engineering flavoprotein dehydrogenases to react with molecular oxygen to this day remains a challenging endeavor. *Pa*DADH is part of a two-enzyme racemic system involved in the racemization of D- to L-arginine. The presence of two enzymes instead of a typical single racemase could potentially serve as a regulatory mechanism. Further investigation of *Pa*DADH and engineering variants that display oxygen reactivity can be utilized for enzymatic synthesis of various α-keto acids and the separation of racemic amino acid mixtures which are of potential interest to the industry.

Table 2.1 Crystal structures of *Pa*DADH deposited in PDB.

PDB ID	Resolution (Å)	Redox state of flavin	Ligand
3NYC	1.06	Mixed*	Iminoarginine
3NYE	1.30	Reduced	Iminoarginine
3NYF	1.30	Reduced	Iminohistidine
3SM8	1.07	Reduced	D-leucine N5 flavin adduct

*Ligand-free and product-bound conformations for *Pa*DADH.

The crystal structures of *Pa*DADH exhibit the same space group $P2_12_12_1$.

Table 2.2 Steady-State Kinetic Parameters for *Pa*DADH**.**

Substrate	k_{cat}/K_m, M^{-1} s^{-1}	k_{cat}, s^{-1}	K_m, mM
D-arginine	(3.4 ± 0.3) x 10^6	204 ± 3	0.06 ± 0.01
D-lysine	(5.3 ± 0.2) x 10^5	141 ± 3	0.26 ± 0.01
D-tyrosine	27600 ± 3800	23 ± 1	0.8 ± 0.1
D-methionine	14800 ± 600	154 ± 3	10 ± 1
D-phenylalanine	6900 ± 300	75 ± 3	11 ± 1
D-histidine	3140 ± 30	35 ± 1	11 ± 1
D-leucine	515 ± 60	6.4 ± 0.3	12 ± 1
D-proline	420 ± 10	-[a]	-
D-tryptophan	245 ± 3	-	-
D-isoleucine	195 ± 3	-	-
D-glutamine	186 ± 3	-	-
D-valine	47 ± 1	-	-
D-alanine	41 ± 1	-	-
D-asparagine	16 ± 1	-	-
D-serine	3.8 ± 0.1	-	-
D-threonine	0.75 ± 0.01	-	-
D-glutamate	-	-	-
D-aspartate	-	-	-
L-arginine	-	-	-
glycine	-	-	-
D-cysteine	nd[b]	nd	nd

Enzyme activity was measured varying concentrations of the desired amino acid and 1 mM PMS in 20 mM Tris-HCl, pH 8.7, at 25 °C. [a]Cannot be saturated with substrate thereby k_{cat} and K_m values are not reported. [b]Not determined. PMS was reduced nonenzymatically by cysteine.

2.10 REFERENCES

[1] Gal, J. (2008) The discovery of biological enantioselectivity: Louis Pasteur and the fermentation of tartaric acid, 1857--a review and analysis 150 yr later, Chirality 20, 5-19.

[2] Pasteur, L. (1848) Mémoire sur la relation qui peut exister entre la forme cristalline et la composition chimique, et sur la cause de la polarisation rotatoire, Comptes rendus de l'Académie des sciences 26, 535–538.

[3] Pasteur, L. (1848) Sur les relations qui peuvent exister entre la forme cristalline, la composition chimique et le sens de la polarisation rotatoire, Annales de Chimie et de Physique 24, 442–459.

[4] Friedman, M. (1999) Chemistry, nutrition, and microbiology of D-amino acids, J Agric Food Chem 47, 3457-3479.

[5] Fujii, N. (2002) D-amino acids in living higher organisms, Orig Life Evol Biosph 32, 103-127.

[6] Krebs, H. A. (1935) Metabolism of amino-acids: Deamination of amino-acids, Biochem J 29, 1620-1644.

[7] Pollegioni, L., Piubelli, L., Sacchi, S., Pilone, M. S., and Molla, G. (2007) Physiological functions of D-amino acid oxidases: from yeast to humans, Cell Mol Life Sci 64, 1373-1394.

[8] Pilone, M. S. (2000) D-Amino acid oxidase: new findings, Cell Mol Life Sci 57, 1732-1747.

[9] Job, V., Marcone, G. L., Pilone, M. S., and Pollegioni, L. (2002) Glycine oxidase from Bacillus subtilis. Characterization of a new flavoprotein, J Biol Chem 277, 6985-6993.

[10] Trickey, P., Wagner, M. A., Jorns, M. S., and Mathews, F. S. (1999) Monomeric sarcosine oxidase: structure of a covalently flavinylated amine oxidizing enzyme, Structure 7, 331-345.

[11] Leys, D., Basran, J., and Scrutton, N. S. (2003) Channelling and formation of 'active' formaldehyde in dimethylglycine oxidase, EMBO J 22, 4038-4048.

[12] Urich, K. (1968) [D-Glutamate oxidase from the antennal gland of the crayfish Oronectes limosus: purification and characterization], Z Naturforsch B 23, 1508-1511.

[13] Olsiewski, P. J., Kaczorowski, G. J., and Walsh, C. (1980) Purification and properties of D-amino acid dehydrogenase, an inducible membrane-bound iron-sulfur flavoenzyme from Escherichia coli B, J Biol Chem 255, 4487-4494.

[14] Satomura, T., Ishikura, M., Koyanagi, T., Sakuraba, H., Ohshima, T., and Suye, S. (2015) Dye-linked D-amino acid dehydrogenase from the thermophilic bacterium Rhodothermus marinus JCM9785: characteristics and role in trans-4-hydroxy-L-proline catabolism, Appl Microbiol Biotechnol 99, 4265-4275.

[15] Tsukada, K. (1966) D-amino acid dehydrogenases of Pseudomonas fluorescens, J Biol Chem 241, 4522-4528.

[16] Li, C., Yao, X., and Lu, C. D. (2010) Regulation of the dauBAR operon and characterization of D-amino acid dehydrogenase DauA in arginine and lysine catabolism of Pseudomonas aeruginosa PAO1, Microbiology 156, 60-71.

[17] Fischer, L., Gabler, M., Horner, R., and Wagner, F. (1996) Microbial D-amino acid oxidases (EC .4.3.3), Ann N Y Acad Sci 799, 683-688.

[18] Rodriguez-Crespo, I. (2008) D-amino acids in the brain: pyridoxal phosphate-dependent amino acid racemases and the physiology of D-serine, FEBS J 275, 3513.

[19] D'Aniello, A., D'Onofrio, G., Pischetola, M., D'Aniello, G., Vetere, A., Petrucelli, L., and Fisher, G. H. (1993) Biological role of D-amino acid oxidase and D-aspartate oxidase. Effects of D-amino acids, J Biol Chem 268, 26941-26949.

[20] Pollegioni, L., and Sacchi, S. (2010) Metabolism of the neuromodulator D-serine, Cell Mol Life Sci 67, 2387-2404.

[21] Negri, A., Massey, V., and Williams, C. H., Jr. (1987) D-aspartate oxidase from beef kidney. Purification and properties, J Biol Chem 262, 10026-10034.

[22] Tishkov, V. I., and Khoronenkova, S. V. (2005) D-Amino acid oxidase: structure, catalytic mechanism, and practical application, Biochemistry (Mosc) 70, 40-54.

[23] Li, C., and Lu, C. D. (2009) Arginine racemization by coupled catabolic and anabolic dehydrogenases, Proc Natl Acad Sci U S A 106, 906-911.

[24] Jann, A., Matsumoto, H., and Haas, D. (1988) The fourth arginine catabolic pathway of Pseudomonas aeruginosa, J Gen Microbiol 134, 1043-1053.

[25] Gannavaram, S., Sirin, S., Sherman, W., and Gadda, G. (2014) Mechanistic and computational studies of the reductive half-reaction of tyrosine to phenylalanine active site variants of D-arginine dehydrogenase, Biochemistry 53, 6574-6583.

[26] Rejsek, K., Formanek, P., and Vranova, V. (2010) The soil amino acids : quality, distribution, and site ecology, Nova Science Publishers, Hauppauge, N.Y.

[27] Erikson, O., Hertzberg, M., and Nasholm, T. (2004) A conditional marker gene allowing both positive and negative selection in plants, Nat Biotechnol 22, 455-458.

[28] Aldag, R. W., and Young, J. L. (1970) Aspects of D-leucine and D-lysine metabolism in maize and ryegrass seedlings, Planta 95, 187-201.

[29] Errico, F., Napolitano, F., Nistico, R., and Usiello, A. (2012) New insights on the role of free D-aspartate in the mammalian brain, Amino Acids 43, 1861-1871.

[30] Sacchi, S. (2013) D-Serine metabolism: new insights into the modulation of D-amino acid oxidase activity, Biochem Soc Trans 41, 1551-1556.

[31] Snyder, S. H., and Kim, P. M. (2000) D-amino acids as putative neurotransmitters: focus on D-serine, Neurochem Res 25, 553-560.

[32] Yoshimura, T., and Goto, M. (2008) D-amino acids in the brain: structure and function of pyridoxal phosphate-dependent amino acid racemases, FEBS J 275, 3527-3537.

[33] Yoshimura, T., and Esak, N. (2003) Amino acid racemases: functions and mechanisms, J Biosci Bioeng 96, 103-109.

[34] Cava, F., Lam, H., de Pedro, M. A., and Waldor, M. K. (2011) Emerging knowledge of regulatory roles of D-amino acids in bacteria, Cell Mol Life Sci 68, 817-831.

[35] Radkov, A. D., and Moe, L. A. (2014) Bacterial synthesis of D-amino acids, Appl Microbiol Biotechnol 98, 5363-5374.

[36] Fu, G., Yuan, H., Li, C., Lu, C. D., Gadda, G., and Weber, I. T. (2010) Conformational changes and substrate recognition in Pseudomonas aeruginosa D-arginine dehydrogenase, Biochemistry 49, 8535-8545.

[37] Fu, G., Yuan, H., Wang, S., Gadda, G., and Weber, I. T. (2011) Atomic-resolution structure of an N5 flavin adduct in D-arginine dehydrogenase, Biochemistry 50, 6292-6294.

[38] Dixon, D. A., Lindner, D. L., Branchaud, B., and Lipscomb, W. N. (1979) Conformations and electronic structures of oxidized and reduced isoalloxazine, Biochemistry 18, 5770-5775.

[39] Kao, Y. T., Saxena, C., He, T. F., Guo, L., Wang, L., Sancar, A., and Zhong, D. (2008) Ultrafast dynamics of flavins in five redox states, J Am Chem Soc 130, 13132-13139.

[40] Todone, F., Vanoni, M. A., Mozzarelli, A., Bolognesi, M., Coda, A., Curti, B., and Mattevi, A. (1997) Active site plasticity in D-amino acid oxidase: a crystallographic analysis, Biochemistry 36, 5853-5860.

[41] Mattevi, A., Vanoni, M. A., Todone, F., Rizzi, M., Teplyakov, A., Coda, A., Bolognesi, M., and Curti, B. (1996) Crystal structure of D-amino acid oxidase: a case of active site mirror-image convergent evolution with flavocytochrome b2, Proc Natl Acad Sci U S A 93, 7496-7501.

[42] Ball, J., Bui, Q. V., Gannavaram, S., and Gadda, G. (2015) Importance of glutamate 87 and the substrate alpha-amine for the reaction catalyzed by D-arginine dehydrogenase, Arch Biochem Biophys 568, 56-63.

[43] Pollegioni, L., Diederichs, K., Molla, G., Umhau, S., Welte, W., Ghisla, S., and Pilone, M. S. (2002) Yeast D-amino acid oxidase: structural basis of its catalytic properties, J Mol Biol 324, 535-546.

[44] Northrop, D. B. (1998) On the meaning of K-m and V/K in enzyme kinetics, J Chem Educ 75, 1153-1157.

[45] Yuan, H., Fu, G., Brooks, P. T., Weber, I., and Gadda, G. (2010) Steady-state kinetic mechanism and reductive half-reaction of D-arginine dehydrogenase from Pseudomonas aeruginosa, Biochemistry 49, 9542-9550.

[46] Meyer, E. A., Castellano, R. K., and Diederich, F. (2003) Interactions with aromatic rings in chemical and biological recognition, Angew Chem Int Ed Engl 42, 1210-1250.

[47] Komarova, N. V., Golubev, I. V., Khoronenkova, S. V., Chubar, T. A., and Tishkov, V. I. (2012) Engineering of substrate specificity of D-amino acid oxidase from the yeast Trigonopsis variabilis: directed mutagenesis of Phe258 residue, Biochemistry (Mosc) 77, 1181-1189.

[48] Pudek, M. R., and Bragg, P. D. (1976) Redox potentials of the cytochromes in the respiratory chain of aerobically grown Escherichia coli, Arch Biochem Biophys 174, 546-552.

[49] Yuan, H., Xin, Y., Hamelberg, D., and Gadda, G. (2011) Insights on the mechanism of amine oxidation catalyzed by D-arginine dehydrogenase through pH and kinetic isotope effects, J Am Chem Soc 133, 18957-18965.

[50] Gadda, G., and Fitzpatrick, P. F. (2000) Iso-mechanism of nitroalkane oxidase: 1. Inhibition studies and activation by imidazole, Biochemistry 39, 1400-1405.

[51] Rouviere, N., Mayer, M., Tegoni, M., Capeillere-Blandin, C., and Lederer, F. (1997) Molecular interpretation of inhibition by excess substrate in flavocytochrome b2: a study with wild-type and Y143F mutant enzymes, Biochemistry 36, 7126-7135.

[52] Wang, Z., Chernyshev, A., Koehn, E. M., Manuel, T. D., Lesley, S. A., and Kohen, A. (2009) Oxidase activity of a flavin-dependent thymidylate synthase, FEBS J 276, 2801-2810.

[53] Itoh, K., Asakawa, T., Hoshino, K., Adachi, M., Fukiya, K., Watanabe, N., and Tanaka, Y. (2009) Functional analysis of aldehyde oxidase using expressed chimeric enzyme between monkey and rat, Biol Pharm Bull 32, 31-35.

[54] Igarashi, K., Momohara, I., Nishino, T., and Samejima, M. (2002) Kinetics of inter-domain electron transfer in flavocytochrome cellobiose dehydrogenase from the white-rot fungus Phanerochaete chrysosporium, Biochem J 365, 521-526.

[55] Cook, P. F., Kenyon, G. L., and Cleland, W. W. (1981) Use of pH studies to elucidate the catalytic mechanism of rabbit muscle creatine kinase, Biochemistry 20, 1204-1210.

[56] Ralph, E. C., Anderson, M. A., Cleland, W. W., and Fitzpatrick, P. F. (2006) Mechanistic studies of the flavoenzyme tryptophan 2-monooxygenase: deuterium and 15N kinetic isotope effects on alanine oxidation by an L-amino acid oxidase, Biochemistry 45, 15844-15852.

[57] Emanuele, J. J., and Fitzpatrick, P. F. (1995) Mechanistic studies of the flavoprotein tryptophan 2-monooxygenase. 2. pH and kinetic isotope effects, Biochemistry 34, 3716-3723.

[58] Ouedraogo, D., Souffrant, M., Vasquez, S., Hamelberg, D., and Gadda, G. (2017) Importance of Loop L1 Dynamics for Substrate Capture and Catalysis in Pseudomonas aeruginosa D-Arginine Dehydrogenase, Biochemistry.

[59] Gora, A., Brezovsky, J., and Damborsky, J. (2013) Gates of enzymes, Chem Rev 113, 5871-5923.

[60] Boselli, A., Sacchi, S., Job, V., Pilone, M. S., and Pollegioni, L. (2002) Role of tyrosine 238 in the active site of Rhodotorula gracilis D-amino acid oxidase. A site-directed mutagenesis study, Eur J Biochem 269, 4762-4771.

[61] Stoisser, T., Brunsteiner, M., Wilson, D. K., and Nidetzky, B. (2016) Conformational flexibility related to enzyme activity: evidence for a dynamic active-site gatekeeper function of Tyr(215) in Aerococcus viridans lactate oxidase, Scientific reports 6, 27892.

[62] Johnson, T. A., McLeod, M. J., and Holyoak, T. (2016) Utilization of Substrate Intrinsic Binding Energy for Conformational Change and Catalytic Function in Phosphoenolpyruvate Carboxykinase, Biochemistry 55, 575-587.

[63] Sampson, N. S., and Knowles, J. R. (1992) Segmental movement: definition of the structural requirements for loop closure in catalysis by triosephosphate isomerase, Biochemistry 31, 8482-8487.

[64] Schnell, J. R., Dyson, H. J., and Wright, P. E. (2004) Structure, dynamics, and catalytic function of dihydrofolate reductase, Annu Rev Biophys Biomol Struct 33, 119-140.

[65] Newby, Z., Lee, T. T., Morse, R. J., Liu, Y., Liu, L., Venkatraman, P., Santi, D. V., Finer-Moore, J. S., and Stroud, R. M. (2006) The role of protein dynamics in thymidylate synthase catalysis: variants of conserved 2'-deoxyuridine 5'-monophosphate (dUMP)-binding Tyr-261, Biochemistry 45, 7415-7428.

3 A SINGLE POINT MUTATION IN D-ARGININE DEHYDROGENASE UNLOCKS A TRANSIENT CONFORMATIONAL STATE RESULTING IN ALTERED COFACTOR REACTIVITY

(This chapter has been published verbatim in A. Iyer, R.A.G. Reis, S. Gannavaram, M. Momin, A. M. Spring-Connell, Y. Orozco-Gonzalvez, J. Agniswamy, D. Hamelberg, I.T. Weber, S. Gozem, S. Wang, M.W. Germann, and G. Gadda (2021), Biochemistry, 60, 9, 711–724; The author contributed to study design, protein expression, purification, crystallization, and data collection and refinement, 6-OH-FAD characterization, and mechanism, writing of the manuscript and editing)

3.1 ABSTRACT

Proteins are inherently dynamic, and proper enzyme function relies on conformational flexibility. In this study, we demonstrated how an active site residue changes an enzyme's reactivity by modulating fluctuations between conformational states. Replacement of tyrosine 249 (Y249) with phenylalanine in the active site of the flavin-dependent D-arginine dehydrogenase yielded an enzyme with both an active yellow FAD (Y249F-y) and an inactive chemically modified green FAD, identified as 6-OH-FAD (Y249F-g) through various spectroscopic techniques. Structural investigation of Y249F-g and Y249F-y variants by comparison to the wild-type enzyme showed no differences in the overall protein structure and fold. A closer observation of the active site of the Y249F-y enzyme revealed an alternative conformation for some active site residues and the flavin cofactor. Molecular dynamics simulations probed the alternate conformations observed in the Y249F-y enzyme structure and showed that the enzyme variant with FAD samples a metastable conformational state, not available to the wild-type enzyme.

Hybrid quantum/molecular mechanical calculations identified differences in flavin electronics between the wild-type and the alternate conformation of the Y249F-y enzyme. The computational studies further indicated that the alternate conformation in the Y249F-y enzyme is responsible for higher spin density at the C6 atom of flavin, which is consistent with the formation of 6-OH-FAD in the variant enzyme. The observations in this study are consistent with an alternate conformational space that results in fine-tuning the microenvironment around a versatile cofactor playing a critical role in enzyme function.

3.2 INTRODUCTION

Enzymes catalyze chemical reactions in biological processes.[1] Understanding how enzymes perform otherwise inaccessible reactions under physiological conditions has been of interest for both fundamental and applied purposes. The majority of biochemical and structural studies have focused on the electrostatic contribution to enzyme catalysis.[2] While the inherent flexibility observed in enzymes is widely accepted to play a role in substrate capture and product release, the contribution of dynamic processes to enzyme catalysis is still not entirely accepted and well understood.[3, 4] All proteins are inherently dynamic and exist in solution as ensembles of conformations.[5-7] Protein motions span a wide range of timescales, from ultrafast atom vibrations occurring in sub-picosecond timescales and fast side-chain motions occurring in sub-nanosecond timescales to slow domain movements ranging from microseconds to seconds.[5, 8, 9] Conformational changes in enzymes facilitate many events like substrate capture, stabilization of transition states, and product release, which are essential for enzyme function.[10] The role of dynamics in catalysis has been investigated in many enzymes.[11, 12] Different stages of catalysis, such as the binding of substrate and cis/trans isomerization, often require conformational changes in enzymes.[5, 13, 14]

Protein conformations can be pooled into conformational "substates" based on structural and energetic similarities.[15-17] Methods like NMR relaxation dispersion have previously demonstrated the existence of such transient and sparsely populated conformational substates.[6, 11, 18, 19] Early studies on myoglobin by Frauenfelder *et al.* in 1982 revealed multiple conformational substates that are coupled to function.[12, 13, 17, 20-22] The population and sampling of protein conformational substates can be modulated by site-specific mutations, as demonstrated in bacterial phosphotriesterase, *Escherichia coli* dihydrofolate reductase (*Ec*DHFR), and cyclophilin A/proline isomerase.[11, 23-25] Studies on *Ec*DHFR variants established that while the wild-type and mutant enzymes are similar in structure, they vary significantly in their ability to access specific conformational substates.[11]

D-Arginine dehydrogenase (EC 1.4.99.6; UniProtKB Q9HXE3; *Pa*DADH) from *Pseudomonas aeruginosa* PAO1 is an FAD-dependent enzyme that oxidizes D-arginine to 2-imino-arginine.[26] The enzyme is part of a two-enzyme system with L-arginine dehydrogenase for the irreversible conversion of D-arginine to L-arginine. [27] In nutrient-limiting conditions, the two-enzyme system enables *P. aeruginosa* to utilize D-arginine as the sole carbon and nitrogen source.[27] The physiological substrate that oxidizes the enzyme-bound flavin in *Pa*DADH is unknown, but the enzyme is unreactive with molecular oxygen.[26] *In vitro* kinetic studies have used phenazine methosulfate (PMS) as an electron acceptor. *Pa*DADH has a broad substrate specificity with D-amino acids, with D-arginine being the best substrate, as shown by a k_{cat}/K_m value of 10^6 $M^{-1}s^{-1}$.[26] A direct hydride ion transfer from the α-carbon atom of the deprotonated substrate to the enzyme-bound flavin oxidizes the substrate,[28] with a mechanism that is common to other flavin-dependent enzymes that oxidize amino acids, such as L-amino acid oxidase, D-amino acid oxidase, and monomeric sarcosine oxidase among others. [29] The atomic resolution crystal structures of

*Pa*DADH showed two conformations of the active site loop L1,[26] with the side-chain of Y53 forming hydrogen bonds with either T137 in the ligand-free conformation or the product's carboxylate in the product-bound enzyme, demonstrating conformational flexibility of enzyme.[26] In the product-bound enzyme, the side-chain of Y249 forms a hydrogen bond with the product's carboxylate.[26] Interestingly, upon replacing either Y53 or Y249 with phenylalanine, substrate binding is minimally affected, but flavin reduction becomes reversible, suggesting modulation of flavin reactivity by the tyrosine residues.[28] Replacement of Y249 with phenylalanine also yielded two enzyme populations, with an active enzyme variant containing yellow FAD (Y249F-y), which was characterized in a previous study, and an inactive enzyme variant harboring a green modified flavin cofactor (Y249F-g).[28]

This study has carried out a biochemical, structural, and computational characterization of the yellow and green Y249F variant enzymes of *Pa*DADH. Our results show that a modified flavin cofactor, 6-OH-FAD, is responsible for the green-colored enzyme variant and establish that the side-chain hydroxyl of Y249 plays a vital role in the wild-type enzyme preventing the formation of the 6-OH-FAD. Indeed, removing the Y249 hydroxyl changed the protein conformational landscape, altering the flavin electronic structure, thus modifying its reactivity.

3.3 EXPERIMENTAL PROCEDURES

3.3.1 Materials.

D-arginine, phenazine methosulfate, and PEG (3350, 5000, 6000) were purchased from Sigma-Aldrich (St. Louis, MO). D-Alanine was obtained from Alfa Aesar (Wardhill, MA). Synthesized 6-OH-FAD was a kind gift of Dr. Bruce A. Palfey at the University of Michigan, Ann Arbor, MI. All other reagents used were obtained in their highest purity commercially available.

3.3.2 Enzyme Preparation.

The Y249F enzyme was prepared by site-directed mutagenesis using the cloned wild-type gene pET20b(+)/PA3863 as a template, as described in previous work.[28] Expression and purification of the Y249F enzyme were described previously.[28] The purified Y249F-g and Y249F-y enzymes were stored in 20 mM Tris-HCl, pH 8.0, 10% glycerol, at a concentration of 10 mg/mL. The expression, purification, and storage of the Y249F enzyme were also carried out in the absence of glycerol to improve the quality of the spectra in the MS-ESI analysis. The enzyme concentration was quantified using the Bradford method.[30, 31] The UV-visible absorption spectrum of the Y249F-y and Y249F-g enzymes was recorded with an Agilent Technologies model HP8453 PC diode-array spectrophotometer equipped with a thermostated water bath.

3.3.3 Flavin Extraction and MS-ESI Analysis.

The flavin cofactors were extracted from the Y249F-g and Y249F-y enzymes by treatment with ice-cold 7% (v/v) TCA for 30 min on an ice-bath, followed by centrifugation at 10,000 g for 10 min to remove precipitated protein. The procedure was repeated on the supernatant to ensure the complete absence of protein. The extracted flavins were purified with an SCL-10A VP SHIMADZU HPLC equipped with diode array detection. The stationary phase was a µBondapak C_{18}-column (15 cm x 4.6 mm), the mobile phase was H_2O + 0.01% TFA as solvent A, and 5% acetonitrile + 0.01% TFA as solvent B. The flavin cofactors were loaded onto the column at 5% solvent B and eluted with a linear gradient from 5% to 100% of solvent B developed in 60 min at a flow rate of 0.5 mL/min. FAD eluted at 21 min and 6-OH-FAD at 24 min. The flavin cofactors extracted from the Y249F-y and Y249F-g enzymes were analyzed using mass spectrometry (MS) in the negative electrospray ionization (ESI) mode at the Mass Spectrometry Laboratory of Georgia State University. Accurate mass analysis was carried out using a Thermo Fisher Orbitrap

Elite mass spectrometer equipped with an ESI source in negative ion mode. The samples were analyzed with an LC-MS profile without using a column and isocratic elution with 20% acetonitrile and 0.1% formic acid at a flow rate of 8 µL/min.

3.3.4 6-OH-FAD pK_a Determination.

After extraction and purification by HPLC, the 6-OH-FAD was vacuum concentrated for ~14 h and dissolved in 20 mM sodium phosphate, 20 mM sodium pyrophosphate, pH 6.0. The concentration of 6-OH-FAD was calculated using ε_{422} = 19.6 $mM^{-1}cm^{-1}$.[32] The UV-visible absorption spectra of the 6-OH-FAD solution were recorded after serial additions of 1 M NaOH (1-10 µL) while the mixture was being stirred until the pH was incrementally changed. After each careful and slow addition of the base, the solution could equilibrate until no changes in the pH value or absorbance were observed, which typically required 2-3 min. The pH dependence of the absorbance at 585 nm was fit to Eq 1, where C_L and C_H are the pH-independent limiting values for the absorbance at 585 nm at low and high pH, respectively.

$$Abs_{585\,nm} = \frac{C_L + C_H}{1 + 10^{pKa - pH}}$$

Equation 3.1

3.3.5 Lack of Reduction of the Y249F-g Enzyme with D-Arginine

A sample containing a mixture of the Y249F-y and Y249F-g enzymes (Y249F-yg) was prepared by gel filtration through a PD-10 desalting column (General Electric, Fairfield, CT) in 20 mM Tris-HCl, pH 8.7, and 25 oC. The Y249F-yg enzyme was incubated with 1.0 mM D-arginine in 50 mM Tris-HCl, pH 8.7 and 25 oC, and the UV-visible absorption spectrum was recorded before and after incubation with the amino acid substrate to establish whether the latter could reduce the Y249F-g enzyme. The Y249F-y enzyme present in the sample was used as an internal control since it was immediately reduced with the addition of D-arginine.

3.3.6 NMR Analysis.

NMR experiments were conducted on a Bruker Avance 600 MHz spectrometer equipped with a 5 mm QXI ^{1}H (^{31}P, ^{13}C, ^{15}N) probe (Bruker, Billerica, MA). 1D ^{1}H spectra were collected using the watergate W5 pulse sequence for water suppression.[33] Heteronuclear ^{1}H-^{13}C HSQC spectra were processed with a shifted squared sine bell multiplication in both dimensions (SSB=2). A 100 ms mixing time was used for TOCSY spectra. Samples were prepared in 10 mM sodium phosphate, pH 7.0, and referenced to 4,4-dimethyl-4-silapentane-1-sulfonic acid (DSS) at 25 °C. Sample concentrations of HPLC-purified flavins ranged from 15 to 30 μM for 6-OH-FAD and ~100 μM for FAD; commercial FAD and synthesized 6-OH-FAD sample concentrations were 300 μM.

3.3.7 Conversion of FAD to 6-OH-FAD in the Y249F-y Enzyme.

The Y249F-y enzyme was incubated with 15 mM D-alanine in 20 mM Tris-HCl at pH 8.0 and 4 ^{o}C under aerobic conditions with constant stirring for 48 h. The flavin cofactors were extracted by treating the enzyme with 50% acetonitrile, 0.1% TCA, and centrifugation at 10,000 *g* to remove precipitated protein. The centrifugation step was repeated on the supernatant until no precipitation was observed. The resulting supernatant was vacuum concentrated for ~1h. Serial additions of 1 M NaOH were made to the samples after recording the initial UV-visible absorption spectrum at pH ~2.0 to incrementally raise the pH to ~10.0 and visualize the characteristic 540-800 nm band of the 6-OH-FAD.[32]

3.3.8 ^{18}O-Incorporation into 6-OH-FAD.

A Y249F-y enzyme solution (15 μM, 1 mL) in 50 mM Tris-HCl, pH 8.0, was placed in a tonometer with a small stirring bar and a concentrated D-alanine solution in the side-arm. The tonometer was made anaerobic by a 30-cycle treatment of flushing with oxygen-free argon and

gas removal by applying vacuum. After the side-arm solution was mixed with the enzyme, the resulting concentration of D-alanine was 15.0 mM. After mixing, the enzyme solution was incubated with constant stirring at 4 ^{o}C in the presence of $^{18}O_2$ gas by connecting a pressurized cylinder with the $^{18}O_2$ mixture to the tonometer. After 48 h, the protein was denatured with 50% acetonitrile previously cooled down to -20 ^{o}C. The slurry was spun down at 10,000 *g* to remove precipitated protein, and the step was repeated on the supernatant until no precipitation was observed with centrifugation. The resulting supernatant was vacuum concentrated for ~4 h. The MS analysis for the extracted flavins was carried out on a Waters QTof micro mass spectrometer equipped with ESI source in negative ion mode through a direct infusion at 5 μL/min flow rate. The ESI tuning settings were capillary voltage at 3000, sample cone voltage at 40, extraction voltage at 1, desolvation temperature at 100 ^{o}C, and source temperature at 70 ^{o}C.

3.3.9 Enzyme Crystallization.

Crystals of the Y249F-g and Y249-y enzymes were grown by the hanging-drop vapor diffusion method; 2 μL of protein solution and 2 μL of reservoir solution were mixed and equilibrated against 500 μL reservoir solution. Crystals of the Y249F-g enzyme were grown at room temperature using 50 mM Tris-HCl, pH 7.0, 10% glycerol, and 13% (w/v) PEG 3350, 6% (w/v) PEG 5000, as the well solution. Green pyramidal crystals were observed within one week and grew to a size of 0.2-0.3 mm^3 in 2 weeks. Crystals of the Y249F-y enzyme were grown at room temperature in 50 mM Tris-HCl, pH 7.0, 10% glycerol, and 13% (w/v) PEG 3350, 6% PEG 6000. Yellow crystals were observed within one week.

3.3.10 X-Ray Data Collection and Processing.

A single crystal of either the Y249F-g or Y249F-y enzyme was soaked for 2 seconds in the reservoir solution with 25% glycerol as a cryoprotectant and flash-frozen immediately in liquid nitrogen. Diffraction data were collected at 100 K on beamline 22-ID with an MX300HS detector of the Southeast Regional Collaborative Access Team (SER-CAT) at the Advanced Photon Source, Argonne National Laboratory. One hundred eighty images were collected at 1° oscillation per image with a crystal-to-detector distance of 190 mm, and exposure of 1.5 s per image. The data for Y249F-g and Y249F-y were processed using iMOSFLM and scaled with SCALA tools included in CCP4i Suite.[34, 35]

3.3.11 Structure Solution and Refinement.

The coordinates of wild-type *Pa*DADH (PDB ID: 3NYE) were used for the molecular replacement step to obtain the initial phases for both the Y249F-y and Y249F-g enzymes.[36] The tool Phaser found a unique solution in the orthorhombic space group $P2_12_12_1$ with one molecule in the asymmetric unit for both Y249F-y and Y249F-g.[37] The crystal structures were refined with Phenix_refine.[38] Manual fitting and rebuilding were performed using the molecular graphics program Coot.[39] The 6-OH-FAD cofactor (6FA) coordinates were constructed using phenix_elbow and added during the refinement of the Y249F-g enzyme structure.[40] FAD was available in the PDB library and was added during refinement for the Y249F-y enzyme. Refined atomic coordinates and experimental structure factors were deposited in the Protein Data Bank (Y249-g-PDB ID: 6PLD and Y249-y-PDB ID: 6P9D). All structural figures were made using UCSF Chimera.[41]

3.3.12 Molecular Dynamics Simulations.

Molecular Dynamics (MD) simulations were carried out using the Amber16 suite of programs and the AMBER ff14SB, a modified version of the Cornell *et al.* force field.[42, 43] Initial coordinates of the systems were taken from the wild-type enzyme structure (PDB: 3NYE) and the Y249F-y structure (PDB: 6P9D).[36] The AmberTools xleap program was used to construct the appropriate system required for each MD simulation. The parameters of the FAD cofactor was obtained from the general AMBER force field (GAFF).[44] Each system was solvated in a periodic octahedron pre-equilibrated TIP3P[45, 46] water box. The edges of the octahedron were at least 10 Å away from the protein. All crystallographic water molecules were maintained. The systems were then neutralized using Na^+ or Cl^- counterions and equilibrated to 300 K and 1 bar.

A detailed equilibration protocol can be found in Momin *et al.*[47] More specifically, the systems were energy minimized for 5,000 steps with the positions of the protein atoms held by harmonic constraints. Five rounds of energy minimization were performed, where the force constant of the positional constraints was gradually reduced from 500 to 0 kcal·mol^{-1}·Å^{-2}. The system was heated from 100 K to 300 K for 500 ps using a 1 fs time step and positional constraints on the protein atoms, and the temperature was maintained using the Langevin thermostat with a collision frequency of 1.0 ps^{-1} under the NVT ensemble. Five rounds of heating were performed, where the force constant of restraint was set to 500, 300, 100, 50, and 5 (kcal·mol^{-1}·Å^{-2}), respectively. A final equilibration step was carried out for 1 ns with a time step of 2 fs and no positional constraints under the NPT ensemble at a constant temperature of 300 K and constant pressure of 1 bar using the Monte Carlo barostat with coupling constant of 1.0 ps. All production simulations were carried out for 1.2 μs. The first 200 ns was considered to be an extension of the equilibration phase, and the last 1.0 μs was used for analysis. The particle-mesh Ewald (PME) summation[48] was used to evaluate long-range electrostatic interactions. A 9 Å cutoff was used for all short-range nonbonded

interactions. All bonds involving hydrogen atoms were constrained using the SHAKE algorithm.[49] The snapshots of the trajectories were saved every 1 ps (500 steps).

3.3.13 Molecular Dynamics Simulations with O_2 Molecules.

Additional molecular dynamics simulations of the wild-type and mutant enzymes with O_2 molecules were carried out for 1.2 μs, similar to the description above. In addition to the above, four O_2 molecules were added randomly to the solution around the protein molecule.

3.3.14 Principal Component Analysis.

Principal Component Analysis (PCA) was performed using the CPPTRAJ program[50] in AMBER 16 suite of programs on the MD simulation trajectories. The backbone atoms for all the snapshots were structurally superposed. The eigenvectors and eigenvalues were calculated from the covariance matrix characterizing the internal motions of all the heavy atoms of the active site residues. Each eigenvector represents a principal component (PC), and the associated eigenvalue describes the structural variation captured by the PC. The top two PCs (PC1 and PC2) captured the largest structural variance and were used to project back on the simulation trajectories to represent the conformational dynamics for the active sites of the wild-type and mutant.

3.3.15 Hybrid Quantum Mechanical/Molecular Mechanical (QM/MM) Calculations.

Hybrid QM/MM calculations were carried out for the wild-type and for different conformations of the Y249F-y enzymes to determine the spin densities on the atoms of the flavin isoalloxazine moiety. Specifically, the protocol used is based on the Average Solvent Electrostatic Environment - Free Energy Gradient (ASEC-FEG) approach used previously for rhodopsins,[51] which was extended here to flavoproteins. Briefly, the ASEC-FEG approach computes quantum mechanical properties of the cofactor in a superposition of several protein conformations instead

of using a single protein structure. ASEC-FEG, therefore, accounts for the effect of local protein flexibility on the quantum mechanically computed properties. The ASEC-FEG QM/MM models were constructed by dividing each enzyme into three subsystems, labeled QM, MM_1, and MM_2.

The QM subsystem, shown in Figure 3.1 with shaded atoms, was described using quantum mechanics and included all atoms of the reduced anionic lumiflavin moiety, up to the link atom (LA). The LA lies at the frontier between the QM and the MM_1 subsystems and is a hydrogen atom that caps the valency created by breaking a C_{QM}-C_{MM1} bond.[52] The position of the LA was restrained according to the Morokuma scheme, such that it remains colinear with the C_{QM}-C_{MM1} bond.[53] The MM_1 subsystem, also shown in Figure 3.1, includes some of the $FADH^-$ ribityl atoms near the LA. The MM_1 subsystem was treated using molecular mechanics with the AMBER99sb[54, 55] force field, and is optimized along with the QM subsystem during QM/MM optimization steps of the protocol. The MM_2 subsystem includes all other atoms of the $FADH^-$, the *Pa*DADH protein, and surrounding water molecules and ions, i.e., all atoms not shown in Figure 3.1. The MM_2 subsystem was treated with molecular mechanics with the AMBER99sb,[54, 55] and TIP3P[56] force fields for the protein and water molecules, respectively, and was sampled to generate the ASEC configurations.

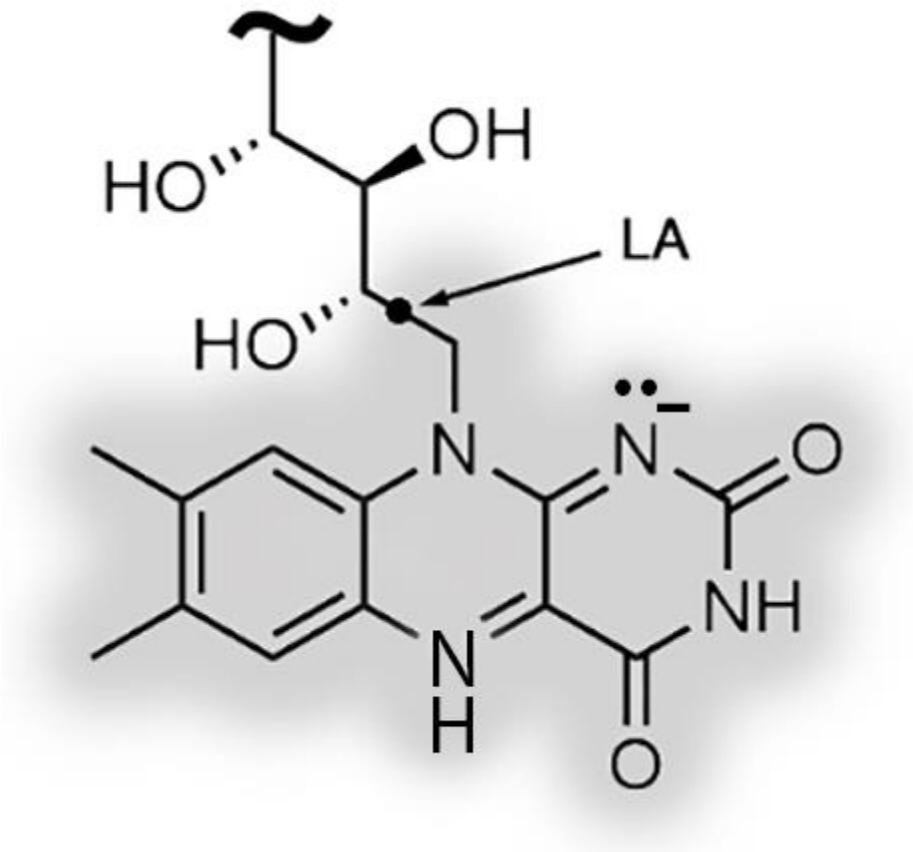

Figure 3.1. The division of $FADH^-$ into QM (shaded atoms) and MM atoms. The frontier valency is saturated by a hydrogen link atom (LA).

QM/MM calculations were performed for wild-type *Pa*DADH and for different conformational substates of the Y249F-y enzyme obtained from the 1,000 ns MD simulations discussed in the previous section using the following protocol. These proteins were re-solvated in a 10 nm cubic water box with 17 Na^+ counterions to ensure a globally neutral system.

Periodic boundary conditions were used to avoid boundary effects. Short MD simulations were then performed for the MM_2 subsystem while keeping the QM and MM_1 subsystems frozen to generate the ASEC configurations for the proteins while maintaining each system in the same sub-state sampled by the long MD simulations. Specifically, the sampling MD simulations were run for a total of 11.3 ns, just long enough to sample local side-chain rotations and flexibility within

each protein substate. Those include a 0.3 ns heating simulation, where the temperature was slowly increased from 0 K to 300 K, a 1 ns thermalization in the NPT ensemble to equilibrate the volume of the system, a 5 ns NVT equilibration run, and a 5 ns production run. The GROMACS code[57] was used for these MD simulations. The MD simulations were used to select 100 statistically uncorrelated snapshots to generate an "ASEC" configuration of the MM_2 subsystem, which is a superposition of the 100 protein configurations with scaled charges and van der Waals parameters such that the QM-MM interaction energy is computed under conditions mimicking thermodynamic equilibrium conditions.[51, 58] The QM and MM_1 subsystems were then optimized within the resulting ASEC environment. The QM/MM calculations were performed using the MOLCAS[59]/TINKER[60] QM/MM interface.[61] QM/MM geometry optimizations were performed using the CASSCF/ANO-L-VDZP[62, 63] level of theory with 14 orbitals and 18 electrons (for $FADH^-$) or 17 electrons (for FADH• or FAD^{-}•) included in the active space. The optimized geometry was used to obtain updated charge parameters for the cofactor using the RESP protocol,[64] and another MD simulation was performed to obtain a new ASEC configuration based on the QM/MM optimized geometry and charges. The iterative process described above was used to obtain a self-consistent $QM/MM_1/MM_2$(ASEC) system.

The optimized QM/MM structures with the updated ASEC configurations were then used to generate four models for the wild-type *Pa*DADH and the different conformational substates Y249F-y. The resulting four sets of data represent different sets of assumptions to accommodate all possible mechanisms and timescales of proton movements in the oxidative reaction catalyzed by the enzyme, which was not known; these were:

- **FADH• at equilibrium**. This data set considers the possibility that the reduced $FADH^-$ state is oxidized to a neutral FADH• that is long-lived enough for the QM/MM environment to

equilibrate around it. In this case, the MM_2(ASEC) and QM/MM_1 optimizations and spin densities are consistently generated for FADH•.

- **FADH• not at equilibrium**. This data set considers the possibility that the reduced $FADH^-$ state is oxidized to a neutral FADH•, but that FADH• reacts instantaneously with O_2. In this case, the MM_2(ASEC) is generated for $FADH^-$ but the QM/MM_1 optimizations and spin densities are computed for FADH•, i.e., we assumed the protein environment would not have time to equilibrate before FADH• reacts.
- **$FAD•^-$ at equilibrium**. This data set considers the possibility that the reduced $FADH^-$ state is oxidized to an anionic flavosemiquinone, i.e., FAD^{-}•, that is long-lived enough for the QM/MM environment to equilibrate around it. In this case, the MM_2(ASEC) and QM/MM_1 optimizations and spin densities are consistently computed for FAD^{-}•.
- **$FAD•^-$ not at equilibrium**. This data set considers the possibility that the reduced $FADH^-$ state is oxidized to a FAD^{-}• that reacts instantaneously with O_2. In this case, the MM_2(ASEC) is generated for $FADH^-$ but the QM/MM_1 optimizations and spin densities are computed for FAD^{-}•, i.e., we assumed the protein environment would not have time to equilibrate before FAD^{-}• reacts.

The Mulliken spin densities were computed using the same CASSCF/ANO-L-VDZP/AMBER99sb level of theory used for the optimization. The spin density calculations were also repeated using unrestricted B3LYP[65]/ANO-L-VDZP calculations for comparison. UB3LYP has been successfully used to model several properties of flavin in different redox states[66, 67] while the CASSCF/AMBER QM/MM approach is widely used to perform multi-configurational electronic structure calculations of protein-bound molecules.[68] Both UB3LYP and CASSCF

calculations showed the same trends in spin densities, so only the CASSCF values are reported in the results.

3.4 RESULTS

3.4.1 UV-Visible Absorbance of the Y249F-y and Y249F-g Enzymes.

The Y249F variant of *Pa*DADH was isolated in three fractions with yellow, light green, and green colors (Figure 3.2A inset) that could be separated using a DEAE-Sepharose column. The yellow enzyme, Y249F-y, was active, contained FAD, and was previously characterized.[23] The Y249F-y enzyme showed a UV-visible absorption spectrum at pH 8.7 with maximal absorbance at 370 nm and 445 nm and no absorbance above 540 nm (Figure 3.2A).

The green enzyme, Y249F-g, showed a broad band in the 540-800 nm region and maximal absorbance at 350 nm and 429 nm (Figure 3.2A). The light green enzyme contained a mixture of yellow and green enzymes (Y249F-yg).

3.4.2 MS-ESI Analysis of 6-OH-FAD.

To establish the atomic composition of the green modified flavin in the Y249F-g enzyme, the enzyme was denatured, and the extracted flavin was subjected to mass spectrometry. An MS-ESI analysis showed an *m/z* (-) value of 800.14 amu for the extracted green modified flavin (Figure 3.2B), consistent with an extra O atom being present on FAD. A control experiment of the yellow flavin extracted from the Y249F-y enzyme yielded an *m/z* (-) value of 784.05 amu (data not shown), in agreement with the expected value of 784.55 amu for FAD. These data are consistent with the green flavin being a hydroxylated form of FAD,[69] but do not establish the site of modification on the flavin cofactor.

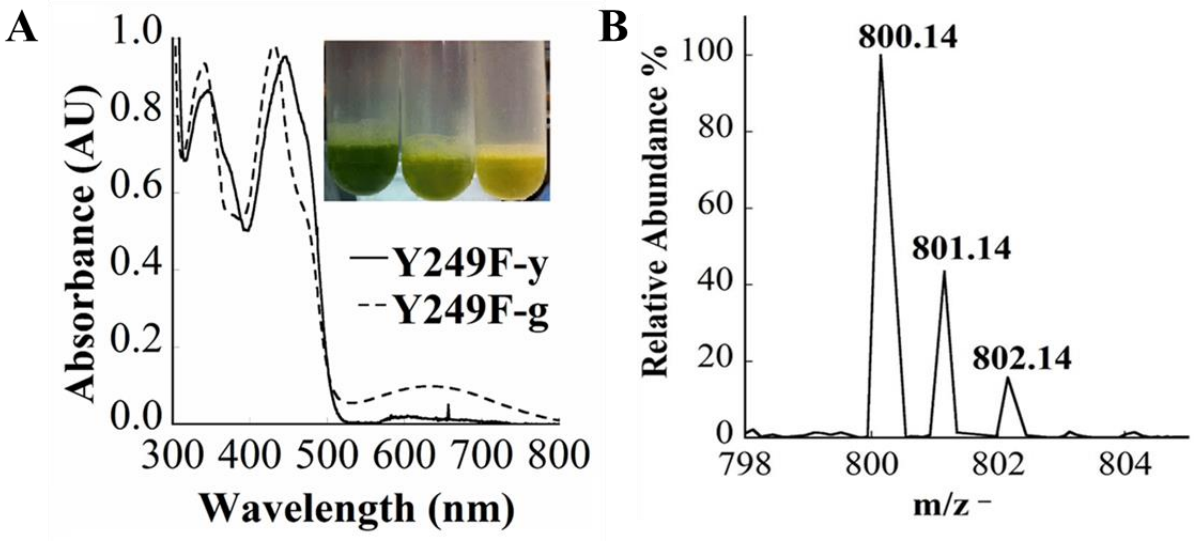

Figure 3.2. Spectroscopic characterization of the green flavin.
A) The UV-visible absorption spectra of the Y249F-y (solid curve) and Y249F-g (dashed curve) enzymes were acquired at pH 8.7. The inset shows the enriched green inactive fraction Y249F-g, a mixture of the Y249F-y and Y249F-g enzyme fractions (Y249F-yg), and the enriched Y249F-y fraction after ion-exchange chromatography. B) MS-ESI spectrum of the green flavin extracted from the Y249F-g enzyme in negative ion mode, showing an m/z (-) value at 800.14 amu and naturally abundant isotopic pattern.

3.4.3 Determination of the pK_a Value of 6-OH-FAD.

The pK_a value of the extracted green modified flavin was determined in a pH titration of the UV-visible absorption spectrum (Figure 3.3A). A plot of the absorbance at 585 nm vs. pH yielded a pK_a value of 7.1 ± 0.1 (Figure 3.3A inset), which agrees with previous data on proton-exchangeable equilibria of 6- or 9-OH-FAD in bulk solution.[32, 70, 71]

3.5 Lack of Activity of Y249F-g Enzyme.

To establish whether the 6-OH-FAD could be reduced in the active site of *Pa*DADH, the enzyme containing a mixture of both 6-OH-FAD and FAD, i.e., Y249F-yg, was incubated with 1.0 mM D-arginine at pH 8.7, and the UV-visible absorption spectrum was acquired. The variant enzyme containing both flavins was chosen because it provided an internal standard, i.e., the FAD., which was expected to be reduced in the substrate's presence. The absorbance at 445 nm of the

Y249F-yg enzyme immediately decreased upon incubation of the enzyme with the substrate (Figure 3.3B), consistent with the enzyme with FAD being active. Instead, the long-wavelength band in the 540-800 nm region of the spectrum persisted after incubation with D-arginine (Figure 3.3B), indicating that the amino acid substrate could not reduce the variant enzyme containing the green modified flavin. Thus, the enzyme with the green modified flavin was not active, in agreement with previous results in other systems showing that enzymes containing 6-hydroxylated flavins retain low to no activity with their physiological substrates.[32, 72-75]

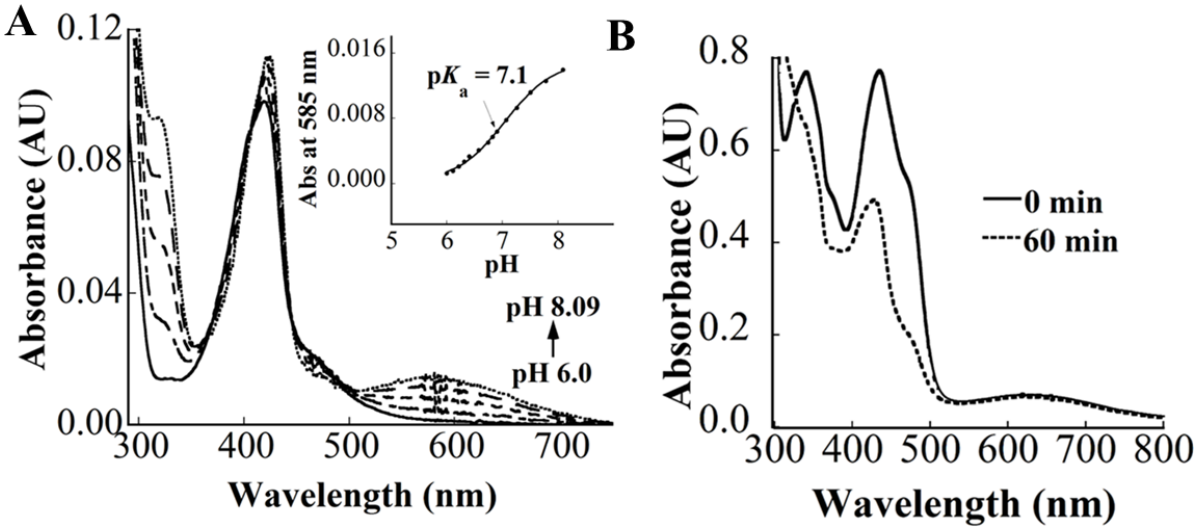

Figure 3.3. Spectroscopic characterization of the green flavin.
A) The UV-visible absorption spectra of the green flavin extracted from the Y249F-g enzyme as a function of pH, with inset showing the determined pK_a value; for clarity, only select spectra are shown between pH 6.0 and 8.1. B) Functional assessment of the Y249F-yg enzyme containing a mixture of FAD and 6-OH-FAD: oxidized enzyme before (solid curve) and after 60 min incubation with 1 mM D-arginine (dotted curve).

3.5.1 NMR Analyses of 6-OH-FAD.

The green flavin extracted from the Y249F-g enzyme was subjected to NMR analysis to establish whether the extra OH group was on the flavin C6 or C9 atom. A synthesized 6-OH-FAD standard and commercially available FAD were also analyzed for reference. Three aromatic peaks

are observed in the ^{1}H NMR spectra of the extracted green flavin sample: 7.8 ppm, 8.35 ppm, and a novel resonance at 6.75 ppm, and are identical to the synthesized 6-OH-FAD sample (Figure 3.4A). The adenosine resonances were identified via comparison to the FAD standard, leaving the resonance at 6.75 ppm corresponding to a proton on the isoalloxazine ring (Figure 3.4B). Analysis of TOCSY spectra obtained from the synthesized 6-OH-FAD and the green flavin extracted from the Y249F-g sample reveal identical coupling between the aromatic peak at 6.75 ppm and the isoalloxazine methyl proton at 2.4 ppm (Figure 3.4C& 3.D). Thus, by direct comparison with standards, the ^{1}H-NMR, TOCSY, and HSQC analyses established that the green flavin's modification was on the C6 atom and not the C9 atom.

3.5.1 Conversion of FAD to 6-OH-FAD in the Y249F-y Enzyme.

The 6-OH-FAD in *Pa*DADH could be formed through an ionic mechanism in which the flavin hydroquinone is a required intermediate, as previously proposed for trimethylamine dehydrogenase.[76] To determine whether the hydroquinone was required to convert FAD to 6-OH-FAD in the active site of *Pa*DADH, the Y249F-y enzyme was reduced aerobically with 15 mM D-alanine at pH 8.0 and 4 ºC, and the resulting UV-visible absorption spectrum was acquired. As shown in Figure 3.5A, the aerobic treatment of the enzyme with the D-alanine resulted in FAD's conversion to 6-OH-FAD. An MS-ESI analysis of the modified flavin after extraction from the enzyme confirmed the formation of the 6-OH-FAD, with an *m/z* (-) value of 800.19 amu in the mass spectrometry spectrum (Figure 3.5B). In the absence of D-alanine, there were no changes in the absorption maxima of the enzyme-bound FAD at 377 nm and 449 nm (Figure 3.5A). Thus, the flavin hydroquinone produced in the substrate-driven reduction of the flavin with D-alanine could be a possible intermediate that allows for the *in vitro* formation of 6-OH-FAD from FAD in the active site of the Y249F-y enzyme.

The aerobic incubation of the Y249F-y enzyme with 15 mM D-alanine was repeated in an atmosphere enriched with $^{18}O_2$ gas to establish whether the O atom incorporated in the 6-OH-FAD originated from molecular O_2. In the MS-ESI spectrum of the extracted flavin reduced with D-alanine in the presence of $^{18}O_2$ gas, the relative intensity of the peak with an *m/z* (-) value of 802.16 amu increased as compared to that treated with atmospheric O_2 gas, consistent with the incorporation of an ^{18}O atom in the newly formed 6-OH-FAD. Thus, the O atom of the 6-OH-FAD originated from molecular O_2.

3.5.1 Proposed Mechanism for the Formation of 6-OH-FAD.

Based on the requirement of a flavin hydroquinone and the observation that the O atom incorporated in the 6-OH-FAD originated from O_2, a mechanism for the formation of 6-OH-FAD could be proposed (Figure 3.5C). Briefly, the enzyme-bound FAD is initially reduced by D-alanine before reacting with O_2 via a single-electron transfer generating a neutral flavosemiquinone and superoxide anion; the two radical species collapse with the formation of a C6-peroxo-FAD, which after elimination of water yields 6-OH-FAD. If one assumes rapid equilibration of protons, an anionic flavosemiquinone could also be considered before forming the 6-peroxo-FAD, as illustrated by the species in brackets in Figure 3.5C. Irrespective of the ionization state of the flavosemiquinone, the proposed mechanism suggests there is an increased tendency for O_2 to react at the C6 carbon of the flavin in the Y249F mutant relative to the wild-type system, where such a reaction does not occur. One possibility is an enhanced reactivity at the C6 carbon of flavin in Y249F, while another possibility is easier O_2 access to the active site. We tested both hypotheses using MD and QM/MM calculations (*see below*).

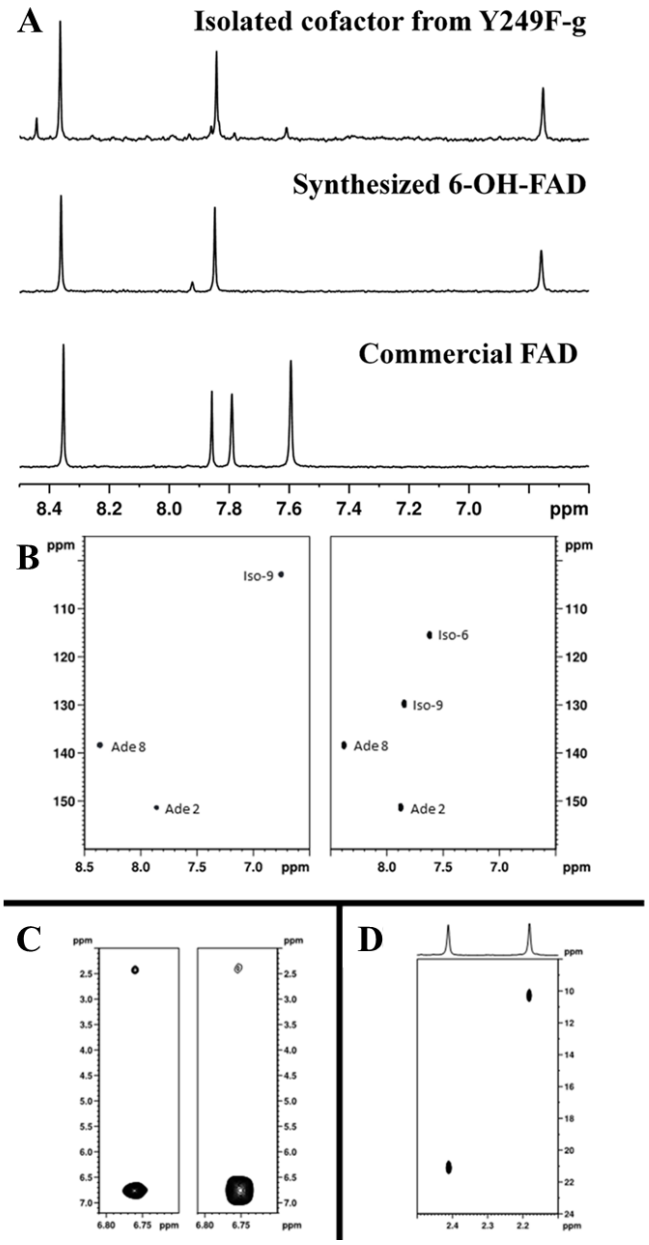

Figure 3.4. ^{1}H-NMR and HSQC spectra of the modified flavin.

A) Comparison of ^{1}H-NMR spectra of the green flavin isolated from the Y249F-g enzyme (top), synthesized 6-OH-FAD (middle), and FAD (bottom). ^{1}H-NMR spectra of the extracted flavin and a chemically synthesized 6-OH-FAD yielded identical chemical shifts, confirming the modification was at the C6 position of the isoalloxazine moiety of FAD. B) HSQC spectra of aromatic regions of synthesized 6-OH-FAD (left) and FAD (right). C) slices from TOCSY spectra showing coupling between position 9 of the isoalloxazine ring and the adjacent methyl protons (left synthesized, right HPLC purified). D) HSQC spectrum of 6-OH-FAD methyl protons. The separation between methyl protons is 0.24 ppm.

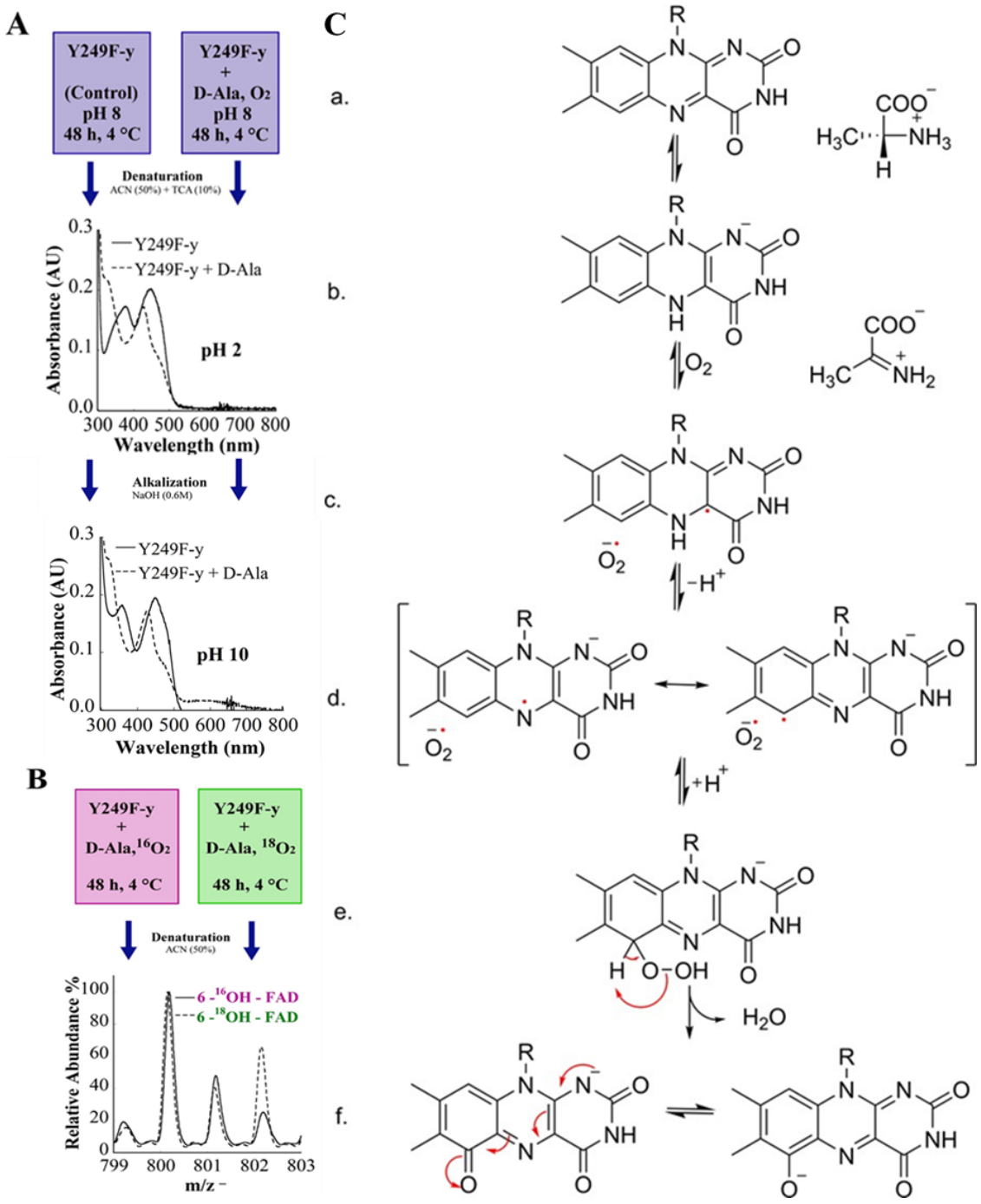

Figure 3.5. Conversion of FAD to 6-OH-FAD in the Y249F-y enzyme.
A) The Y249F-y enzyme was incubated for 48 h in the presence or absence of 15 mM D-alanine at pH 8.0 and 4 ºC (top); UV-visible absorption spectra of the isolated cofactors after the treatment of the enzymes with acidified 50% acetonitrile and centrifugation to remove denatured protein at pH 2.0 (middle) and alkalization with 0.6 M NaOH (bottom). B) MS-ESI spectra of the extracted cofactors after aerobic incubation of the Y249F-y enzyme with 15 mM D-alanine in natural and $^{18}O_2$ gas-enriched atmospheres after extraction with 50% acetonitrile. C) Proposed mechanism for hydroxylation of FAD in the active site of the Y249F-y enzyme. The description is in the text.

3.5.2 X-Ray Crystal Structures of the Y249F-g and Y249F-y Enzymes.

The high-resolution X-ray crystal structures of the Y249F enzymes with either 6-OH-FAD or FAD were independently solved in space group $P2_12_12_1$. The space group was the same as that previously seen for the structure of wild-type *Pa*DADH.[36] The structure of the Y249F-g enzyme with 6-OH-FAD (PDB: 6PLD) was refined to an *R* factor of 0.16 and a resolution of 1.55 Å and that of the yellow Y249F-y enzyme with FAD (PDB: 6P9D) to an *R* factor of 0.13 and a resolution of 1.33 Å. The crystallographic and refinement statistics are presented in Table 3.1.

Superposition of the backbone atoms of either the Y249F-g or the Y249F-y enzyme with the structure of the wild-type enzyme previously determined (PDB: 3NYE) yielded RMSD values ≤0.38 Å over 375 polypeptide backbone atoms (Figure 3.6). The structure of the Y249F-g enzyme lacked electron density on the C4 atom of F249, as expected due to the mutation of Y249 to phenylalanine. Additional electron density was present on the flavin C6 atom (Figure 3.), consistent with 6-OH-FAD in the Y249F-g enzyme. In contrast, the structure of the Y249F-y enzyme lacked electron density on both the C4 atom of F249 and the flavin C6 atom, consistent with the mutation of Y249 to phenylalanine and the presence of unmodified FAD.

The Y249F-g and wild-type enzymes shared identical conformations of all the active site residues and flavin (Figure 3.7B). In the Y249F-y enzyme, instead, the conformations of both the guanidino group of R222 and R305 could only be modeled between 60 and 80% occupancy (Figure 3.7C-D). This enzyme conformation was labeled conformation-A. The guanidino group of R222 was also present in an alternative conformation that could be modeled for 40% occupancy (Figure 3.7C-D), which was labeled conformation-B. Although residual electron density for the side chain of R305 was observed at lower sigma levels, a unique alternative conformation of the guanidino

group of R305 could not be modeled with confidence. Residual electron density for the FAD was also observed in the Y249F-y enzyme, but again a unique alternative conformation could not be modeled with confidence (Figure 3.7C). Thus, the FAD and the side chains of R222 and R305 in the Y249F-y enzyme appeared to be mobile. A similar case of FAD being in multiple conformations was previously observed in the crystal structure of an enzyme variant of *p*-hydroxybenzoate hydroxylase, in which Y222 was replaced with phenylalanine.[77]

3.5.1 MD Simulations.

To probe whether replacement of Y249 with phenylalanine was responsible for the unique conformational substate seen in the X-ray structure of the Y249F-y enzyme, i.e., conformation-B, MD simulations were carried out on the wild-type and the two conformations of the Y249F-y enzyme. Unrestrained MD simulations were carried out for 1.2 μs to generate an ensemble of accessible conformations of the Y249F-y and wild-type enzymes.[78] Principal component analysis (PCA) showed that the Y249F-y and wild-type enzymes share most of the conformational landscape, i.e., conformation-A (Figure 3.8). The Y249F-y enzyme had an extra conformational substate in the PCA involving the guanidino groups of R222 and R305 and the FAD that was not available to the wild-type enzyme (Figures 3.8 & 3.9). Thus, the replacement of Y249 with phenylalanine permits a conformational substate in the mutant enzyme that is impeded in the wild-type enzyme, i.e., conformation-B is available to the Y249F enzyme but not the wild-type *Pa*DADH.

3.5.2 O_2 localization in the active site.

To establish whether the effect of the single point mutation unlocking a transient conformational state in the protein was due to altered localization of O_2 to the flavin C6 atom, additional MD simulations with O_2 molecules were carried out. O_2 molecules were able to freely

access the active site of the wild-type and mutant enzymes. There was no significant difference in the localization of O_2 around the flavin C6 atom in the Y249F-y and wild-type enzymes. The replacement of Y249 with phenylalanine yielded minimal, if any, steric control of the formation of 6-OH-FAD in the active site of *Pa*DADH, suggesting that the modification was due to the change in the electronic configuration of the flavin.

3.5.3 Hybrid QM/MM Electron Spin Density Flavin Computations.

To determine whether the transient conformational substate unlocked in the Y249F-y enzyme by the single point mutation yielded an altered chemical reactivity of the flavin, hybrid QM/MM calculations were used to model the electron spin density of the flavin in conformation-A and conformation-B of the Y249F-y enzyme and the wild-type enzyme. As described in the QM/MM methodology section, multiple models were considered to allow for both the neutral flavosemiquinones, anionic flavosemiquinones, and the protein equilibrated before and after electron transfer. The latter requirements allowed for either rapid formation of 6-peroxo-FAD after superoxide formation or slow enough reactivity to allow protein equilibration, since this was not experimentally established and was beyond the scope of the present study. As shown in Table 3.2, the QM/MM analysis showed that the flavin C6 atom in the Y249F-y enzyme's conformation-B had a higher spin density than in conformation-A, irrespective of protein equilibration or the flavosemiquinone ionization's state. The same result was obtained for UB3LYP spin-density calculations. Thus, the replacement of Y249 with phenylalanine is associated with a change in protein dynamics, unlocking a conformational substate with an altered FAD reactivity, which likely results in the formation of 6-OH-FAD in the active site of *Pa*DADH.

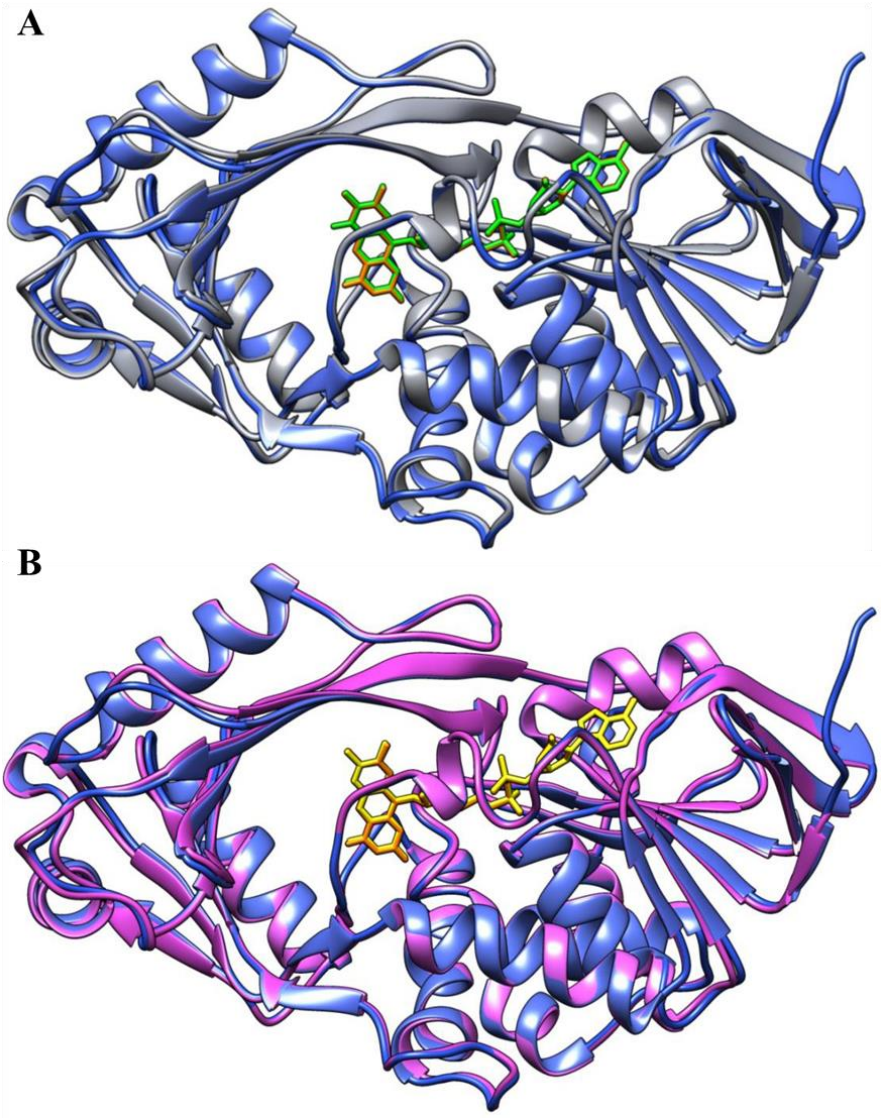

Figure 3.6. The overall structure of the Y249F-g and Y249F-y enzymes.
A) Overlay of the Y249F-g (gray) and wild-type (purple) structures, showing similar overall folds, with RMSD values of 0.36 Å over 375 polypeptide backbone atoms. B) Overlay of the Y249F-y (pink) and wild-type (purple) structures, showing similar overall folds, with RMSD values of 0.38 Å over 375 polypeptide backbone atoms.

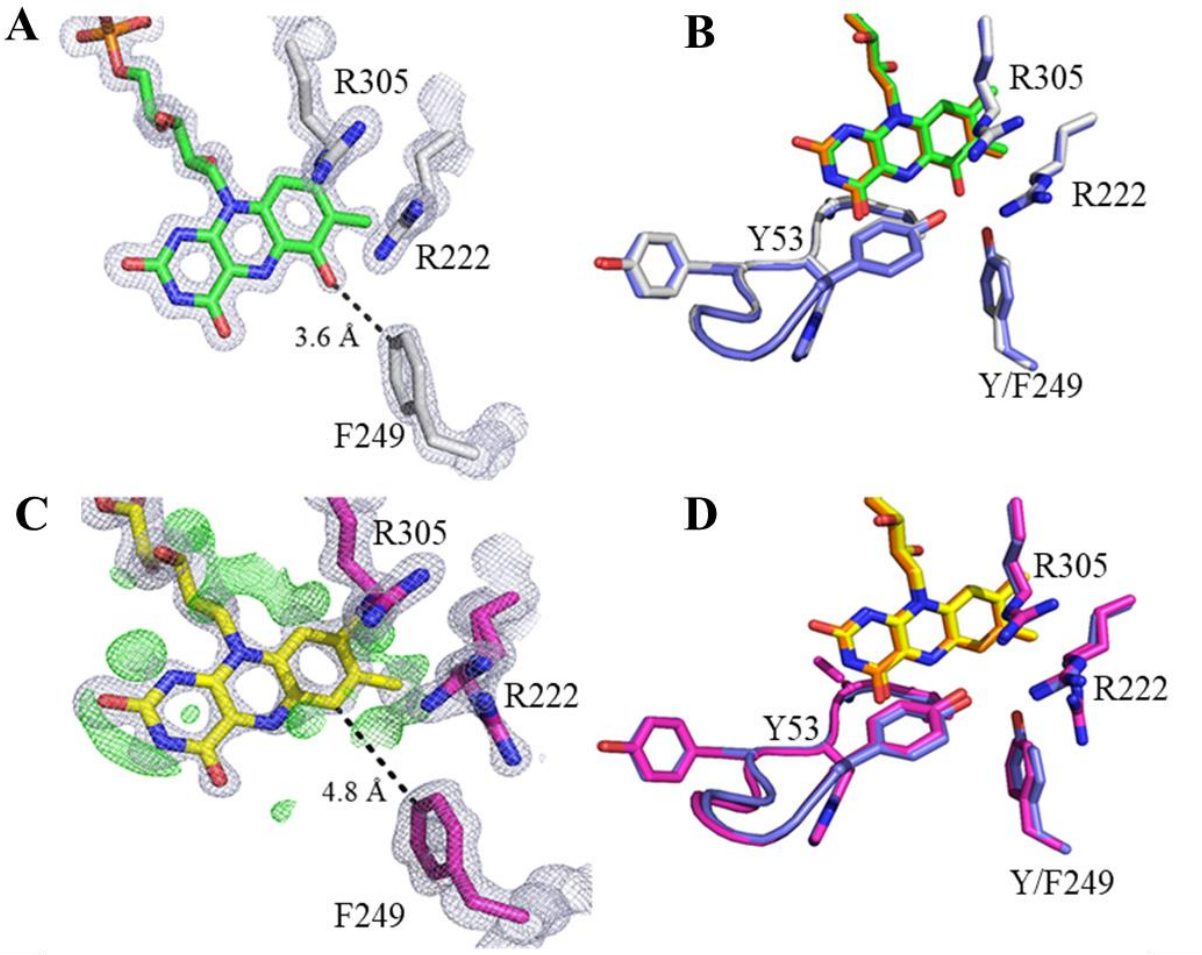

Figure 3.7. The active sites of the Y249F-y and Y249F-g enzymes.

A) Electron density map (2Fo-Fc contoured at 2σ) of the Y249F-g enzyme, showing 6-OH-FAD. B) Active site overlay of the Y249F-g (gray) and wild-type *Pa*DADH (purple), demonstrating no changes in the active site. C) Electron density map (2Fo-Fc contoured at 1.3σ, in gray, and Fo-Fc contoured at 3.0σ, in green) of the flavin and electron density map (2Fo-Fc contoured at 1.3σ, in gray) of R305, R222, and F249 in the active site of the Y249F-y enzyme. D) Active site overlay of the Y249F-y (pink) and wild-type *Pa*DADH (purple) demonstrating two major conformations for the side chain of R222.

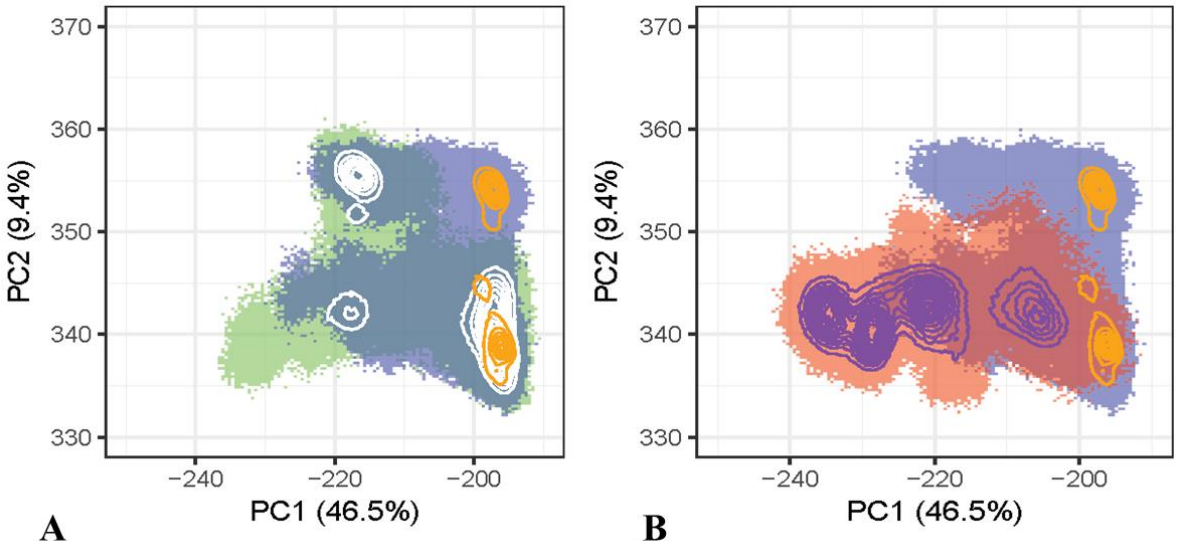

Figure 3.8. Conformational flexibility of active site in the Y249F-y variant.
A). Principal component analysis as a scatter plot for wild-type *Pa*DADH (purple), Y249F-y conformation-A (green), demonstrating significant overlap between the wild-type *Pa*DADH and Y249F-y conformation-A. The concentric circles in orange indicate the highest density areas for the wild-type and in white for Y249F-y conformation-A. B) Principal component analysis as a scatter plot for wild-type *Pa*DADH (purple) and Y249F-y conformation-B (red) demonstrating overlap between the Y249F-y conformation-B to a lower degree, compared to the Y249F-y conformation-A and a novel conformational state in the conformation-B. The concentric circles in orange indicate the highest density areas for the wild-type and purple for Y249F-y conformation-B.

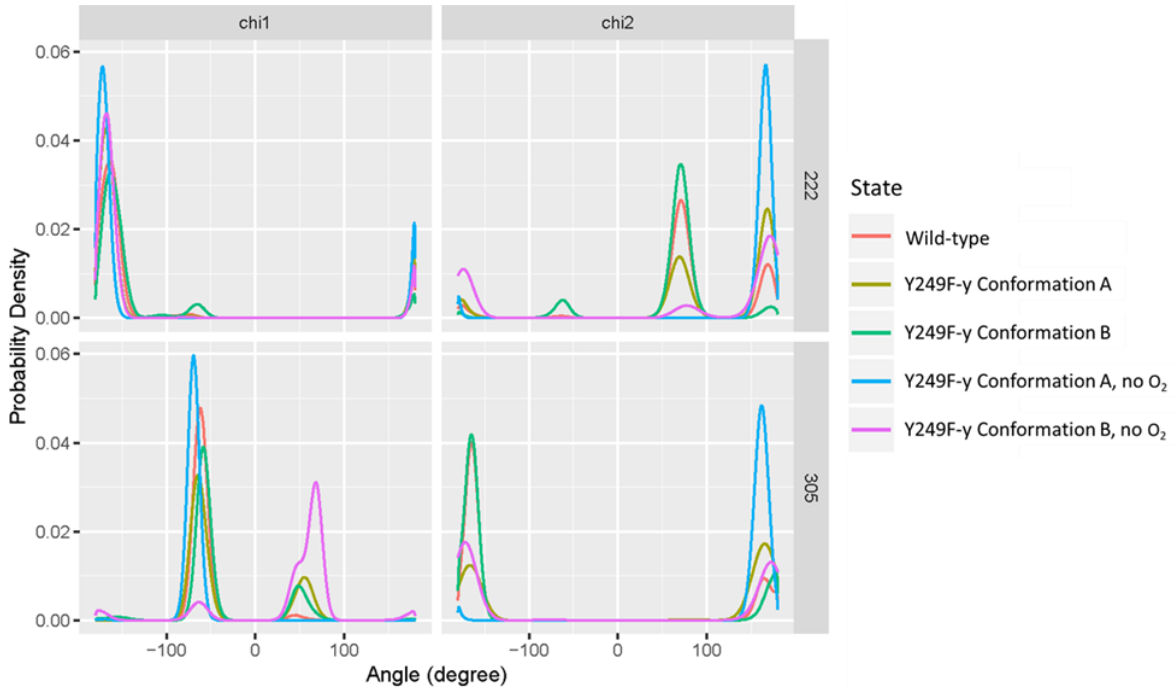

Figure 3.9. Side-chain flexibility for R222 and R305.
Probability distribution plot for the side-chain dihedral angles for arginine 222 and 305. The plot demonstrates the frequency of dihedral angle space accessed at chi1 and chi2 of R222 and R305 for WT PaDADH, conformations A and B of Y249F-y, in the presence and absence of O_2.

3.6 DISCUSSION

The biochemical, structural, and computational investigation presented here demonstrates that Y249 in *Pa*DADH exerts a tight control on the reactivity of flavin by limiting the ensemble of conformational substates that could be otherwise sampled by the protein in the absence of the Y249 hydroxyl group. The X-ray structures of the mutant enzyme before and after the formation of 6-OH-FAD, i.e., the Y249F-y enzyme in conformation-A and the Y249F-g enzyme, are identical to the wild-type enzyme. The crystal structure does, however, suggest an alternative conformation for some flexible residues but does not entirely explain what features may alter the reactivity of the flavin. However, MD simulations demonstrate that, upon removing the Y249 hydroxyl by mutation to phenylalanine, the protein samples a new conformational landscape not available to the wild-type enzyme, i.e., Y249F-y conformation-B. MD simulations also indicate no difference in O_2 localization in the mutant and wild-type enzymes, while hybrid QM/MM spin density

calculations indicate that conformation-B has altered flavosemiquinone reactivity. This suggests that Y249F-g is formed only in the transient conformation-B substate of Y249F, which is not observed in the wild-type protein.

Proteins are dynamic and sample a wide range of conformations to stabilize transition states, control substrate access to and product release from the active site, and provide proper electrostatic interactions for catalysis and substrate binding.[79] Any perturbation to the existing ensemble of conformations can severely impact enzyme activity, as demonstrated in *Pa*DADH, where a point mutation removing an O atom from the side-chain of an active site residue modifies protein dynamical pathways and leads to altered cofactor reactivity. This conclusion further expands conclusions from previous studies on *Ec*DHFR showing that mutations affect the enzyme's ability to sample specific conformations associated with the hydride transfer reaction catalyzed by the enzyme.[11, 79] The results presented in the current study suggest that the dynamics of enzymes orchestrate their function due to the highly optimized interactions and coupled motions between the different residues that can be altered with the slightest change in the amino acid sequence.

Apart from the side-chain conformations and protein motions, flavin dynamics also have an essential role in substrate binding and catalysis.[77] The ribityl moiety and the isoalloxazine ring are the most mobile portions of flavins and can be stabilized by hydrogen bonding interactions.[80] *p*-Hydroxybenzoate hydroxylase was one of the first enzymes for which structural evidence for a mobile flavin existing in two conformations, namely "in' and "out," was established in a Y222 to phenylalanine enzyme variant.[81] In contrast to the wild-type enzyme, the flavin in *p*-hydroxybenzoate hydroxylase prefers the "out" conformation, with the isoalloxazine ring away from the substrate-binding site in the Y222F enzyme, with R220 providing a significant stabilizing interaction to maintain the "out" conformation.[77] Interestingly, in both *Pa*DADH and *p*-

hydroxybenzoate hydroxylase protein dynamics is altered when an active site tyrosine is replaced with phenylalanine, although a rationale is not immediately clear. Perhaps Nature has exploited the ability of the tyrosine's hydroxyl side chain to act concomitantly as both hydrogen bond donor and acceptor to firmly limit the ensemble of conformational substates potentially available to the protein. More recently, studies on enzymes like N-hydroxylases/monooxygenase, tetracycline resistance enzymes amongst other flavin monooxygenases have focused on elucidating the role of cofactor dynamics and how it can be coupled to substrate binding and catalysis.[82-85]

Cofactor versatility and the fine-tuning of the cofactor reactivity are other aspects that dictate enzyme activity.[86] The effect of the protein microenvironment on the flavin cofactor is evident in the Y249F-y variant conformation B, where a higher spin density on the C6 position of the flavosemiquinone species was observed. Another flavin-dependent enzyme where the microenvironment's effect can be demonstrated on the flavin cofactor is trimethylamine dehydrogenase (TMADH). A substrate-assisted mechanism proposed for the formation of 6-OH-FAD in Y249F-y was also proposed for the C30 to alanine variant of TMADH.[76] The FMN cofactor in wild-type TMADH is covalently attached to the protein through a 6-S-cysteinyl bond, and on mutating the cysteine responsible for covalent attachment, the FMN undergoes a substrate-assisted reduction and reacts with molecular oxygen to form 6-hydroxy-FMN.[76, 87] Interestingly, the wild-type and a W335 to leucine variant were isolated with differing quantities of 6-hydroxy-FMN already present in the active site, thereby not necessarily requiring turnover with the substrate.[87, 88] A different mechanism involving a flavin imininoquinone methide intermediate mechanism was proposed for the W335L variant of TMADH.[88] The flavin cofactor in TMADH does possess an intrinsic susceptibility to 6-hydroxylation or covalent attachment through a cysteinyl bond; it is interesting to note that varying levels of 6-hydroxylation are present depending

on minor changes in the active site environment.[88] Flavins are versatile cofactors, but their potential for catalytic versatility is primarily dictated by the dynamic interactions with the substrate and the protein matrix.[89]

Engineering enzyme by mutagenesis for new applications have necessarily focused on structure-function relationships, often neglecting protein dynamics, which can have an essential role in enzyme catalysis.[11, 22, 24, 90] Studies that include cofactor dynamics, as in the case of tetracycline resistance enzymes, also showcase that inhibitors can be designed to lock the cofactor flavin in an 'inactive' conformation.[82] As our understanding of protein dynamics and the approach for their study further advance, the tools to probe conformational dynamics could be directed towards the rational design of enzymes with novel functions.[7, 91, 92] The current study and the previous computational investigation of *Ec*DHFR demonstrate in different fashions that mutations can modulate the equilibrium between functional and non-functional conformational protein ensembles.[11, 19] The next challenge is how to apply what is learned about protein dynamics, cofactor motions, and conformational space at the active site towards developing new enzyme functions.[91, 93] Studies that examine how enzymes have evolved to optimize protein and cofactor motions and organize the active site by conformational transitions will be beneficial for engineering new enzymes that catalyze novel reactions.[14, 94-96]

3.7 CONCLUSION

In conclusion, our study demonstrates how a simple hydroxyl group can act as a conformational switch. Replacement of a tyrosine with phenylalanine in the active site of *Pa*DADH changed the conformational landscape of the protein, altered the flavin electronic structure, and led to the modification of the cofactor chemical reactivity, ultimately negatively

impacting biological function by allowing the formation of an inactive modified flavin in the active site of the enzyme.

3.8 ACKNOWLEDGEMENTS

The authors thank Dr. Bruce A. Palfey for the generous donation of synthesized 6-OH-FAD. The authors also recognize Daniel Kneller and Shelley Hinkle Burnaman for their valuable input for the X-ray crystallography portion of the project. For assistance during X-ray data collection, we thank the staff at the Southeast Regional-Collaborative Access Team (SER-CAT) at the Advanced Photon Source (APS), Argonne National Laboratory (ANL). Use of the Advanced Photon Source was supported by the U. S. Department of Energy, Office of Science, Office of Basic Energy Sciences, under Contract No. W-31-109-Eng-38. Molecular graphics and analyses were performed with UCSF Chimera, developed by the Resource for Biocomputing, Visualization, and Informatics at the University of California, San Francisco, with support from NIH P41-GM103311. Y.O.G. and S. Gozem are grateful to NSF XSEDE for computational resources from research allocation CHE180027 and to the Advanced Research Computing Technology, and Innovation Core (ARCTIC) resources supported by NSF-MRI grant CNS-1920024.

Table 3.1. Data collection and refinement statistics for X-ray crystal structures.

	*Pa*DADH Y249F-g (PDB ID 6PLD)	*Pa*DADH Y249F-y (PDB ID 6P9D)
Data collection		
Space group	$P2_12_12_1$	$P2_12_12_1$
Cell dimensions		
a, *b*, *c* (Å)	59.78, 73.91, 76.98	60.10, 74.03, 77.19
α, β, γ (°)	90.00, 90.00, 90.00	90.00, 90.00, 90.00
Resolution (Å)	59.78-1.55 (1.58-1.55) *	59.74-1.34 (1.58-1.34) *
R_{merge}	0.103 (0.488)	0.020 (0.200)
$I / \sigma I$	10.6 (3.2)	17.2 (3.6)
Completeness (%)	96.1 (93.4)	99.4 (96.9)
Redundancy	7.0 (6.5)	2.0 (2.0)
Refinement		
Resolution (Å)	39.8-1.55	37.01-1.33 (1.38-1.33)
No. of reflections	53764	79364 (7694)
R_{work} / R_{free}	0.16 / 0.20	0.13 / 0.17
No. atoms	3578	3770
Protein	3079	3286
Ligand/ion	109	95
Water	390	389
B-factors	17.0	16.62
Protein	16.20	14.50
Ligand/ion	21.60	23.44
Water	28.28	32.80
R.m.s. deviations		
Bond lengths (Å)	0.006	0.006
Bond angles (°)	1.178	1.23

*Number of crystals for each structure should be noted in the footnote. *Values in parentheses are for the highest-resolution shell.

Table 3.2. QM/MM spin density calculations for flavin C6 atom.

Flavin species	WT	Conformation-A	Conformation-B
FADH•, equilibrium[a]	0.017	0.014	0.035
FADH•, non-equilibrium[b]	0.017	0.015	0.038
$FAD^{\bullet -}$, equilibrium[a]	0.107	0.128	0.136
$FAD^{\bullet -}$, non-equilibrium[b]	0.049	0.107	0.144

[a]The equilibrium models assume that the species is long-lived enough to allow equilibration of the protein environment and sampling the configuration space around the flavosemiquinone. [b]The non-equilibrium models assume that the flavosemiquinone reacts instantaneously, i.e., with the protein in a frozen state in the ASEC configuration corresponding to the fully reduced anionic system.

3.9 REFERENCES

[1] Hammes-Schiffer, S. (2013) Catalytic efficiency of enzymes: a theoretical analysis, *Biochemistry 52*, 2012-2020.

[2] Warshel, A., Sharma, P. K., Kato, M., Xiang, Y., Liu, H. B., and Olsson, M. H. M. (2006) Electrostatic basis for enzyme catalysis, *Chem Rev 106*, 3210-3235.

[3] Kamerlin, S. C. L., and Warshel, A. (2010) At the dawn of the 21st century: Is dynamics the missing link for understanding enzyme catalysis?, *Proteins 78*, 1339-1375.

[4] Okazaki, K., and Takada, S. (2008) Dynamic energy landscape view of coupled binding and protein conformational change: induced-fit versus population-shift mechanisms, *Proc. Natl. Acad. Sci. U. S. A. 105*, 11182-11187.

[5] Henzler-Wildman, K., and Kern, D. (2007) Dynamic personalities of proteins, *Nature 450*, 964-972.

[6] Kern, D. (2007) Dynamic personality of an enzyme studied by crystallography, NMR, computation and single molecule FRET, *Faseb J 21*, A90-A90.

[7] Maria-Solano, M. A., Serrano-Hervas, E., Romero-Rivera, A., Iglesias-Fernandez, J., and Osuna, S. (2018) Role of conformational dynamics in the evolution of novel enzyme function, *Chem Commun (Camb) 54*, 6622-6634.

[8] Hammes-Schiffer, S., and Benkovic, S. J. (2006) Relating protein motion to catalysis, *Annu Rev Biochem 75*, 519-541.

[9] van den Bedem, H., and Fraser, J. S. (2015) Integrative, dynamic structural biology at atomic resolution--it's about time, *Nat. Methods 12*, 307-318.

[10] Kraut, D. A., Carroll, K. S., and Herschlag, D. (2003) Challenges in enzyme mechanism and energetics, *Annu Rev Biochem 72*, 517-571.

[11] Bhabha, G., Lee, J., Ekiert, D. C., Gam, J., Wilson, I. A., Dyson, H. J., Benkovic, S. J., and Wright, P. E. (2011) A Dynamic Knockout Reveals That Conformational Fluctuations Influence the Chemical Step of Enzyme Catalysis, *Science 332*, 234-238.

[12] Iorgu, A. I., Baxter, N. J., Cliff, M. J., Levy, C., Waltho, J. P., Hay, S., and Scrutton, N. S. (2018) Nonequivalence of Second Sphere "Noncatalytic" Residues in Pentaerythritol Tetranitrate Reductase in Relation to Local Dynamics Linked to H-Transfer in Reactions with NADH and NADPH Coenzymes, *ACS Catal. 8*, 11589-11599.

[13] Eisenmesser, E. Z., Bosco, D. A., Akke, M., and Kern, D. (2002) Enzyme dynamics during catalysis, *Science 295*, 1520-1523.

[14] Eisenmesser, E. Z., Millet, O., Labeikovsky, W., Korzhnev, D. M., Wolf-Watz, M., Bosco, D. A., Skalicky, J. J., Kay, L. E., and Kern, D. (2005) Intrinsic dynamics of an enzyme underlies catalysis, *Nature 438*, 117-121.

[15] Ramanathan, A., Savol, A. J., Langmead, C. J., Agarwal, P. K., and Chennubhotla, C. S. (2011) Discovering Conformational Sub-States Relevant to Protein Function, *Plos One 6*, e15827.

[16] Fraser, J. S., and Jackson, C. J. (2011) Mining electron density for functionally relevant protein polysterism in crystal structures, *Cell Mol Life Sci 68*, 1829-1841.

[17] Frauenfelder, H., Sligar, S. G., and Wolynes, P. G. (1991) The energy landscapes and motions of proteins, *Science 254*, 1598-1603.

[18] Baldwin, A. J., Hansen, D. F., Vallurupalli, P., and Kay, L. E. (2009) Measurement of methyl axis orientations in invisible, excited states of proteins by relaxation dispersion NMR spectroscopy, *J. Am. Chem. Soc. 131*, 11939-11948.

[19] Boehr, D. D., McElheny, D., Dyson, H. J., and Wright, P. E. (2006) The dynamic energy landscape of dihydrofolate reductase catalysis, *Science 313*, 1638-1642.

[20] Hartmann, H., Parak, F., Steigemann, W., Petsko, G. A., Ponzi, D. R., and Frauenfelder, H. (1982) Conformational substates in a protein: structure and dynamics of metmyoglobin at 80 K, *Proc. Natl. Acad. Sci. U. S. A. 79*, 4967-4971.

[21] Klinman, J. P., and Kohen, A. (2014) Evolutionary aspects of enzyme dynamics, *J. Biol. Chem. 289*, 30205-30212.

[22] Agarwal, P. K. (2006) Enzymes: An integrated view of structure, dynamics and function, *Microb. Cell Fact. 5*, 2.

[23] Fraser, J. S., Clarkson, M. W., Degnan, S. C., Erion, R., Kern, D., and Alber, T. (2009) Hidden alternative structures of proline isomerase essential for catalysis, *Nature 462*, 669-U149.

[24] Jackson, C. J., Foo, J. L., Tokuriki, N., Afriat, L., Carr, P. D., Kim, H. K., Schenk, G., Tawfik, D. S., and Ollis, D. L. (2009) Conformational sampling, catalysis, and evolution of the bacterial phosphotriesterase, *Proc. Natl. Acad. Sci. U. S. A. 106*, 21631-21636.

[25] Camilloni, C., Sahakyan, A. B., Holliday, M. J., Isern, N. G., Zhang, F., Eisenmesser, E. Z., and Vendruscolo, M. (2014) Cyclophilin A catalyzes proline isomerization by an electrostatic handle mechanism, *Proc. Natl. Acad. Sci. U. S. A. 111*, 10203-10208.

[26] Yuan, H., Fu, G., Brooks, P. T., Weber, I., and Gadda, G. (2010) Steady-state kinetic mechanism and reductive half-reaction of D-arginine dehydrogenase from Pseudomonas aeruginosa, *Biochemistry 49*, 9542-9550.

[27] Li, C., and Lu, C. D. (2009) Arginine racemization by coupled catabolic and anabolic dehydrogenases, *Proc. Natl. Acad. Sci. U. S. A. 106*, 906-911.

[28] Gannavaram, S., Sirin, S., Sherman, W., and Gadda, G. (2014) Mechanistic and computational studies of the reductive half-reaction of tyrosine to phenylalanine active site variants of D-arginine dehydrogenase, *Biochemistry 53*, 6574-6583.

[29] Fitzpatrick, P. F. (2010) Oxidation of amines by flavoproteins, *Arch Biochem Biophys 493*, 13-25.

[30] Bradford, M. M. (1976) A rapid and sensitive method for the quantitation of microgram quantities of protein utilizing the principle of protein-dye binding, *Anal Biochem 72*, 248-254.

[31] Noble, J. E. (2014) Quantification of protein concentration using UV absorbance and Coomassie dyes, *Methods Enzymol 536*, 17-26.

[32] Mayhew, S. G., Whitfield, C. D., Ghisla, S., and Schuman-Jorns, M. (1974) Identification and properties of new flavins in electron-transferring flavoprotein from Peptostreptococcus elsdenii and pig-liver glycolate oxidase, *Eur. J. Biochem. 44*, 579-591.

[33] Liu, M. L., Mao, X. A., Ye, C. H., Huang, H., Nicholson, J. K., and Lindon, J. C. (1998) Improved WATERGATE pulse sequences for solvent suppression in NMR spectroscopy, *J. Magn. Reson. 132*, 125-129.

[34] Battye, T. G., Kontogiannis, L., Johnson, O., Powell, H. R., and Leslie, A. G. (2011) iMOSFLM: a new graphical interface for diffraction-image processing with MOSFLM, *Acta Crystallogr., Sect. D: Biol. Crystallogr. 67*, 271-281.

[35] Evans, P. (2006) Scaling and assessment of data quality, *Acta Crystallogr., Sect. D: Biol. Crystallogr. 62*, 72-82.

[36] Fu, G., Yuan, H., Li, C., Lu, C. D., Gadda, G., and Weber, I. T. (2010) Conformational changes and substrate recognition in Pseudomonas aeruginosa D-arginine dehydrogenase, *Biochemistry 49*, 8535-8545.

[37] McCoy, A. J., Grosse-Kunstleve, R. W., Adams, P. D., Winn, M. D., Storoni, L. C., and Read, R. J. (2007) Phaser crystallographic software, *J. Appl. Crystallogr. 40*, 658-674.

[38] Afonine, P. V., Grosse-Kunstleve, R. W., Echols, N., Headd, J. J., Moriarty, N. W., Mustyakimov, M., Terwilliger, T. C., Urzhumtsev, A., Zwart, P. H., and Adams, P. D. (2012) Towards automated crystallographic structure refinement with phenix.refine, *Acta Crystallogr D 68*, 352-367.

[39] Emsley, P., Lohkamp, B., Scott, W. G., and Cowtan, K. (2010) Features and development of Coot, *Acta Crystallogr., Sect. D: Biol. Crystallogr. 66*, 486-501.

[40] Moriarty, N. W., Grosse-Kunstleve, R. W., and Adams, P. D. (2009) electronic Ligand Builder and Optimization Workbench (eLBOW): a tool for ligand coordinate and restraint generation, *Acta Crystallogr., Sect. D: Biol. Crystallogr. 65*, 1074-1080.

[41] Pettersen, E. F., Goddard, T. D., Huang, C. C., Couch, G. S., Greenblatt, D. M., Meng, E. C., and Ferrin, T. E. (2004) UCSF Chimera--a visualization system for exploratory research and analysis, *J. Comput. Chem. 25*, 1605-1612.

[42] Maier, J. A., Martinez, C., Kasavajhala, K., Wickstrom, L., Hauser, K. E., and Simmerling, C. (2015) ff14SB: Improving the Accuracy of Protein Side Chain and Backbone Parameters from ff99SB, *J. Chem. Theory Comput. 11*, 3696-3713.

[43] Cornell, W. D., Cieplak, P., Bayly, C. I., Gould, I. R., Merz, K. M., Ferguson, D. M., Spellmeyer, D. C., Fox, T., Caldwell, J. W., and Kollman, P. A. (1995) A Second

Generation Force Field for the Simulation of Proteins, Nucleic Acids, and Organic Molecules, *J. Am. Chem. Soc. 117*, 5179-5197.

[44] Wang, J., Wolf, R. M., Caldwell, J. W., Kollman, P. A., and Case, D. A. (2004) Development and testing of a general amber force field, *J Comput Chem 25*, 1157-1174.

[45] Mark, P., and Nilsson, L. (2001) Structure and Dynamics of the TIP3P, SPC, and SPC/E Water Models at 298 K, *The Journal of Physical Chemistry A 105*, 9954-9960.

[46] Jorgensen, W. (1982) Revised TIPS for simulations of liquid water and aqueous solutions, *Journal of Chemical Physics 77*, 4156-4163.

[47] Momin, M., Yao, X. Q., Thor, W., and Hamelberg, D. (2018) Substrate Sequence Determines Catalytic Activities, Domain-Binding Preferences, and Allosteric Mechanisms in Pin1, *J. Phys. Chem. B 122*, 6521-6527.

[48] Darden, T., York, D., and Pedersen, L. (1993) Particle mesh Ewald: An N·log(N) method for Ewald sums in large systems, *The Journal of Chemical Physics 98*, 10089-10092.

[49] Ryckaert, J.-P., Ciccotti, G., and Berendsen, H. J. C. (1977) Numerical integration of the cartesian equations of motion of a system with constraints: molecular dynamics of n-alkanes, *Journal of Computational Physics 23*, 327-341.

[50] Roe, D. R., and Cheatham, T. E., 3rd. (2013) PTRAJ and CPPTRAJ: Software for Processing and Analysis of Molecular Dynamics Trajectory Data, *J Chem Theory Comput 9*, 3084-3095.

[51] Orozco-Gonzalez, Y., Manathunga, M., Marin, M. D. C., Agathangelou, D., Jung, K. H., Melaccio, F., Ferre, N., Haacke, S., Coutinho, K., Canuto, S., and Olivucci, M. (2017) An Average Solvent Electrostatic Configuration Protocol for QM/MM Free Energy

Optimization: Implementation and Application to Rhodopsin Systems, *J. Chem. Theory Comput. 13*, 6391-6404.

[52] Singh, U. C., and Kollman, P. A. (1986) A combined ab initio quantum mechanical and molecular mechanical method for carrying out simulations on complex molecular systems: Applications to the CH3Cl + Cl− exchange reaction and gas phase protonation of polyethers, *J. Comput. Chem. 7*, 718-730.

[53] Humbel, S., Sieber, S., and Morokuma, K. (1996) The IMOMO method: Integration of different levels of molecular orbital approximations for geometry optimization of large systems: Test for n-butane conformation and SN2 reaction: RCl+Cl−, *J. Chem. Phys. 105*, 1959-1967.

[54] Hornak, V., Abel, R., Okur, A., Strockbine, B., Roitberg, A., and Simmerling, C. (2006) Comparison of multiple Amber force fields and development of improved protein backbone parameters, *Proteins 65*, 712-725.

[55] Hornak, V., Okur, A., Rizzo, R. C., and Simmerling, C. (2006) HIV-1 protease flaps spontaneously open and reclose in molecular dynamics simulations, *Proc. Natl. Acad. Sci. U. S. A. 103*, 915-920.

[56] Jorgensen, W. L., Chandrasekhar, J., Madura, J. D., Impey, R. W., and Klein, M. L. (1983) Comparison of simple potential functions for simulating liquid water, *J. Chem. Phys. 79*, 926-935.

[57] Pronk, S., Pall, S., Schulz, R., Larsson, P., Bjelkmar, P., Apostolov, R., Shirts, M. R., Smith, J. C., Kasson, P. M., van der Spoel, D., Hess, B., and Lindahl, E. (2013) GROMACS 4.5: a high-throughput and highly parallel open source molecular simulation toolkit, *Bioinformatics 29*, 845-854.

[58] Coutinho, K., Georg, H. C., Fonseca, T. L., Ludwig, V., and Canuto, S. (2007) An efficient statistically converged average configuration for solvent effects, *Chemical Physics Letters 437*, 148-152.

[59] Aquilante, F., De Vico, L., Ferre, N., Ghigo, G., Malmqvist, P. A., Neogrady, P., Pedersen, T. B., Pitonak, M., Reiher, M., Roos, B. O., Serrano-Andres, L., Urban, M., Veryazov, V., and Lindh, R. (2010) MOLCAS 7: the next generation, *J. Comput. Chem. 31*, 224-247.

[60] Ponder, J. W., and Case, D. A. (2003) Force fields for protein simulations, *Adv. Protein Chem. 66*, 27-85.

[61] Strambi, A., Coto, P. B., Frutos, L. M., Ferré, N., and Olivucci, M. (2008) Relationship between the Excited State Relaxation Paths of Rhodopsin and Isorhodopsin, *J. Am. Chem. Soc. 130*, 3382-3388.

[62] Roos, B. O. (2007) The Complete Active Space Self-Consistent Field Method and its Applications in Electronic Structure Calculations, In *Adv. Chem. Phys.*, pp 399-445.

[63] Widmark, P.-O., Malmqvist, P.-Å., and Roos, B. O. (1990) Density matrix averaged atomic natural orbital (ANO) basis sets for correlated molecular wave functions, *Theor. Chem. Acc. 77*, 291-306.

[64] Bayly, C. I., Cieplak, P., Cornell, W. D., and Kollman, P. A. (1993) A Well-Behaved Electrostatic Potential Based Method Using Charge Restraints for Deriving Atomic Charges - the Resp Model, *J. Phys. Chem. 97*, 10269-10280.

[65] Lee, C., Yang, W., and Parr, R. G. (1988) Development of the Colle-Salvetti correlation-energy formula into a functional of the electron density, *Phys. Rev. B 37*, 785-789.

[66] Kabir, M. P., Orozco-Gonzalez, Y., and Gozem, S. (2019) Electronic spectra of flavin in different redox and protonation states: a computational perspective on the effect of the electrostatic environment, *Physical Chemistry Chemical Physics 21*, 16526-16537.

[67] Choe, Y.-K., Nagase, S., and Nishimoto, K. (2007) Theoretical study of the electronic spectra of oxidized and reduced states of lumiflavin and its derivative, *Journal of Computational Chemistry 28*, 727-739.

[68] Gozem, S., Luk, H. L., Schapiro, I., and Olivucci, M. (2017) Theory and Simulation of the Ultrafast Double-Bond Isomerization of Biological Chromophores, *Chemical Reviews 117*, 13502-13565.

[69] Schollnhammer, G., and Hemmerich, P. (1974) Nucleophilic addition at the photoexcited flavin cation: synthesis and properties of 6- and 9-hydroxy-flavocoenzyme chromophores, *Eur J Biochem 44*, 561-577.

[70] Huang, C. H., Winkler, A., Chen, C. L., Lai, W. L., Tsai, Y. C., Macheroux, P., and Liaw, S. H. (2008) Functional roles of the 6-S-cysteinyl, 8alpha-N1-histidyl FAD in glucooligosaccharide oxidase from Acremonium strictum, *J. Biol. Chem. 283*, 30990-30996.

[71] Huang, L., Scrutton, N. S., and Hille, R. (1996) Reaction of the C30A mutant of trimethylamine dehydrogenase with diethylmethylamine, *J. Biol. Chem. 271*, 13401-13406.

[72] Ghisla, S., Kenney, W. C., Knappe, W. R., McIntire, W., and Singer, T. P. (1980) Chemical synthesis and some properties of 6-substituted flavins, *Biochemistry 19*, 2537-2544.

[73] Ghisla, S., Massey, V., and Yagi, K. (1986) Preparation and some properties of 6-substituted flavins as active site probes for flavin enzymes, *Biochemistry 25*, 3282-3289.

[74] Ghisla, S., and Mayhew, S. G. (1976) Identification and properties of 8-hydroxyflavin--adenine dinucleotide in electron-transferring flavoprotein from Peptostreptococcus elsdenii, *Eur. J. Biochem. 63*, 373-390.

[75] Massey, V., Ghisla, S., and Yagi, K. (1986) 6-Azido- and 6-aminoflavins as active-site probes of flavin enzymes, *Biochemistry 25*, 8095-8102.

[76] Lu, X., Nikolic, D., Mitchell, D. J., van Breemen, R. B., Mersfelder, J. A., Hille, R., and Silverman, R. B. (2003) A mechanism for substrate-Induced formation of 6-hydroxyflavin mononucleotide catalyzed by C30A trimethylamine dehydrogenase, *Bioorg. Med. Chem. Lett. 13*, 4129-4132.

[77] Gatti, D. L., Palfey, B. A., Lah, M. S., Entsch, B., Massey, V., Ballou, D. P., and Ludwig, M. L. (1994) The mobile flavin of 4-OH benzoate hydroxylase, *Science 266*, 110-114.

[78] David, C. C., and Jacobs, D. J. (2014) Principal component analysis: a method for determining the essential dynamics of proteins, *Methods Mol. Biol. 1084*, 193-226.

[79] Agarwal, P. K. (2005) Role of protein dynamics in reaction rate enhancement by enzymes, *J. Am. Chem. Soc. 127*, 15248-15256.

[80] Crozier-Reabe, K., and Moran, G. R. (2012) Form follows function: structural and catalytic variation in the class a flavoprotein monooxygenases, *Int J Mol Sci 13*, 15601-15639.

[81] Zheng, Y., Dong, J., Palfey, B. A., and Carey, P. R. (1999) Using Raman spectroscopy to monitor the solvent-exposed and "buried" forms of flavin in p-hydroxybenzoate hydroxylase, *Biochemistry 38*, 16727-16732.

[82] Park, J., Gasparrini, A. J., Reck, M. R., Symister, C. T., Elliott, J. L., Vogel, J. P., Wencewicz, T. A., Dantas, G., and Tolia, N. H. (2017) Plasticity, dynamics, and inhibition of emerging tetracycline resistance enzymes, *Nat Chem Biol 13*, 730-736.

[83] Setser, J. W., Heemstra, J. R., Jr., Walsh, C. T., and Drennan, C. L. (2014) Crystallographic evidence of drastic conformational changes in the active site of a flavin-dependent N-hydroxylase, *Biochemistry 53*, 6063-6077.

[84] Manenda, M. S., Picard, M. E., Zhang, L., Cyr, N., Zhu, X., Barma, J., Pascal, J. M., Couture, M., Zhang, C., and Shi, R. (2020) Structural analyses of the Group A flavin-dependent monooxygenase PieE reveal a sliding FAD cofactor conformation bridging OUT and IN conformations, *J Biol Chem 295*, 4709-4722.

[85] Campbell, A. C., Stiers, K. M., Martin Del Campo, J. S., Mehra-Chaudhary, R., Sobrado, P., and Tanner, J. J. (2020) Trapping conformational states of a flavin-dependent N-monooxygenase in crystallo reveals protein and flavin dynamics, *J Biol Chem 295*, P13239-13249.

[86] Miura, R. (2001) Versatility and specificity in flavoenzymes: control mechanisms of flavin reactivity, *Chem Rec 1*, 183-194.

[87] Trickey, P., Basran, J., Lian, L. Y., Chen, Z., Barton, J. D., Sutcliffe, M. J., Scrutton, N. S., and Mathews, F. S. (2000) Structural and biochemical characterization of recombinant wild type and a C30A mutant of trimethylamine dehydrogenase from methylophilus methylotrophus (sp. W(3)A(1)), *Biochemistry 39*, 7678-7688.

[88] Mewies, M., Basran, J., Packman, L. C., Hille, R., and Scrutton, N. S. (1997) Involvement of a flavin iminoquinone methide in the formation of 6-hydroxyflavin mononucleotide in trimethylamine dehydrogenase: a rationale for the existence of 8alpha-methyl and C6-linked covalent flavoproteins, *Biochemistry 36*, 7162-7168.

[89] Piano, V., Palfey, B. A., and Mattevi, A. (2017) Flavins as Covalent Catalysts: New Mechanisms Emerge, *Trends Biochem Sci 42*, 457-469.

[90] Furst, M., Romero, E., Gomez Castellanos, J. R., Fraaije, M. W., and Mattevi, A. (2018) Side-Chain Pruning Has Limited Impact on Substrate Preference in a Promiscuous Enzyme, *ACS Catal. 8*, 11648-11656.

[91] Bhabha, G., Biel, J. T., and Fraser, J. S. (2015) Keep on moving: discovering and perturbing the conformational dynamics of enzymes, *Acc. Chem. Res. 48*, 423-430.

[92] Gardner, J. M., Biler, M., Risso, V. A., Sanchez-Ruiz, J. M., and Kamerlin, S. C. L. (2020) Manipulating Conformational Dynamics To Repurpose Ancient Proteins for Modern Catalytic Functions, *ACS Catalysis 10*, 4863-4870.

[93] Tokuriki, N., and Tawfik, D. S. (2009) Protein dynamism and evolvability, *Science 324*, 203-207.

[94] Pandya, C., Farelli, J. D., Dunaway-Mariano, D., and Allen, K. N. (2014) Enzyme promiscuity: engine of evolutionary innovation, *J. Biol. Chem. 289*, 30229-30236.

[95] Pabis, A., Risso, V. A., Sanchez-Ruiz, J. M., and Kamerlin, S. C. (2018) Cooperativity and flexibility in enzyme evolution, *Curr Opin Struc Biol 48*, 83-92.

[96] Crean, R. M., Gardner, J. M., and Kamerlin, S. C. L. (2020) Harnessing Conformational Plasticity to Generate Designer Enzymes, *J. Am. Chem. Soc. 142*, 11324–11342.

4 DISCOVERY OF A NEW FLAVIN N5-ADDUCT IN A TYROSINE TO PHENYLALANINE VARIANT OF D-ARGININE DEHYDROGENASE

(This chapter will be published verbatim as A. Iyer, R.A.G. Reis, J. Agniswamy, I.T. Weber, and G. Gadda (2022) to *Archives of Biochemistry and Biophysics Archives of Biochemistry and Biophysics*, Volume 715, 109100. The author contributed to study design, protein expression, purification, crystallization, and data collection and refinement, 6-OH-FAD and N5-(4-guanidino-oxobutyl)-FAD characterization with mechanism, writing of the manuscript and editing)

4.1 ABSTRACT

D-Arginine dehydrogenase from *Pseudomonas aeruginosa* (*Pa*DADH) catalyzes the flavin-dependent oxidation of D-arginine and other D-amino acids. Here, we report the crystal structure at 1.29 Å resolution for *Pa*DADH-Y249F expressed and co-crystallized with D-arginine. The overall structure of *Pa*DADH-Y249F resembled *Pa*DADH-WT, but the electron density for the flavin cofactor was ambiguous, suggesting the presence of modified flavins. Electron density maps and mass spectrometric analysis confirmed the presence of both N5-(4-guanidino-oxobutyl)-FAD and 6-OH-FAD in a single crystal of *Pa*DADH-Y249F and helped with the further refinement of the X-ray crystal structure. The versatility of the reduced flavin is apparent in the *Pa*DADH-Y249F structure and is evidenced by the multiple functions it can perform in the same active site.

4.2 INTRODUCTION

Flavins are among the most versatile enzyme cofactors, along with non-heme iron, pyridoxal phosphate, and the heme group. [1-4] Flavins participate in many redox reactions, such as oxygenation, hydroxylation, epoxidation, oxidation, and reduction. [1] The spectroscopic properties and reactivity of flavins change when functional groups like methyl, hydroxyl, cyano, thiol, amino, bromide, formyl, or chloride are attached covalently to the 7,8-dimethyl-isoalloxazine moiety. [5-11] Modified flavins have also been synthesized and used as probes of chemical mechanisms in flavoenzymes. [1] The 6-hydroxy-flavin is among the most abundant modified flavins in nature, with 6-OH flavin-containing enzymes usually existing as a mixture of FAD, or FMN, and 6-OH flavin. [7, 10, 12] Most enzymes containing 6-OH modified flavins have a seemingly elusive functional relevance and exhibit low to no enzymatic activity. [7, 10, 13, 14]

While the reactivity of flavin cofactors has been studied for decades, recent advances have established new reactivities like the functional prenylated flavins and flavin-N5-iminium/peroxo/oxide adducts. [15] The flavin C4a and N5 atoms are the most reactive centers; they participate in the redox chemistry by enabling the entry and exit of electrons and forming covalent adducts. [1, 5] For decades, the flavin C4a atom was a center for covalent catalysis, e.g., the short-lived C4a-hydroperoxide intermediate often observed in flavin-dependent monooxygenases. [1] The most common function of the flavin N5 atom was to accept a hydride to form the reduced flavin during enzyme catalytic cycles. [15] Recent studies on the functionalization of the N5 atom in flavins have widened the possibilities of new reactions for the reduced flavin cofactor. [15-18]

D-Arginine dehydrogenase (*Pa*DADH, EC 1.4.99.6) from *Pseudomonas aeruginosa* PAO1 uses a tightly bound, non-covalent FAD to catalyze the oxidation of D-arginine to iminoarginine, which can be non-enzymatically hydrolyzed to α-ketoarginine and ammonia. *Pa*DADH and NAD(P)H-

dependent L-arginine dehydrogenase form a novel two-enzyme system for converting D- to L-arginine, enabling *P. aeruginosa* to survive using D-arginine as the sole carbon and nitrogen source. [19, 20] The enzyme has a broad substrate specificity, with D-arginine and D-lysine being the best substrates, as shown by k_{cat}/K_m values ranging from 10^5 to 10^6 $M^{-1}s^{-1}$. [19] Crystal structures of the wild-type enzyme are available for the substrate-free form (1.06 Å, PDB: 3NYC) and complexes with either iminoarginine (1.30 Å, PDB: 3NYE) or iminohistidine (1.30 Å, PDB: 3NYF), providing insights on substrate binding. [19] The side chain of E87 interacts with the guanidino group of D-arginine, explaining the enzyme specificity for D-amino acids with positively charged side chains. A covalent N5-(4-methyl-2-pentanone)-FAD adduct (1.07 Å, PDB: 3SM8) was previously observed in the structure of the enzyme crystallized with D-leucine. [21] In a *Pa*DADH enzyme variant in which Y249 was replaced with phenylalanine to evaluate the residue's role in substrate binding due to its proximity to substrate carboxylate, the formation of 6-OH-FAD was recently reported. [14] The structures of the *Pa*DADH-Y249F with 6-OH-FAD (1.55 Å, PDB: 6PLD) or FAD (1.34 Å, PDB: 6P9D) bound at the active site were recently determined [14], demonstrating no differences in the overall fold of the enzyme with the native and the modified flavin. Molecular dynamics and quantum mechanical/molecular mechanical calculations suggested that the formation of the 6-OH-FAD ensued from altered protein dynamics through sampling a conformational landscape unavailable to the wild-type enzyme, which changed the reactivity of the flavin. [14] The same study also showed that 6-OH-FAD could be formed *in vitro* from FAD in the active site of the *Pa*DADH-Y249F. [14]

In this study, *Pa*DADH-Y249F was expressed and co-crystallized in the presence of D-arginine to gain further insights into the enzyme. The resulting electron density map revealed that the enzyme-bound FAD contained additional electron density at both the flavin N5 and C6 atoms,

suggesting covalent adducts at both positions. Mass spectrometry was used on the flavin sample extracted after solubilizing the crystals to establish that multiple modified FAD cofactors were present in a single crystal as deduced from the electron density map. The study highlights the enhanced versatility of the flavin cofactor in the active site of *Pa*DADH-Y249F, where the reduced flavin can perform at least three different functions, including exchanging a hydride ion during conventional catalytic turnover with D-amino acids and radical and nucleophilic reactions that lead to two different covalent flavins in the same active site.

4.3 MATERIALS AND METHODS

4.3.1 Materials.

D-arginine, phenazine methosulfate (PMS), and PEG (3350, 5000, 6000) were purchased from Sigma-Aldrich (St. Louis, MO). D-Alanine was obtained from Alfa Aesar (Wardhill, MA). All other reagents used were obtained in their highest purity commercially available.

4.3.2 Expression and purification

The expression and purification of *Pa*DADH-Y249F was carried out as previously described [22], except for the presence of 100 µM D-arginine during the 18 h induction at 4 °C with 100 µM IPTG.

4.3.3 Crystallization conditions

Crystals of *Pa*DADH-Y249F were grown by the hanging-drop vapor diffusion method; 2 µL of a reservoir solution and 2 µL of the protein solution, which were mixed and equilibrated against 500 µL of a reservoir solution. The protein was stored in a solution of 20 mM TRIS-HCL pH 8.0, 10 % (v/v) glycerol, and the protein crystals were grown at room temperature with a reservoir solution that contained 13% (w/v) PEG 3350, 6% (w/v) PEG 6000, 20 mM TRIS-HCl, pH 7.0,

10% (v/v) glycerol, 5 mM D-arginine. Green-colored pyramidal crystals were observed within one week, could grow to 0.2-0.3 mm^3 within two weeks.

4.3.4 MS-ESI (-) analysis conditions

Fifty protein crystals of *Pa*DADH-Y249F expressed and co-crystallized with D-arginine were harvested from the hanging drops, washed by passing through 2 µL drops of Milli Q H_2O, and collected in a 1.5 mL microcentrifuge tube containing 100 µL of Milli Q H_2O. The crystals were crushed using a micro pestle and vortexing. The flavin was extracted by denaturing the protein with chilled (-20 °C) 50% CH_3CN. The slurry was spun down at 10,000 g to remove precipitated protein, and the step was repeated on the supernatant until no precipitate was observed with centrifugation. The supernatant was vacuum concentrated for ~4 h before MS-ESI (-) analysis. The MS-ESI (-) analysis was carried out on a Waters Q-TOF micro-mass spectrometer equipped with an electrospray ionization source in negative ion mode through a direct infusion at a 5 µL/min flow rate. The ESI tuning settings were capillary voltage at 3000, sample cone voltage at 40, extraction voltage at 1, desolvation temperature at 100 °C, and source temperature at 70 °C.

4.3.5 X-ray data collection and processing

A single crystal was cryocooled in the reservoir solution with 25% (w/v) glycerol. X-ray data were collected at 100 K on beamline 22-ID of the Southeast Regional Collaborative Access Team (SER-CAT) at the Advanced Photon Source, Argonne National Laboratory. One hundred and eighty images were collected with 1° oscillation per image with a 190 mm crystal-to-detector distance and 1.5 s exposure. The X-ray data were processed using iMOSFLM [23] and scaled with SCALA. [24] Data collection and processing statistics are summarized in Table 4.1.

4.3.6 Structure solution and refinement

The coordinates of the *Pa*DADH-WT structure (PDB: 3NYE) were used to obtain the initial phases for the *Pa*DADH-Y249F structure by molecular replacement using PHASER in the CCP4i suite. [25, 26] The crystal structure was refined using Phenix_refine. [27] Manual adjustments and rebuilding were performed using the molecular graphics program COOT. [28] The cofactor ligands 6-OH-FAD (PDB ID: 6FA) and N5-(4-guanidino-oxobutyl)-FAD (PDB ID: 4R2) were constructed using Phenix_elbow. [29] The model quality was checked for steric clashes, incorrect stereochemistry, and rotamer outliers using MolProbity. [30] All structural figures were made using UCSF Chimera. [31] Refined atomic coordinates and experimental structure factors were deposited in the Protein Data Bank (PDB: 7RDF). Refinement statistics and validation statistics are shown in Table 4.1.

4.3.7 UV-Visible absorption spectra

A UV-Visible absorption spectrum of a solution containing *Pa*DADH-Y249F was determined at 25 °C using an Agilent Technologies model HP8453 PC diode-array spectrophotometer equipped with a thermostated water bath. The conditions in the solution were 50 mM Tris-HCl, pH 8.0, and 10 % (v/v) glycerol. The *Pa*DADH-Y249F was then incubated with 15 mM D-arginine in 50 mM Tris-HCl, pH 8.0, and 10 % (v/v) glycerol at 25 °C with constant stirring. The UV-Visible absorption spectrum was recorded right after the addition of D-arginine and after an 8-day incubation with the amino acid substrate to generate spectra consistent with the formation of an N5 acyl adduct as observed in the crystal structure.

4.4 RESULTS

*Pa*DADH-Y249F was expressed in *Escherichia coli* in the presence of 0.1 mM D-arginine and purified to a high level as judged by visual inspection of an SDS-PAGE, using the same protocol

used for *Pa*DADH-WT. [32] Three protein fractions with yellow (enriched with oxidized, unmodified FAD) , light-green (unresolved mixture with FAD and 6-OH-FAD), and green (enriched with 6-OH-FAD) colors were separated on a DEAE-Sepharose column, as recently reported for *Pa*DADH-Y249F expressed in the absence of D-arginine. [14] The three protein fractions were crystallized in the conditions listed in the methods section, in the presence of 5 mM D-arginine to investigate whether the *Pa*DADH-Y249F with 6-OH-FAD could still bind D-arginine in its active site or the modification precluded substrate binding. Green pyramidal crystals were obtained with the largest crystals appearing in the drops with the light-green fraction of *Pa*DADH-Y249F. The high-resolution structure of the enzyme was determined in the orthorhombic space group $P2_12_12_1$ with one molecule per asymmetric unit up to a resolution of 1.29 Å by molecular replacement using the structure of *Pa*DADH-WT as the search model (PDB: 3NYE) (Table 1). [19] All 375 protein residues in the structure were clearly defined in the electron density map. Additional electron density protruding from both the flavin N5 and C6 atoms was also observed, consistent with a portion of the flavin occupancy being 6-OH-FAD, as recently reported for *Pa*DADH-Y249F (PDB: 6PLD) [14], and the rest being a flavin N5-acyl adduct (Figure 4. 1). Thus, *Pa*DADH-Y249F expressed and crystallized in the presence of D-arginine yielded either a doubly modified flavin or two distinctly modified cofactors in the protein crystals. After cofactor extraction from the crystals, MS-ESI (-) analysis yielded two peaks, consistent with the presence of two distinctly modified cofactors. A peak with m/z (-) value of 800.26 amu corresponded to 6-OH-FAD, as shown in a recent study for *Pa*DADH-Y249F [14]; a peak with m/z (-) value of 913.46 amu was attributed to an N5-(4-guanidino-oxobutyl)-FAD, based on a calculated m/z value of 913.24 amu (Figure 4. 1).

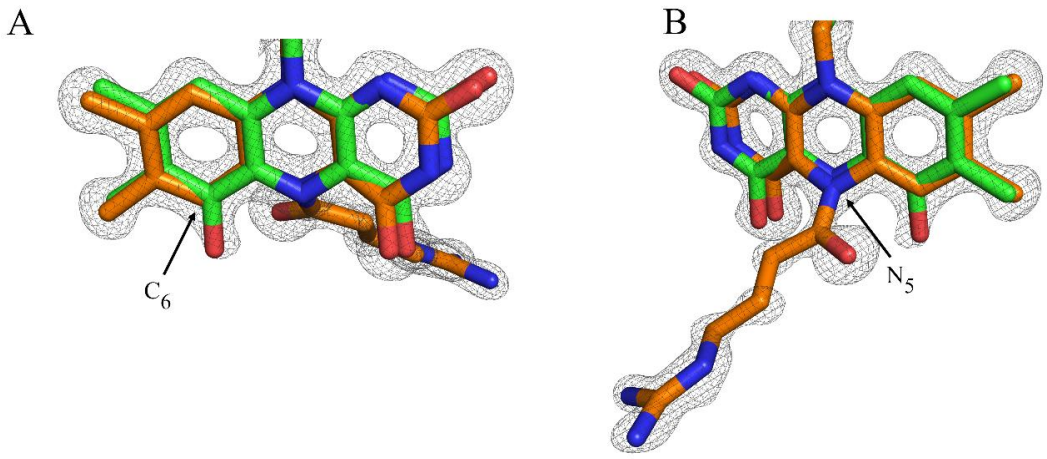

Figure 4.1. 2Fo-Fc electron density map (contoured at 1.2σ) for the two modified cofactors in the active site of PaDADH-Y249F. The left panel shows the additional density on the flavin C6 atom, i.e., 6-hydroxy-FAD (green). The right panel is in a different orientation and shows the protruding density from the flavin N5 atom, i.e., N5-(4-guanidino-oxobutyl)-FAD (orange).

The *Pa*DADH-Y249F structure was refined to an R-factor of 12.6% and an R-free of 15.7% with the addition of two distinctly modified cofactors (Table 1). As previously reported for *Pa*DADH-WT, the protein folded into an FAD-binding domain that includes residues 1-82, 147-217, and 309-375, and a substrate-binding domain comprised of residues 83-142 and 218-297. [19] Electron density for the C4 atom of F249 was consistent with mutation to phenylalanine. The occupancy of the 6-OH-FAD (6FA) was 29%, and the occupancy of the N5-(4-guanidino-oxobutyl)-FAD (FDE) was 71%. The overall structure of *Pa*DADH-Y249F closely resembled that of *Pa*DADH-WT (PDB: 3NYE), *Pa*DADH-WT with an N5 acyl adduct (PDB: 3SM8), and *Pa*DADH-Y249F with 6-OH-FAD (PDB: 6P9D) or FAD bound (PDB: 6PLD), with RMSD values ≤ 0.50 Å for 375 Cα atoms (Figure 4. 2). [14, 19, 21] Thus, the overall fold of the enzyme was not altered by the mutation of Y249 to phenylalanine or the covalent modification of the flavin N5 and C6 atoms. In the *Pa*DADH-Y249F structure, the major conformations of the carboxylate groups

of E87 and E246 could be modeled only between ~65% and ~60% occupancy. An alternative conformation of the carboxylate groups of E87 and E246 could not be modeled with confidence.

The FAD adopted an elongated conformation with the 7,8-dimethylisoalloxazine ring located at the interface of the substrate- and FAD-binding domains (Figure 4. 2). The angle defined by the flavin C4a-N5-C5a atoms was 179.5° for the 6-OH-FAD and 144.9° for the N5-(4-guanidino-oxobutyl)-FAD, reflecting the different sp^2 and sp^3 hybridizations for the flavin N5 atom in the two modified flavins (Figure 4. 2), similar to the 'butterfly bend' found in proline dehydrogenase.[33-35] Most of the hydrogen-bonds previously seen in the *Pa*DADH-WT structure linking the pyrimidine portion of the isoalloxazine and the backbone atoms of the protein were conserved in the *Pa*DADH-Y249F structure, e.g., the flavin O2 atom with the N atom of I335 and the flavin N3-H atom with the O atom of H48 and a water molecule. [19] In contrast, the hydrogen bonds between the flavin O2 atom and the N atom of Q336 and the flavin O4 atom with the N atom of H48 were not observed in the *Pa*DADH-Y249F structure with the two modified flavins. [19] No differences were observed in the van der Waals contacts between the xylene portion of the flavin and R44, R222, W301, G303, and R305 upon comparing the *Pa*DADH-Y249F and *Pa*DADH-WT structures. [19] All the interactions of the adenosyl, diphosphatidyl, and ribityl moieties of the modified flavins with the protein were identical to those previously described for *Pa*DADH-WT. [19]

The N5-(4-guanidino-oxobutyl)-FAD established several interactions with active site residues in *Pa*DADH-Y249F. The carbonyl oxygen atom of the N5-(4-guanidino-oxobutyl)-FAD formed a hydrogen bond with the guanidino group of R222, as previously observed in the structure of the *Pa*DADH-WT with N5-(4-methyl-2-pentanone) obtained by co-crystallization of the enzyme with D-leucine (Figure 4. 3). [21] The guanidino group of the N5-(4-guanidino-oxobutyl)-FAD formed

two ion pairs with two glutamate residues in the active site of the enzyme. The side chain of E87 formed a weak monodentate interaction (2.7 Å) with the guanidino group of the N5-(4-guanidino-oxobutyl) adduct (Figure 4. 3 & 4). In contrast, in the *Pa*DADH-WT structure in complex with iminoarginine non-covalently bound in the active site, E87 formed a strong bidentate ion pair (2.5 Å, 2.5 Å) with the guanidino group of the ligand (Figure 4.4). The weaker interactions of E87 with the guanidino group of the N5-(4-guanidino-oxobutyl)-FAD in *Pa*DADH-Y249F originated from a different spatial localization of the ligand guanidino group dictated by the covalent attachment to FAD. The side chain of E246 in *Pa*DADH-Y249F established a monodentate ion pair (3.2 Å) with the guanidino group of the N5-(4-guanidino-oxobutyl)-FAD (Figure 4. 3) in a slightly different conformation than previously observed in the *Pa*DADH-WT structure. [19] In contrast to the *Pa*DADH-WT structure, showing an open and closed conformation for Loop L1 (residues 45-56) at the active site entrance [19], the *Pa*DADH-Y249F structure reported here is in the closed conformation, which is identical to that previously described in *Pa*DADH-WT. The positions of all the other residues in the enzyme active site were identical in the *Pa*DADH-Y249F and *Pa*DADH-WT structures. [19, 21]

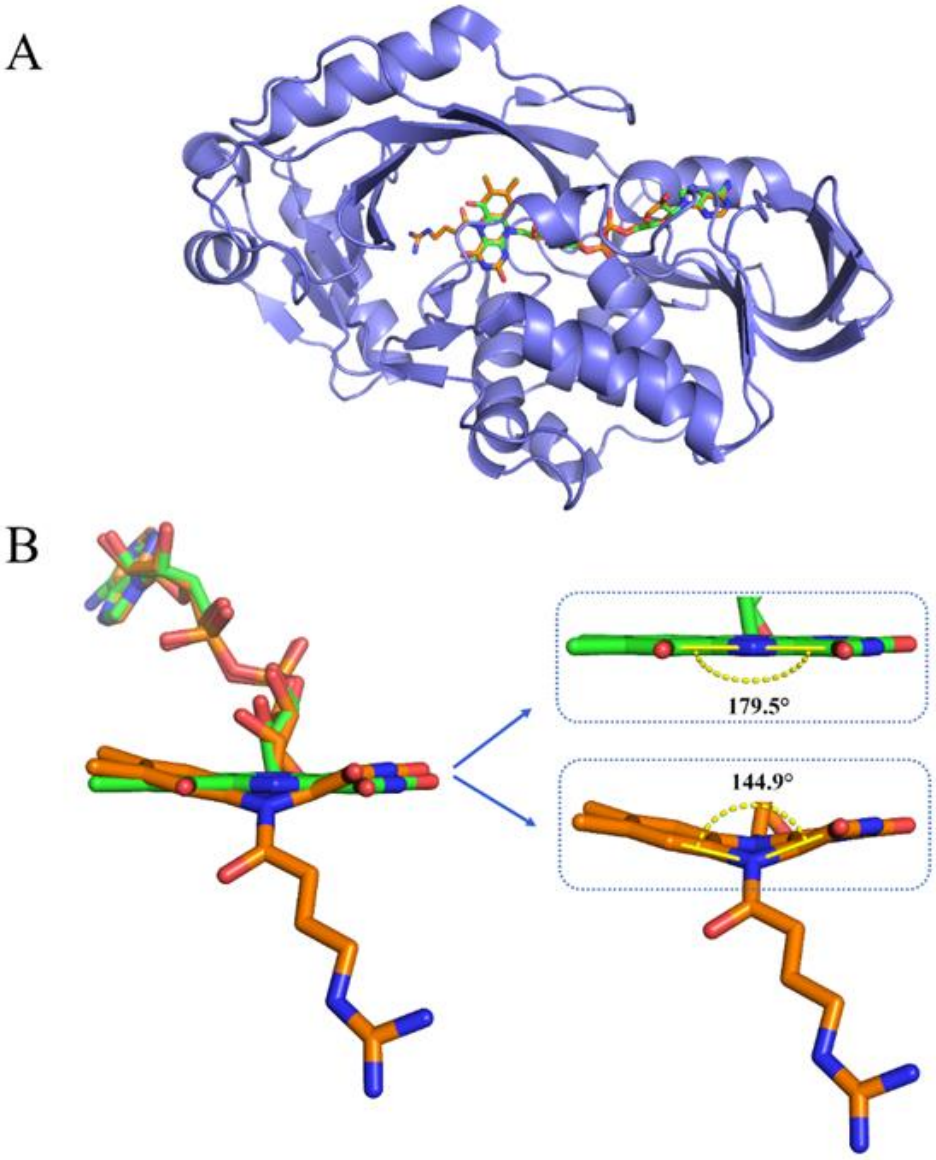

Figure 4.2. A) The overall structure of the PaDADH-Y249F (blue). The 6-OH -FAD is shown with green carbons, and the N5-(4-guanidino-oxobutyl)-FAD in orange carbons. B) The geometry of the two modified flavin cofactors observed in the active site of PaDADH-Y249F, showing the angle defined by the flavin C4a-N5-C5a atoms being co-planar in the 6-OH-FAD and bent in the N5-(4-guanidino-oxobutyl)-FAD.

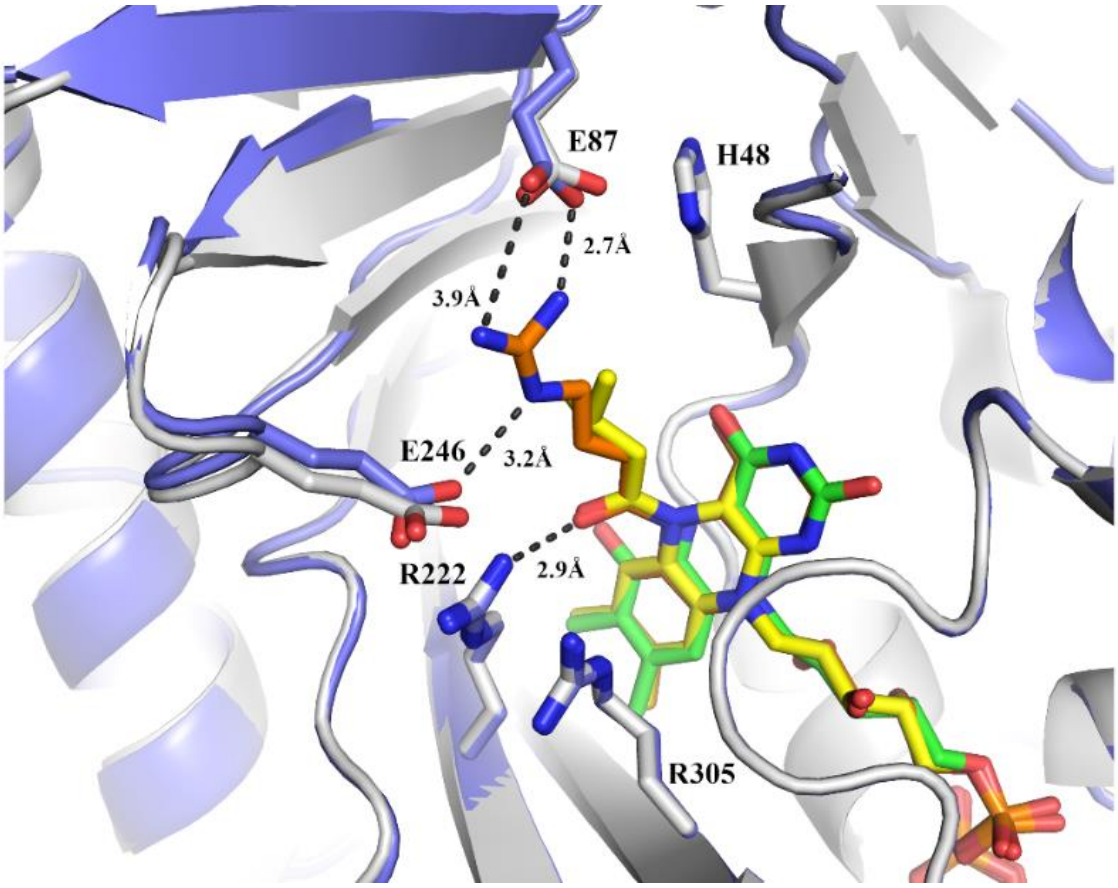

Figure 4.3. Structural overlay of the PaDADH-Y249F (blue) with the N5-(4-guanidino-oxobutyl)-FAD (orange) and the PaDADH-WT (gray) with the N5-(4-methyl-2-pentanone)-FAD (yellow) and 6-OH-FAD shown (green).

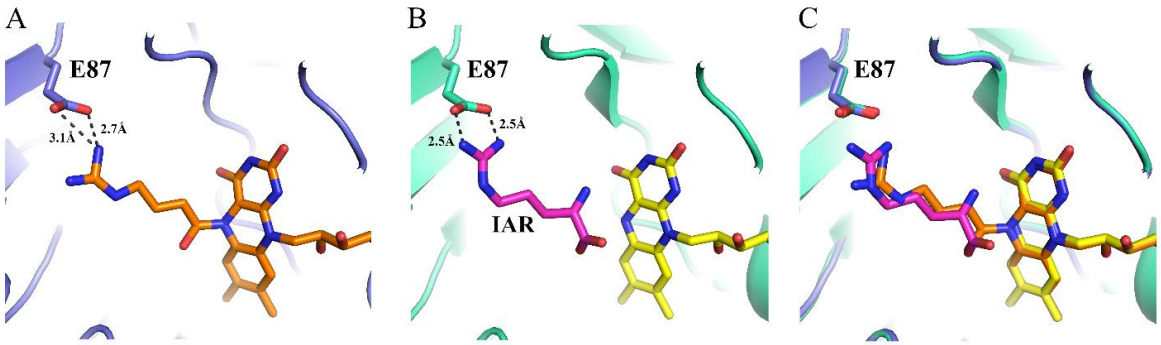

Figure 4.4. A) The active site of PaDADH-Y249F(blue), where residue E87 interacts with the guanidium group of the N5-(4-guanidino-oxobutyl)-FAD (orange). B) The active site of PaDADH-WT (green) shows residue E87 with the guanidinium group of the oxidized product iminoarginine (pink). C) Overlay of the active sites of PaDADH-Y249F (blue) and PaDADH-WT (green).

The formation of a flavin N5-(4-guanidino-oxobutyl)-FAD adduct was independently validated with UV-visible absorption spectroscopy of *Pa*DADH-Y249F incubated aerobically with 15 mM D-arginine at pH 8.0, 4 °C. As shown in Figure 4.5, the enzyme was immediately reduced upon mixing with the substrate, as evidenced by the bleaching of absorption peaks at 345 nm and 445 nm. A slow increase in the absorbance at 445 nm occurred over the next 8 days at 4 °C, indicating a slow oxidation of the reduced enzyme by molecular oxygen (Figure 4.5). Additionally, an increase in absorbance in the 300-420 nm region was observed, yielding a final absorption spectrum different from that of the initial oxidized enzyme (Figure 4. 5). The difference spectrum of the final oxidized enzyme minus the initial oxidized enzyme showed a peak with maximal absorbance at 360 nm, consistent with the formation of a covalent flavin N5 acyl adduct (Figure 4. 5-inset), as previously reported for other N5 adducts in lactate oxidase, monoamine oxidase, nitroalkane oxidase, UDP-galactopyranose mutase and proline dehydrogenase. [33-41] A red-shift of the absorption spectrum of the oxidized enzyme as compared to the initial oxidized enzyme was also observed in the 420-540 nm region, suggesting the formation of a non-covalent complex of the oxidized enzyme incubated in the presence of D-arginine that was devoid of the flavin N5 adduct with excess D-arginine, as previously reported for sarcosine oxidase in complex with sarcosine analogs. [42]

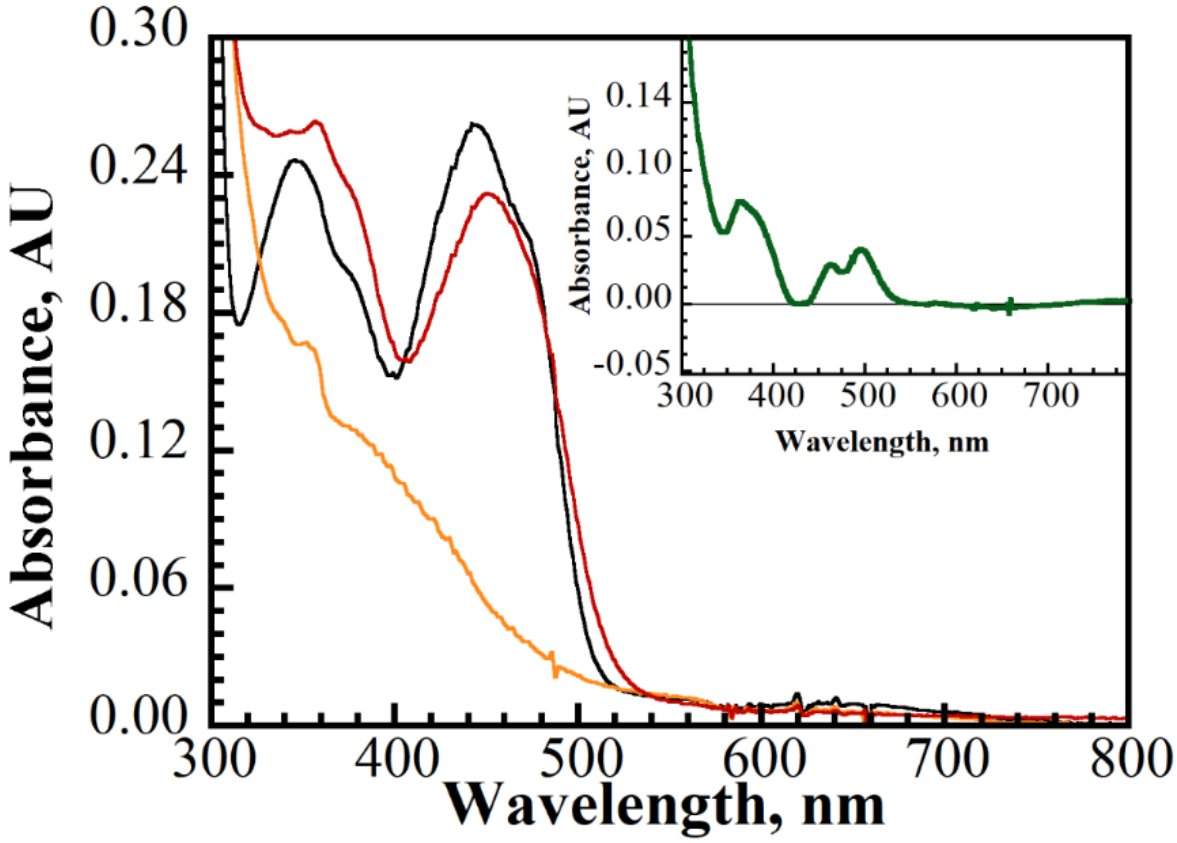

Figure 4.5. UV-Visible absorption spectra of the PaDADH-Y249F. Oxidized enzyme (black) was treated with 15 mM D-arginine to obtain the spectra of the reduced enzyme (orange). Over 8 days of incubation, the reduced enzyme was slowly reoxidized along with an extra feature appearing around 360 nm (red). (Inset) The difference spectra of the enzyme incubated over 8 days and the initial oxidized enzyme with 16% of the oxidized enzyme added back to the spectra (green) to account for the incomplete formation of an N5-acyl adduct.

4.5 DISCUSSION

The versatility of the flavin is apparent in this study, with the reduced flavin in *Pa*DADH-Y249F performing three different functions, e.g., a hydride transfer reaction, a radical, and a nucleophilic reaction resulting in the formation of flavin N5 and C6 adducts (Scheme 4.1). The reduced flavin is oxidized to FAD during regular turnover with a D-amino acid and an electron acceptor like PMS. The reduced flavin forms 6-OH-FAD in the presence of D-alanine and molecular oxygen. The reduced flavin forms a covalent N5-(4-guanidino-oxobutyl) FAD after prolonged incubation

with D-arginine. Previous studies have established that *Pa*DADH-Y249F could turnover with D-arginine and PMS with steady-state kinetic parameters k_{cat}, $k_{cat}/K_{m,}$ and K_m ≤2.5-times lower than those of *Pa*DADH-WT [22]. Moreover, the structure of *Pa*DADH-Y249F reported here contains 6-OH-FAD and N5-(4-guanidino-oxobutyl)-FAD in the active site, both of which require the reduced flavin for their formation (Scheme 1). Thus, the reduced flavin in *Pa*DADH-Y249F can perform at least three documented reactions in the same active site environment.

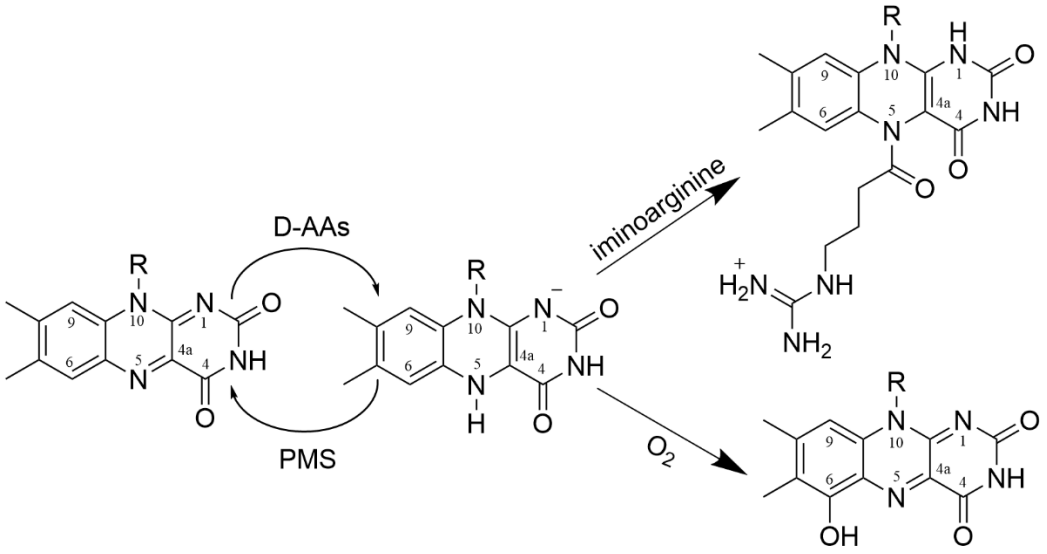

Scheme 4.1. The versatility of the reduced flavin in *Pa*DADH-Y249F.

Previous studies using pH and multiple kinetic isotope effects established that *Pa*DADH binds preferentially the protonated form of the D-amino acid substrate, which is then deprotonated through the release of the α-amino proton to bulk solvent, without the involvement of active site residues [43]. In this respect, the enzyme is like other enzymes that oxidize amino acid substrates, such as L-amino acid oxidase, DAAO, and sarcosine oxidase, which have been shown to oxidize their substrates without the involvement of an active site base [42, 44, 45]. With *Pa*DADH-Y249F previous multiple kinetic isotope effects established that a hydride transfer reaction resulting in the oxidation of D-amino acids occurs with the synchronous cleavage of the substrate NH and CH

bonds [22]. In contrast, the hydride transfer mechanism previously determined with *Pa*DADH-WT demonstrated an asynchronous NH and CH bond cleavage [22, 46]. These results are consistent with the Y249F mutation having a minimal effect on the oxidation reaction catalyzed by the enzyme and a proposed role of the hydroxyl group of Y249 in stabilizing the transition state for bond cleavage [22, 46].

The mechanism for the formation of 6-OH-FAD with *Pa*DADH-Y249F was recently proposed based on $^{18}O_2$ isotope incorporation experiments [14]. As shown in Scheme 4.2, it is proposed that after D-alanine reduces the enzyme-bound FAD, it reacts with O_2 via a single-electron transfer reaction. The resulting flavosemiquinone and superoxide anion then form an unstable C6-hydroperoxo intermediate, which decays to yield 6-OH-FAD.

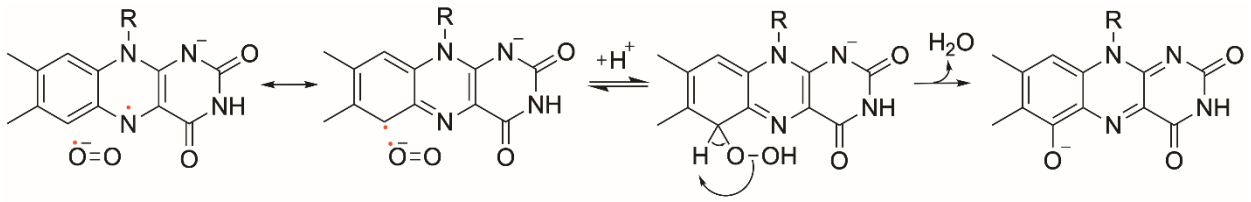

Scheme 4.2. Proposed mechanism for the formation of 6-OH-FAD in *Pa*DADH-Y249F.

The proposed mechanism for the formation of the N5-(4-guanidino-oxobutyl)-FAD in *Pa*DADH-Y249F is illustrated in Scheme 4.3. Briefly, after the oxidized enzyme reacts with D-arginine, the reduced FAD and iminoarginine are formed in the active site of the enzyme. The lone pair electrons of the flavin N5 atom in the reduced FAD then performs a nucleophilic reaction with the carbonyl C atom of the bound iminoarginine forming an unstable (1-carboxyl-4-guanidino-1-iminobutyl)-N5 adduct, which then is hydrolyzed to the N5-(4-guanidino-oxobutyl)-FAD with the elimination of CO_2 and NH_3. Due to a pK_a value of ≥20 [47], at pH 8.0, only a tiny fraction of the reduced flavin has the N5 atom unprotonated, which is required for the nucleophilic reaction, thereby making the formation of the N5 acyl adduct extremely slow. The proposed mechanism for

the formation of N5-(4-guanidino-oxobutyl) in *Pa*DADH-Y249F is similar to the N5-flavin adduct formation reaction previously proposed for D-amino acid oxidase (DAAO), in which it was shown that the reaction of the enzyme with a ketoacid lead to decarboxylation of the ketoacid after its covalent linkage with the flavin N5 atom [48].

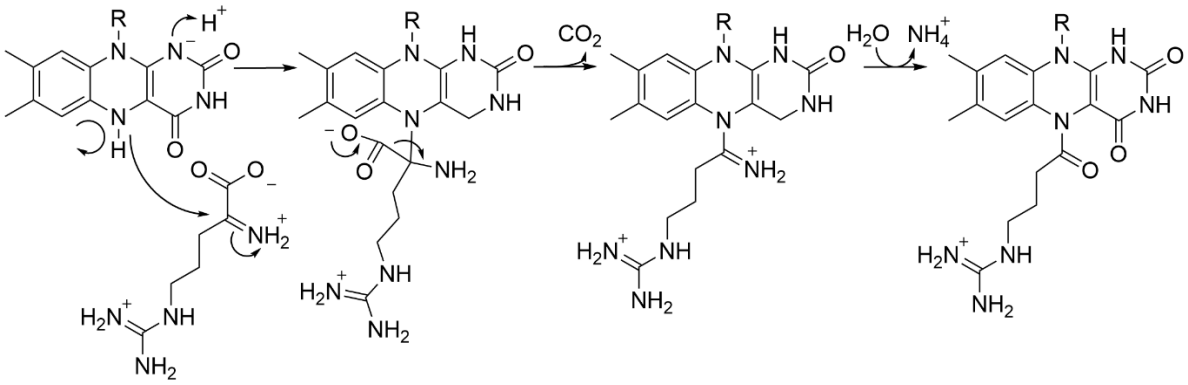

Scheme 3. Proposed mechanism for the formation of N5-(4-guanidino-oxobutyl)-FAD in *Pa*DADH-Y249F**.**

Multiple structures with covalent flavin adducts have been reported previously for many flavin-dependent enzymes [15, 21, 39, 48-53]. However, the presence of two covalently modified flavin cofactors has never been reported in the same crystal structure. In this study, the *Pa*DADH-Y249F structure was determined with 6-OH-FAD and N5-(4-guanidino-oxobutyl)-FAD. The propensity of the enzyme active site to form covalent flavin N5 adducts is supported by a previous structure for *Pa*DADH-WT determined with an N5-(4-methyl-2-pentanone)-FAD in the active site [21]. Another enzyme in the same structural family as *Pa*DADH, DAAO (PDB entry 1DAO, 3.20 Å), was also crystallized with a flavin N5 adduct with 3-methyl-2-oxobutyric acid [48], suggesting an enhanced reactivity of the N5 atom in the reduced flavin in this class of enzymes. The only enzyme other than *Pa*DADH-Y249F that showed 6-OH-FAD in its crystal structures is cellobiose dehydrogenase from *Phanerochaete chrysosporium* [12, 54], a member of the GMC oxidoreductase

superfamily. Most enzyme preparations with 6-OH-flavins have been reported to contain a mixture of regular flavin and the hydroxylated flavin cofactor [12, 22, 55, 56]. The presence of two covalently modified flavins in the *Pa*DADH-Y249F structure is evidence of the enhanced versatility of the reduced flavin in *Pa*DADH-Y249F.

The mutation of tyrosine to phenylalanine and the modifications on the flavin do not affect the overall structure or fold of the enzyme. Superposition of *Pa*DADH-Y249F structure with *Pa*DADH-WT gave an RMSD value of 0.45 for 375 α-carbons, indicating that the Y249F mutation did not affect the overall effect fold of the enzyme. Similarly, when comparing the structure of the *Pa*DADH-Y249F to the previously published structures of *Pa*DADH-Y249F with FAD or 6-OH-FAD, the calculated RMSD values were 0.25 and 0.32 respectively over 375 α-carbons, indicating that the presence of two covalent FAD-adducts does not alter the overall structure of the enzyme. However, altered protein or cofactor dynamics around the flavin can be a significant factor in modulating the reactivity of the flavin cofactor, as recently demonstrated in a computational, biochemical, and structural study of *Pa*DADH-Y249F with FAD, leading it to form 6-OH-FAD [14].

The prevalence of flavin-N5 adducts in systems like *Pa*DADH or DAAO that employ a hydride transfer mechanism in catalysis indicates that the flavin N5 atom can also participate in covalent catalysis leading to a dead-end adduct in these systems. Covalent catalysis has long been employed by flavin-dependent enzymes, with more examples of uncommon covalent reactions in recent literature [15, 50, 57]. While the flavin C4a atom was the most well-studied center for the covalent catalysis in flavin-dependent enzymes, with more examples of catalytically relevant N5 adducts like those found in nitroalkane oxidase, adenylylsulfate reductase, and UDP-galactopyranose

mutase, the flavin N5 atom has now emerged as a new focal point for covalent catalysis [15, 18, 38, 40, 49, 50].

In conclusion, the study presented here used X-ray crystallography and mass spectrometry to demonstrate that the structure of *Pa*DADH-Y249F contained two flavin modifications, i.e., 6-OH-FAD and N5-(4-guanidino-oxobutyl)-FAD. While it is commonly acknowledged that the primary function of the protein in flavoproteins is to modulate flavin reactivity to the extent that unproductive reactions are suppressed in favor of the specific reaction that needs to be catalyzed, this study highlights that the extraordinary versatility of the flavin in flavoproteins could be uncovered within the same active site through a single mutation. The replacement of a tyrosine with phenylalanine yielded an enzyme that maintained the ability to catalyze a hydride transfer reaction during turnover while also acquiring the ability to form two different flavin adducts through radical and nucleophilic reactions. The study also emphasizes the importance of a seemingly inconspicuous hydroxyl group harbored on the side chain of Y249, which, despite playing no direct roles in catalysis and substrate binding, is important to fine-tuning the reactivity of the flavin toward the hydride transfer reaction that oxidizes the D-amino acid substrate while eliminating alternative flavin chemistries that would modify the flavin and inactivate the enzyme. Insights from this and future studies of modified flavins will help steer the flavin cofactor reactivity towards new directions in engineered enzymes in the future [57].

Table 4.1. Data collection and refinement statistics.

PDB code	7RDF
Space group	$P2_12_12_1$
a, *b*, *c* (Å)	60.01, 76.33, 76.76
α, β, γ (°)	90.00, 90.00, 90.00
Resolution range (Å)	47.28 – 1.29 (1.36 - 1.29)
Total No. of reflections	610871 (61270)
No. of unique reflections	86350 (11210)
Redundancy	7.1 (5.5)
Completeness (%)	97.8 (88.5)
$\langle I/\sigma(I) \rangle$	16.3 (5.3)
$R_{sym\ (\%)}$	8.6 (35.7)
CC1/2	0.995 (0.905)
Wilson B-factor (Å^2)	11.94
R_{work} (%)	12.6 (14.7)
R_{free} (%)	15.7 (18.4)
No. of non-H atoms	3816
Protein	3236
Ligand	148
Water	432
Average *B* factors (Å^2)	17.77
Protein	15.84
Ligand	17.69
Water	32.29
RMSD Bonds (Å)/ Angles (°)	0.005/0.85
Ramachandran analyses	
Favored regions (%)	98.12
Allowed regions (%)	1.88%

4.6 REFERENCES

[1] Walsh, C. T., and Wencewicz, T. A. (2013) Flavoenzymes: versatile catalysts in biosynthetic pathways, Nat Prod Rep 30, 175-200.

[2] Percudani, R., and Peracchi, A. (2009) The B6 database: a tool for the description and classification of vitamin B6-dependent enzymatic activities and of the corresponding protein families, BMC Bioinformatics 10, 273.

[3] Kovaleva, E. G., and Lipscomb, J. D. (2008) Versatility of biological non-heme Fe(II) centers in oxygen activation reactions, Nat Chem Biol 4, 186-193.

[4] Li, C., and Stocker, R. (2009) Heme oxygenase and iron: from bacteria to humans, Redox Rep 14, 95-101.

[5] Bruice, T. C., Hevesi, L., and Shinkai, S. (1973) Mechanisms of formation and equilibria of 4a and 5 adducts of an isoalloxazine. Reaction of 10-(2',6'-dimethylphenyl)-3-methylisoalloxazine-6,8-disulfonate with sulfite in aqueous media, Biochemistry 12, 2083-2089.

[6] Eckstein, J. W., Hastings, J. W., and Ghisla, S. (1993) Mechanism of bacterial bioluminescence: 4a,5-dihydroflavin analogs as models for luciferase hydroperoxide intermediates and the effect of substituents at the 8-position of flavin on luciferase kinetics, Biochemistry 32, 404-411.

[7] Ghisla, S., Massey, V., and Yagi, K. (1986) Preparation and some properties of 6-substituted flavins as active site probes for flavin enzymes, Biochemistry 25, 3282-3289.

[8] Ghisla, S., and Mayhew, S. G. (1980) Isolation, synthesis, and properties of 8-hydroxyflavins, Methods Enzymol 66, 241-253.

[9] Massey, V., Husain, M., and Hemmerich, P. (1980) Photodehalogenation of 7- and 8-halogen-substituted flavins. Photochemistry of the reduced flavin chromophore, J Biol Chem 255, 1393-1398.

[10] Mayhew, S. G., Whitfield, C. D., Ghisla, S., and Schuman-Jorns, M. (1974) Identification and properties of new flavins in electron-transferring flavoprotein from Peptostreptococcus elsdenii and pig-liver glycolate oxidase, Eur J Biochem 44, 579-591.

[11] Palfey, B. A., Ballou, D. P., and Massey, V. (1997) Flavin conformational changes in the catalytic cycle of p-hydroxybenzoate hydroxylase substituted with 6-azido- and 6-aminoflavin adenine dinucleotide, Biochemistry 36, 15713-15723.

[12] Hallberg, B. M., Henriksson, G., Pettersson, G., and Divne, C. (2002) Crystal structure of the flavoprotein domain of the extracellular flavocytochrome cellobiose dehydrogenase, J Mol Biol 315, 421-434.

[13] Massey, V., Ghisla, S., and Yagi, K. (1986) 6-Azido- and 6-aminoflavins as active-site probes of flavin enzymes, Biochemistry 25, 8095-8102.

[14] Iyer, A., Reis, R. A. G., Gannavaram, S., Momin, M., Spring-Connell, A. M., Orozco-Gonzalez, Y., Agniswamy, J., Hamelberg, D., Weber, I. T., Gozem, S., Wang, S., Germann, M. W., and Gadda, G. (2021) A Single-Point Mutation in d-Arginine Dehydrogenase Unlocks a Transient Conformational State Resulting in Altered Cofactor Reactivity, Biochemistry 60, 711-724.

[15] Beaupre, B. A., and Moran, G. R. (2020) N5 Is the New C4a: Biochemical Functionalization of Reduced Flavins at the N5 Position, Front Mol Biosci 7, 598912.

[16] Saleem-Batcha, R., and Teufel, R. (2018) Insights into the enzymatic formation, chemical features, and biological role of the flavin-N5-oxide, Curr Opin Chem Biol 47, 47-53.

[17] Teufel, R., Agarwal, V., and Moore, B. S. (2016) Unusual flavoenzyme catalysis in marine bacteria, Curr Opin Chem Biol 31, 31-39.

[18] Adak, S., and Begley, T. P. (2017) Flavin-N5-oxide: A new, catalytic motif in flavoenzymology, Arch Biochem Biophys 632, 4-10.

[19] Fu, G., Yuan, H., Li, C., Lu, C. D., Gadda, G., and Weber, I. T. (2010) Conformational changes and substrate recognition in Pseudomonas aeruginosa D-arginine dehydrogenase, Biochemistry 49, 8535-8545.

[20] Li, C., and Lu, C. D. (2009) Arginine racemization by coupled catabolic and anabolic dehydrogenases, Proc Natl Acad Sci U S A 106, 906-911.

[21] Fu, G., Yuan, H., Wang, S., Gadda, G., and Weber, I. T. (2011) Atomic-resolution structure of an N5 flavin adduct in D-arginine dehydrogenase, Biochemistry 50, 6292-6294.

[22] Gannavaram, S., Sirin, S., Sherman, W., and Gadda, G. (2014) Mechanistic and computational studies of the reductive half-reaction of tyrosine to phenylalanine active site variants of D-arginine dehydrogenase, Biochemistry 53, 6574-6583.

[23] Battye, T. G., Kontogiannis, L., Johnson, O., Powell, H. R., and Leslie, A. G. (2011) iMOSFLM: a new graphical interface for diffraction-image processing with MOSFLM, Acta Crystallogr D Biol Crystallogr 67, 271-281.

[24] Evans, P. (2006) Scaling and assessment of data quality, Acta Crystallogr D Biol Crystallogr 62, 72-82.

[25] Collaborative Computational Project, N. (1994) The CCP4 suite: programs for protein crystallography, Acta Crystallogr D Biol Crystallogr 50, 760-763.

[26] McCoy, A. J., Grosse-Kunstleve, R. W., Adams, P. D., Winn, M. D., Storoni, L. C., and Read, R. J. (2007) Phaser crystallographic software, J Appl Crystallogr 40, 658-674.

[27] Afonine, P. V., Grosse-Kunstleve, R. W., Echols, N., Headd, J. J., Moriarty, N. W., Mustyakimov, M., Terwilliger, T. C., Urzhumtsev, A., Zwart, P. H., and Adams, P. D. (2012) Towards automated crystallographic structure refinement with phenix.refine, Acta Crystallogr D Biol Crystallogr 68, 352-367.

[28] Emsley, P., Lohkamp, B., Scott, W. G., and Cowtan, K. (2010) Features and development of Coot, Acta Crystallogr D Biol Crystallogr 66, 486-501.

[29] Moriarty, N. W., Grosse-Kunstleve, R. W., and Adams, P. D. (2009) electronic Ligand Builder and Optimization Workbench (eLBOW): a tool for ligand coordinate and restraint generation, Acta Crystallogr D Biol Crystallogr 65, 1074-1080.

[30] Chen, V. B., Arendall, W. B., 3rd, Headd, J. J., Keedy, D. A., Immormino, R. M., Kapral, G. J., Murray, L. W., Richardson, J. S., and Richardson, D. C. (2010) MolProbity: all-atom structure validation for macromolecular crystallography, Acta Crystallogr D Biol Crystallogr 66, 12-21.

[31] Pettersen, E. F., Goddard, T. D., Huang, C. C., Couch, G. S., Greenblatt, D. M., Meng, E. C., and Ferrin, T. E. (2004) UCSF chimera - A visualization system for exploratory research and analysis, J Comput Chem 25, 1605-1612.

[32] Yuan, H., Fu, G., Brooks, P. T., Weber, I., and Gadda, G. (2010) Steady-state kinetic mechanism and reductive half-reaction of D-arginine dehydrogenase from Pseudomonas aeruginosa, Biochemistry 49, 9542-9550.

[33] Campbell, A. C., Becker, D. F., Gates, K. S., and Tanner, J. J. (2020) Covalent Modification of the Flavin in Proline Dehydrogenase by Thiazolidine-2-Carboxylate, ACS Chem Biol 15, 936-944.

[34] White, T. A., Johnson, W. H., Jr., Whitman, C. P., and Tanner, J. J. (2008) Structural basis for the inactivation of Thermus thermophilus proline dehydrogenase by N-propargylglycine, Biochemistry 47, 5573-5580.

[35] Srivastava, D., Zhu, W., Johnson, W. H., Jr., Whitman, C. P., Becker, D. F., and Tanner, J. J. (2010) The structure of the proline utilization a proline dehydrogenase domain inactivated by N-propargylglycine provides insight into conformational changes induced by substrate binding and flavin reduction, Biochemistry 49, 560-569.

[36] Ghisla, S., and Massey, V. (1980) Studies on the catalytic mechanism of lactate oxidase. Formation of enantiomeric flavin-N(5)-glycollyl adducts via carbanion intermediates, J Biol Chem 255, 5688-5696.

[37] Massey, V., Ghisla, S., and Kieschke, K. (1980) Studies on the reaction mechanism of lactate oxidase. Formation of two covalent flavin-substrate adducts on reaction with glycollate, J Biol Chem 255, 2796-2806.

[38] Gadda, G., Edmondson, R. D., Russell, D. H., and Fitzpatrick, P. F. (1997) Identification of the naturally occurring flavin of nitroalkane oxidase from fusarium oxysporum as a 5-nitrobutyl-FAD and conversion of the enzyme to the active FAD-containing form, J Biol Chem 272, 5563-5570.

[39] Nagai, T., Unno, H., Janczak, M. W., Yoshimura, T., Poulter, C. D., and Hemmi, H. (2011) Covalent modification of reduced flavin mononucleotide in type-2 isopentenyl diphosphate isomerase by active-site-directed inhibitors, Proc Natl Acad Sci U S A 108, 20461-20466.

[40] Mehra-Chaudhary, R., Dai, Y., Sobrado, P., and Tanner, J. J. (2016) In Crystallo Capture of a Covalent Intermediate in the UDP-Galactopyranose Mutase Reaction, Biochemistry 55, 833-836.

[41] Albreht, A., Vovk, I., Mavri, J., Marco-Contelles, J., and Ramsay, R. R. (2018) Evidence for a Cyanine Link Between Propargylamine Drugs and Monoamine Oxidase Clarifies the Inactivation Mechanism, Front Chem 6, 169.

[42] Wagner, M. A., Trickey, P., Chen, Z. W., Mathews, F. S., and Jorns, M. S. (2000) Monomeric sarcosine oxidase: 1. Flavin reactivity and active site binding determinants, Biochemistry 39, 8813-8824.

[43] Ball, J., Bui, Q. V., Gannavaram, S., and Gadda, G. (2015) Importance of glutamate 87 and the substrate alpha-amine for the reaction catalyzed by D-arginine dehydrogenase, Arch Biochem Biophys 568, 56-63.

[44] Porter, D. J., and Bright, H. J. (1980) Interpretation of the pH dependence of flavin reduction in the L-amino acid oxidase reaction, J Biol Chem 255, 2969-2975.

[45] Harris, C. M., Pollegioni, L., and Ghisla, S. (2001) pH and kinetic isotope effects in d-amino acid oxidase catalysis, Eur J Biochem 268, 5504-5520.

[46] Yuan, H., Xin, Y., Hamelberg, D., and Gadda, G. (2011) Insights on the mechanism of amine oxidation catalyzed by D-arginine dehydrogenase through pH and kinetic isotope effects, J Am Chem Soc 133, 18957-18965.

[47] Macheroux, P., Ghisla, S., Sanner, C., Ruterjans, H., and Muller, F. (2005) Reduced flavin: NMR investigation of N5-H exchange mechanism, estimation of ionisation constants and assessment of properties as biological catalyst, BMC Biochem 6, 26.

[48] Todone, F., Vanoni, M. A., Mozzarelli, A., Bolognesi, M., Coda, A., Curti, B., and Mattevi, A. (1997) Active site plasticity in D-amino acid oxidase: a crystallographic analysis, Biochemistry 36, 5853-5860.

[49] Fritz, G., Roth, A., Schiffer, A., Buchert, T., Bourenkov, G., Bartunik, H. D., Huber, H., Stetter, K. O., Kroneck, P. M., and Ermler, U. (2002) Structure of adenylylsulfate reductase from the hyperthermophilic Archaeoglobus fulgidus at 1.6-A resolution, Proc Natl Acad Sci U S A 99, 1836-1841.

[50] Leys, D., and Scrutton, N. S. (2016) Sweating the assets of flavin cofactors: new insight of chemical versatility from knowledge of structure and mechanism, Curr Opin Struct Biol 41, 19-26.

[51] Binda, C., Newton-Vinson, P., Hubalek, F., Edmondson, D. E., and Mattevi, A. (2002) Structure of human monoamine oxidase B, a drug target for the treatment of neurological disorders, Nat Struct Biol 9, 22-26.

[52] De Colibus, L., Li, M., Binda, C., Lustig, A., Edmondson, D. E., and Mattevi, A. (2005) Three-dimensional structure of human monoamine oxidase A (MAO A): relation to the structures of rat MAO A and human MAO B, Proc Natl Acad Sci U S A 102, 12684-12689.

[53] Mattevi, A., Fraaije, M. W., Mozzarelli, A., Olivi, L., Coda, A., and van Berkel, W. J. (1997) Crystal structures and inhibitor binding in the octameric flavoenzyme vanillyl-alcohol oxidase: the shape of the active-site cavity controls substrate specificity, Structure 5, 907-920.

[54] Hallberg, B. M., Henriksson, G., Pettersson, G., Vasella, A., and Divne, C. (2003) Mechanism of the reductive half-reaction in cellobiose dehydrogenase, J Biol Chem 278, 7160-7166.

[55] Igarashi, K., Verhagen, M. F., Samejima, M., Schulein, M., Eriksson, K. E., and Nishino, T. (1999) Cellobiose dehydrogenase from the fungi Phanerochaete chrysosporium and Humicola insolens. A flavohemoprotein from Humicola insolens contains 6-hydroxy-FAD as the dominant active cofactor, J Biol Chem 274, 3338-3344.

[56] Huang, L., Scrutton, N. S., and Hille, R. (1996) Reaction of the C30A mutant of trimethylamine dehydrogenase with diethylmethylamine, J Biol Chem 271, 13401-13406.

[57] Piano, V., Palfey, B. A., and Mattevi, A. (2017) Flavins as Covalent Catalysts: New Mechanisms Emerge, Trends Biochem Sci 42, 457-469.

5 CHARACTERIZATION OF A COUPLED-ENZYME D-ARGININE CONVERSION SYSTEM FROM PSEUDOMONAS AERUGINOSA

5.1 ABSTRACT

L-arginine dehydrogenase (*Pa*LADH) and D-arginine dehydrogenase (*Pa*DADH) from *Pseudomonas aeruginosa* are part of a two-enzyme system that catalyzes the irreversible conversion of D-arginine to L-arginine. *Pa*DADH is an FAD-dependent enzyme that catalyzes the oxidation of D-arginine into 2-ketoarginine and ammonia. *Pa*LADH catalyzes the conversion of 2-ketoarginine and ammonia to L-arginine using NADH as a substrate in the forward direction and catalyzes the conversion of L-arginine using NAD^+ in the reverse direction to ketoarginine and ammonia. The coupled-enzyme system enables *P. aeruginosa* to survive solely on D-arginine as a nitrogen and carbon source. The formation of a protein-protein complex of *Pa*LADH and *Pa*DADH was probed using analytical ultracentrifugation and size-exclusion chromatography. The turnover number, k_{cat}, for *Pa*LADH with L-arginine and NAD^+ as substrates was measured using a stopped-flow instrument and for the coupled-enzyme assay in which both enzymes were mixed with the substrates D-arginine, benzoquinone, and NADH. The utilization of the coupled enzyme system to metabolize D-arginine has given *P. aeruginosa* an edge over other bacteria to survive in nutrient-limiting conditions, and further studies will help us further understand the role of this novel system.

5.2 INTRODUCTION

Pseudomonas aeruginosa is a persistent and opportunistic pathogen and is the leading cause of mortality by infection in cystic fibrosis (CF) patients.[1-5] While many other bacteria also colonize the lungs of cystic fibrosis patients, *P. aeruginosa* remains the dominant pathogen.[6, 7] The CF lung environment is very complex, and not a lot is known about the selection pressures for certain strains of microbes over others.[3] *P. aeruginosa* is prone to grow biofilms and can be resistant to antimicrobials in its mucoid form.[3-5, 7, 8] The tracts of CF patients are quite congested with sputum are generally devoid of many high-value nutrients.[7] Gene expression profiles of virulent *P. aeruginosa* strains cultured in minimal media reveal several amino acid transporter genes, amino acid biosynthesis genes, and amino acid degradation genes along with alginate genes are constitutively expressed. Experiments also confirmed the utilization of amino acids from lyophilized sputum to establish the utilization of amino acids by *P. aeruginosa* as a carbon and nitrogen source.[6]

P. aeruginosa PAO1 is one of the few strains known to survive on just D-amino acids as nutrients and can utilize D-alanine, D-glutamate, D-glutamine, and D-arginine as the sole carbon and nitrogen sources.[9-11] DadA, a D-alanine dehydrogenase and a product of the *dadRAX* operon in *P. aeruginosa*, is responsible for D-alanine metabolism and regulation.[10] DadA was characterized to have D-amino acid dehydrogenase activity with broad substrate specificity and is overexpressed in virulent strains of *P. aeruginosa*, suggesting that D-amino acids play a significant role in virulence.[2] PAO1 has multiple operons similar to the *dadRAX* operon to participate in D-amino acid metabolism like *dguR-dguABC* operon established to be essential for D-glutamate catabolism and the *dauBAR* operon reported to be essential for D-arginine utilization. [9, 11, 12]

The expression of the *dauBAR* operon is regulated by two transcriptional regulators, ArgR, which functions as an activator, and DauR, which acts as a repressor.[11] The *dauBAR* operon also encodes DauA, an FAD-dependent D-arginine dehydrogenase (*Pa*DADH), and DauB, L-arginine dehydrogenase (*Pa*LADH), both of which function as a coupled-enzyme D-arginine conversion system in *P. aeruginosa* (Scheme 5.1).[11, 12] *P. aeruginosa* strains with *dauA* and *dauB* knocked out lost the ability to utilize D-arginine as a sole carbon and nitrogen source.[11, 12]

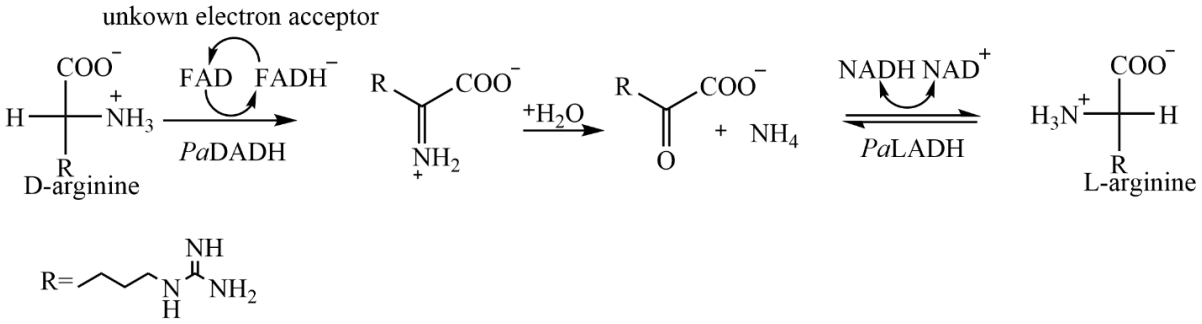

Scheme 5.1. Scheme for the conversion of D-arginine to L-arginine using the two-enzyme system of PaDADH and PaLADH.

*Pa*DADH has been characterized kinetically as a dehydrogenase with broad substrate specificity.[13, 14] The highest activity of *Pa*DADH was shown to be with D-arginine and D-lysine and no activity with D-glutamate and D-aspartate as substrates, highlighting the enzyme's preference for substrates with cationic side chains. [11, 14] *Pa*DADH catalyzes the oxidation of D-arginine to iminoarginine, which is hydrolyzed to form 2-ketoarginine and ammonia. *Pa*DADH is a true dehydrogenase as it does not utilize molecular oxygen, and kinetic assays are determined using an artificial electron acceptor like phenazine methosulfate (PMS) (Scheme 5.1). Multiple structures have also been reported for *Pa*DADH.[13, 14] DauB or *Pa*LADH is the second enzyme in the sequence and can catalyze an NADH-dependent conversion of 2-ketoarginine and ammonia to L-arginine (Scheme 5.1).[12 9, 12] *Pa*LADH can also catalyze the reverse reaction, which converts L-arginine to ketoarginine and ammonia, generating NADH in the process (Scheme 5.1).[12]

Most racemases are commonly single PLP-dependent or PLP-independent enzymes that catalyze the conversion of D- to L- forms, so the function of two enzymes to catalyze a D- to L- conversion seems a little elusive.[15] In this study, we characterize the steady-state kinetic mechanism of *Pa*LADH, investigate the coupled-enzyme D-arginine conversion system through kinetics, and analyze the protein-protein interactions between *Pa*DADH and *Pa*LADH.

5.3 MATERIALS AND METHODS

5.3.1 Materials

The pET20b(+) plasmid harboring the PA3862 gene, which encodes *Pa*LADH optimized for E.coli expression, was purchased from GenScript (Piscataway, NJ). *Escherichia coli* strain Rosetta (DE3) pLysS was from Novagen (Madison, WI). BSA was purchased from Promega (Madison, WI), chloramphenicol, IPTG, lysozyme, sodium hydrosulfite (dithionite), phenazine methosulfate (PMS), and PMSF were obtained from Sigma-Aldrich (St. Louis, MO). Ampicillin was purchased from ICN Biomedicals (Aurora, OH). NADH and NADPH disodium salts were purchased from VWR (Radnor, PA). All other reagents used were of the highest purity commercially available.

5.3.2 Expression and Purification

A permanently frozen stock containing *Escherichia coli* Rosetta (DE3) pLysS harboring the plasmid pET20b (+)/*PA*3862 was used to inoculate 50 mL of Luria-Bertani broth medium containing 100 μg/mL ampicillin and 34 μg/mL chloramphenicol, and cultures were grown at 37 °C for 16 h to be used as a preculture. The starting precultures (30 mL) were used to inoculate 3 L of Terrific Broth medium containing 100 μg/mL ampicillin and 34 μg/mL chloramphenicol. The cell cultures were incubated at 30 °C with shaking at 160 rpm and allowed to reach an optical density of ~0.8 at 600 nm, IPTG was added to a final concentration of 200 μM, and the induced

cultures were incubated for 3 hours at 30 °C. The cells were harvested by centrifugation at 5,000 g for 30 min. The resulting pellet was re-suspended in lysis buffer (10 mM imidazole, 300 mM NaCl, 10% (v/v) glycerol, 1 mM phenylmethylsulphonyl fluoride, 5 mM $MgCl_2$, 2 mg/mL of lysozyme, 5 μg/mL of DNase, 5 μg/mL of RNase, and 20 mM sodium phosphate, pH 7.8 at a ratio of 4 mL per 1 g of wet cell paste and subjected to several cycles of sonication. The resulting cell-free extract obtained after centrifugation at 10,000 g for 25 min was loaded directly onto a HisTrap 5 mL affinity column equilibrated with buffer A (25 mM imidazole, 300 mM NaCl, 10% (v/v) glycerol, and 20 mM potassium phosphate, pH 7.8). After washing with 5 column volumes of buffer A at 5 mL/min, *Pa*LADH was eluted with 35% B (500 mM imidazole, 300 mM NaCl, 10% (v/v) glycerol, and 20 mM sodium phosphate, pH 7.8) and two fractions were collected. The two fractions of the purified *Pa*LADH were dialyzed against 20 mM sodium phosphate, pH 7.8, 10% glycerol, and stored at -20 °C.

5.3.3 Enzymatic Assay

The activity of the two fractions of purified *Pa*LADH was tested using the reverse reaction for *Pa*LADH, which would lead to oxidation of L-arginine to ketoarginine and ammonia, generating NADH from NAD^+. The experiment was conducted on an Agilent UV-Vis spectrophotometer under the following conditions: 50 mM L-arginine, 8 mM NAD^+ in 50 mM Tris-Cl pH 8.0 at 25°C. NADH generation was monitored at 340 nm by plotting the change in absorbance against time (seconds) ($\varepsilon 340 = 6220\ M^{-1}\ cm^{-1}$).

Table 5.1. Purification table for Ni-NTA purification of 6x His-tagged *Pa*LADH.

Sample	Vol (mL)	U/mL	$U_{(total)}$	mg/mL	$mg_{(total)}$	U/mg	Yield
Cell-free extract	53	9.0	477	120.0	6360	0.01	1
Fraction A	15	9.7	145	5.3	80	1.8	0.31
Fraction B	50	3.1	155	1.2	60	2.6	0.33

Conditions: 50 mM Tris-Cl, 30°C, pH 8. Substrates- NAD^+ and L-arginine.

Specific activity (U/mg) is calculated by dividing the total units of activity by the total protein.

5.3.4 Sedimentation velocity analytical ultracentrifugation

The sedimentation profiles of wild-type *Pa*DADH, *Pa*LADH, and the mixture of *Pa*LADH and *Pa*DADH samples were compared using analytical ultracentrifugation (SVAUC) analysis. AUC cells equipped with 12 mm double-sector Epon centerpieces and quartz windows were equilibrated at 20 °C in an AN50 Ti rotor for 1 h and then loaded with the samples. For Experiment 1, the left and right sectors of each cell were loaded with 400 μL of *Pa*DADH (17μM and 66 μM respectively), *Pa*LADH (10 μM and 80 μM respectively) and the mixture of *Pa*LADH and *Pa*DADH (8 μM:10 μM and 20 μM:20 μM respectively). Sedimentation velocity data were collected using a Beckman Optima analytical ultracentrifuge at a rotor speed of 40,000 rpm (128,794 g) at 20 °C. All the samples were buffered with 50 mM TRIS-Cl, pH 8.0, 10% glycerol. The buffer viscosity of 0.01391 Poise and 1.04 g/mL density were calculated using UltraScan (www.ultrascan.uthscsa.edu). Sedimentation velocity data were analyzed using both SEDFIT (www.analyticalultracentrifugation.com) and UltraScan. Continuous sedimentation coefficient distribution (c(s)) analyses were restrained by maximum entropy regularization at $P = 0.95$ confidence interval. The baseline, meniscus, frictional coefficient, systematic time-invariant, and

radial invariant noise were fit. The resulting averaged distribution data were plotted using KaleidaGraph.

5.3.5 Size-exclusion chromatography

The molecular weight of *Pa*DADH, *Pa*LADH, and the protein complex of *Pa*DADH and *Pa*LADH under non-denaturing conditions as determined by size exclusion chromatography. A Sephacryl S-200 HR column was connected to an Akta Start FPLC system and equilibrated with 50 mM sodium phosphate and 50 mM sodium pyrophosphate, pH 9.0, 100 mM NaCl, and 50 mM L-arginine at a flow rate of 0.5 ml/min. The following proteins along with Dextran blue [2000 kDa] were used as standards: Ferritin [440 kDa], Aldolase [158 kDa], Conalbumin [75 kDa], and Ovalbumin [44 kDa].

5.3.6 Kinetics

Time-resolved absorbance spectroscopy was used to measure the kinetics for the reverse reaction of *Pa*LADH using the generation of NADH from NAD^+. NADH or NADPH generation was monitored by following the absorbance at 340 nm ($\varepsilon 340 = 6220\ M^{-1}\ cm^{-1}$) using an SF-61DX2 KinetAsyst high-performance stopped-flow spectrophotometer in 100 mM Tris-HCl (pH 8.0), 10% glycerol, and atmospheric oxygen at 25 °C. The range of concentrations were 0.5 mM to 5.0 mM for NAD^+ and 0.5 mM to 15.0 mM for L-arginine. The enzyme concentration was 0.4 μM.

5.3.7 Coupled-enzyme assay

Time-resolved absorbance spectroscopy was used to measure the kinetics for the coupled-enzyme reaction (Scheme 5.2). D-arginine was provided for D-arginine dehydrogenase along with benzoquinone as an artificial electron acceptor. Syringe A contained a mixture of both the enzymes *Pa*DADH and *Pa*LADH at 0.4 μM each and 10 μM benzoquinone. Syringe B contained D-arginine

[10 µM-300 µM] and NADH or NADPH [8-160 µM]. The SF- 61DX2 KinetAsyst high-performance stopped-flow spectrophotometer was used in single mixing mode to mix the contents of both syringes and monitor the reaction catalyzed by *Pa*LADH using the consumption of NADH at 340 nm. NADH or NADPH oxidation was monitored by following the absorbance at 340 nm (ε_{340} = 6220 M^{-1} cm^{-1}) in 100 mM Tris-HCl (pH 8.0), 10% glycerol, and atmospheric oxygen at 25 °C. The instrument dead time was 2.2 ms. The ranges for D-arginine and NADH were [10 µM-300 µM] and [8-160 µM] respectively, and benzoquinone was kept constant at 10 µM.

5.3.8 Data analysis

Kinetic data were fit using the Kaleidagraph software. The apparent steady-state kinetic parameters were determined by fitting the initial reaction rates derived from the stopped-flow traces (points fit a straight line) to the Michaelis-Menten equation (Equation 1). The steady-state kinetics parameter for the reverse reaction of *Pa*LADH was fit to the ternary-complex equation (Equation 5.2). In these equations, *e* denotes the concentration of enzyme. k_{cat} is the turnover number for the reverse reaction of *Pa*LADH (at saturating concentrations of L-arginine and NAD^+) and the coupled-enzyme assay (at saturating concentrations of D-arginine and NADH). K_a and K_b represent the Michaelis constants for the L-arginine and NAD^+, respectively, and K_{ia} is the substrate inhibition constants for L-arginine.

$$\frac{v_o}{e} = \frac{k_{cat}[A]}{K_m+[A]}$$

Equation 5.1

$$\frac{v}{e} = \frac{k_{\mathrm{cat}}AB}{K_bA+AB+K_{ia}K_b}$$

Equation 5.2

5.3.9 Homology Modeling

A homology model for *Pa*LADH was developed using Robetta, a relatively accurate protein structure prediction service based on deep learning methods: RoseTTAFold and TrRosetta,

and allows for custom sequence alignments for homology modeling.[16-19] Since an experimentally determined model for alanine dehydrogenase (PDB: 1omo) with a high sequence similarity of 70 % to *Pa*LADH existed, comparative modeling was then used to determine the homology model for *Pa*LADH using the structure for alanine dehydrogenase as a template.[20, 21]

5.4 RESULTS

The recombinant protein *Pa*LADH was overexpressed in *E. coli* strain Rosetta (DE3) pLysS and purified with a NiNTA as determined by SDS-PAGE (data not shown). The purified enzyme's activity was tested by monitoring the generation of NADH (Scheme 5.1), as shown in Table 5.1.

As a first step toward characterizing *Pa*LADH kinetically, the steady-state kinetic mechanism was investigated by varying concentrations of NAD^+ and L-arginine at pH 8.0 and 25 °C. The k_{cat}, K_{NAD^+}, $K_{L\text{-}arg}$, k_{cat}/K_{NAD^+}, and $k_{cat}/K_{L\text{-}arg}$ are reported in Table 5.2. A k_{cat} value of 8.0 ± 0.5 s^{-1}, with K_m values obtained for NAD^+ (3.2 ± 0.5 mM) and L-arginine (4.1 ± 0.8 mM), yielded a k_{cat}/ K_{NAD^+} value of (2.5 ± 0.5) x 10^3 $M^{-1}s^{-1}$ and a $k_{cat}/ K_{L\text{-}arg}$ value of (2.0 ± 0.5) x 10^3 $M^{-1}s^{-1}$.

Table 5.2. Steady-State kinetic parameters for *Pa*LADH.

k_{cat}, s^{-1}	8.0 ± 0.5
K_{NAD^+}, mM	3.2 ± 0.5
k_{cat}/ K_{NAD^+}, $M^{-1}s^{-1}$	(2.5 ± 0.5) x 10^3
$K_{L\text{-}arg}$, mM	4.1 ± 0.8
$k_{cat}/ K_{L\text{-}arg}$, $M^{-1}s^{-1}$	(2.0 ± 0.5) x 10^3
K_{ia}	2.1 ± 0.8

Conditions: 100 mM Tris-Cl, 25°C, pH 8.0. Substrates- NAD^+ [0.5 mM-5.0 mM] and L-arginine [0.5 mM-15.0 mM]. Concentration of enzyme was constant at 0.4 μM.

*Pa*LADH follows a ternary-complex mechanism, as evidenced by the double-reciprocal plots (Figure 5.1) as a function of the substrates NAD^+ and L-arg. A ternary-complex mechanism is as expected for an enzyme mechanism that involves a hydride transfer between NAD^+ and L-arginine in the absence of any other associated cofactors (Figure 5.1). *Pa*LADH was also tested against L-lysine in the reverse direction with NAD^+ and pyruvate with NH_4Cl and NADH in the forward direction, and no activity was observed spectroscopically, which demonstrates the strict specificity of *Pa*LADH for arginine and its keto analog.

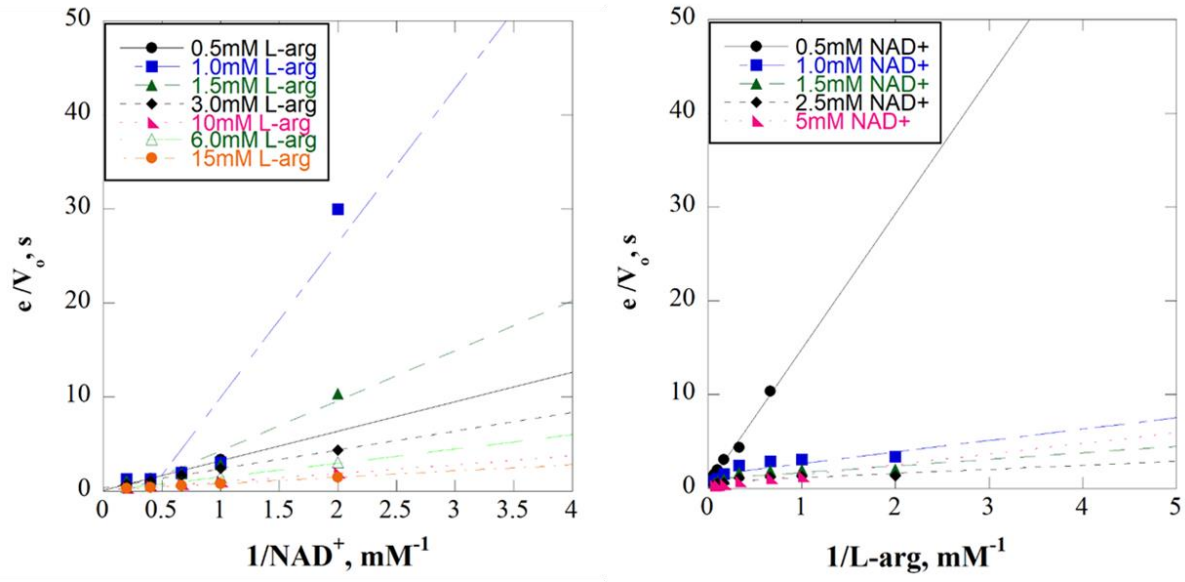

Figure 5.1. Lineweaver−Burk plot for the reverse reaction of *Pa*LADH with NAD^+ and L-arginine as substrates. Data were fit to eq 5.2.

To validate the D-arginine conversion system from *P. aeruginosa* functionally, the kinetics were evaluated with both enzymes as part of the coupled-enzyme reaction. *Pa*DADH is the first enzyme in the D-arginine conversion system. As substrates are provided to the first enzyme *Pa*DADH, the enzyme turns over, generating substrates for the second enzyme *Pa*LADH (Scheme 5.2). D-arginine and benzoquinone as an artificial electron acceptor were used as substrates for *Pa*DADH, present in the reaction mixture with *Pa*LADH and NADH. The oxidation of NADH is

monitored with the stopped-flow spectrophotometer, and the concentration dependence of the coupled-enzyme reaction on D-arginine and NADH is also tested to yield a k_{cat} of 1.3 ± 0.1 s^{-1} along with other kinetic parameters listed in Table 5.3. The K_m value determined for D-arginine for the coupled-enzyme assay was 50 ± 5 µM, while a K_m for NADH could not be established due to the lower limit of the instrument being used to monitor NADH consumption, it is estimated to be below 5 µM. A $k_{cat}/ K_{D\text{-}arg}$ value of (26 ± 3) x 10^3 $M^{-1}s^{-1}$ was determined, and no k_{cat}/ K_{NADH} could be established but is estimated to be in the range of 10^5-10^6 $M^{-1}s^{-1}$. The lower k_{cat} value obtained for the coupled-enzyme reaction probing the forward direction for *Pa*LADH could be due to the formation of the protein-complex between *Pa*DADH and *Pa*LADH being slow, or the kinetics of the transfer of substrates from one enzyme to the other being rate-limiting.

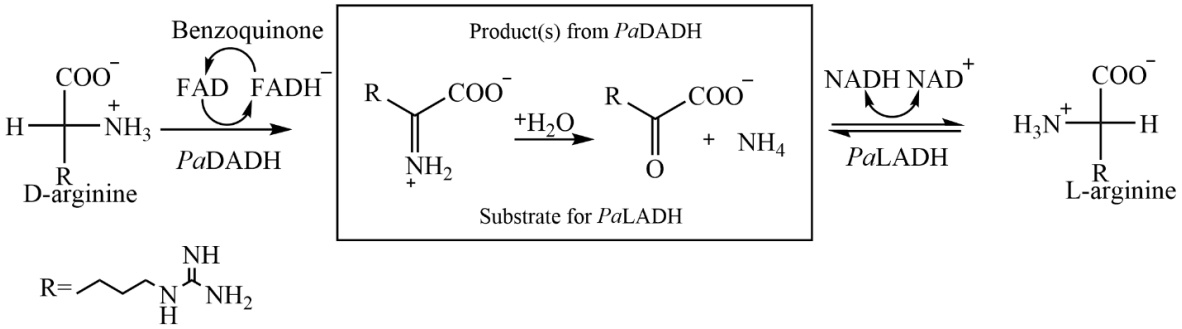

Scheme 5.2. Schematics for the coupled-enzyme assay.

Table 5.3. Kinetic parameters for the coupled-enzyme assay.

k_{cat}, s^{-1}	1.3 ± 0.1
K_{NADH}, µM	≤ 5
k_{cat}/ K_{NADH}, $M^{-1}s^{-1}$	N.D.
$K_{D\text{-}arg}$, µM	50 ± 5
$k_{cat}/ K_{D\text{-}arg}$, $M^{-1}s^{-1}$	(26 ± 3) x 10^3

Conditions: 100 mM Tris-Cl, 25°C, pH 8.0. Substrates- D-arginine [10 µM-300 µM], NADH [8-160 µM] and benzoquinone was kept constant at 10 µM. The concentration of the two enzymes *Pa*DADH and *Pa*LADH were kept constant at 0.4 µM.

As the coupled-enzyme D-arginine conversion system was determined to be functional by the coupled-enzyme assays using stopped-flow kinetics. Multiple techniques were used to test the hypothesis that the two enzymes *Pa*DADH and *Pa*LADH form a protein complex to carry out the D- to L- conversion of D-arginine. Sedimentation velocity analytical ultracentrifugation (SVAUC) analysis was used to establish the oligomeric state of *Pa*DADH, *Pa*LADH, and a possible complex of *Pa*DADH and *Pa*LADH. Data for the *Pa*LADH was inconclusive, as there was significant agglomeration observed in the conditions used. The SVAUC data for *Pa*DADH revealed a sharp peak at 2.8 S (Figure 5.2), estimated to a mass of 42 kDa, which corresponds to a monomer of *Pa*DADH as a standalone unit. The data for the mixture of *Pa*DADH and *Pa*LADH yielded a relatively sharp peak at 3.6 S, estimated to a mass of 75 kDa, which roughly corresponds to a 1:1 protein complex of *Pa*DADH(42 kDa) and *Pa*LADH (35 kDa), theoretically estimated to have a molecular mass of 77 kDa (Figure 5.2). The disappearance of the single peak for *Pa*DADH at 2.8 S and the appearance of the relatively sharp peak at 3.6 S corresponds to a molecular mass of 75 kDa, which is similar to the theoretical mass of the *Pa*DADH: *Pa*LADH complex (77 kDa). While the data for *Pa*LADH on its own was inconclusive due to the protein not being stable, the data for the mixture of *Pa*DADH and *Pa*LADH suggest a protein-complex formation consisting of a heterodimer of *Pa*DADH and *Pa*LADH in a 1:1 stoichiometry.

The oligomerization state of *Pa*LADH, *Pa*LADH, and the mixture of *Pa*DADH and *Pa*LADH were determined by size exclusion chromatography (SEC) onto a Sephacryl S-200 HR column under non-denaturing conditions. The results indicated *Pa*DADH has a molecular weight of 41 kDa, the expected molecular weight for a monomer. The SEC data for *Pa*LADH showed an apparent molecular weight of 69 kDa, which is roughly the expected molecular weight for a homodimer of *Pa*LADH. The apparent molecular weight was calculated for the sample containing

the mixture of *Pa*LADH and *Pa*DADH to be 73 kDa, which is the expected molecular weight for a heterodimer with a 1:1 stoichiometry of *Pa*DADH and *Pa*LADH.

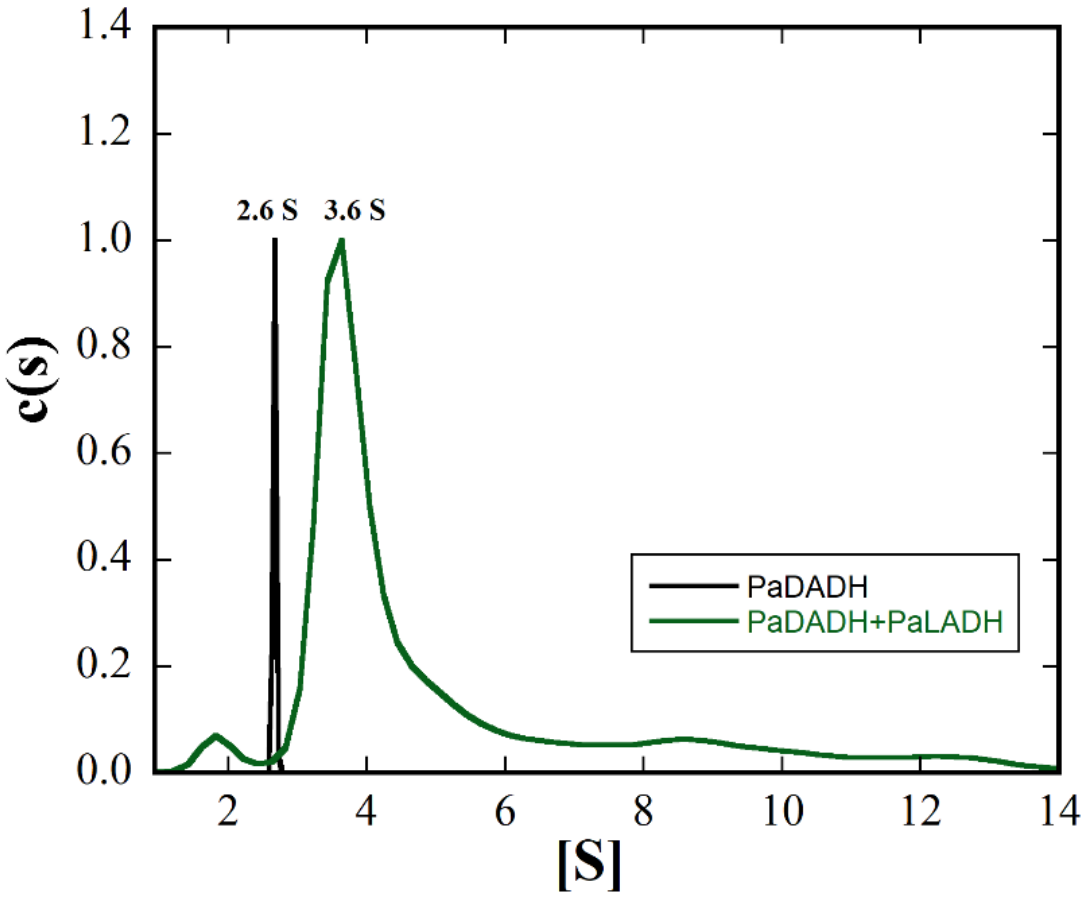

Figure 5.2. Sedimentation velocity analytical ultracentrifugation velocity data for *Pa*LADH and the complex of *Pa*DADH and *Pa*LADH.

Crystallization trials were performed to determine the structure of *Pa*LADH and gain structural insight for the protein-protein complex of *Pa*LADH and *Pa*DADH. However, the crystallization trials were unsuccessful, and a homology model for *Pa*LADH using the Robetta program was determined. The homology model for *Pa*LADH was based on the template structure of alanine dehydrogenase (PDB: 1omo) with a sequence similarity of 70 % and is part of the mu-crystallin protein family.[20] The homology model for *Pa*LADH presented as a dimer, similar to the template alanine dehydrogenase. The homology model for *Pa*LADH displays a typical Rossmann-type

NAD-binding domain in the active site, which is in the cleft of the overall enzyme structure (Figure 5.3)

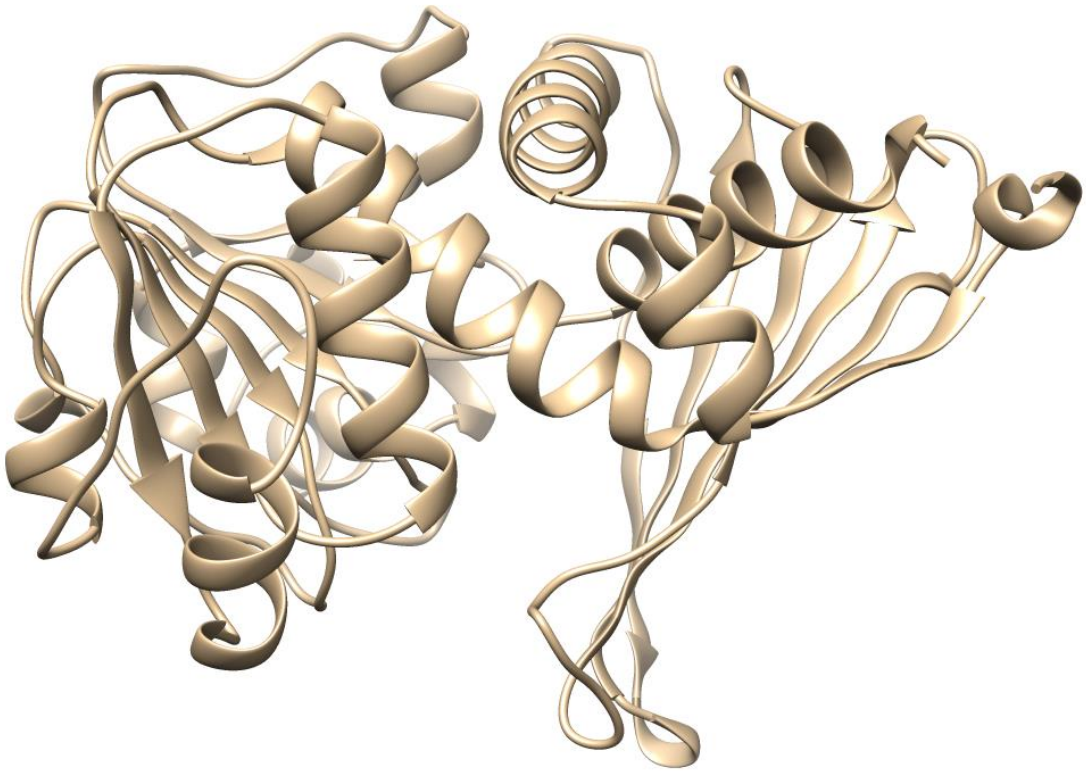

Figure 5.3. Homology model of *Pa*LADH generated by the comparative modeling module of Robetta server using the experimentally determined structure of alanine dehydrogenase (PDB: 1omo).

5.5 DISCUSSION

This study kinetically characterized *Pa*LADH and determined the protein-complex formation of *Pa*DADH and *Pa*LADH in a 1:1 stoichiometry by SVAUC and SEC. A coupled-enzyme assay was also developed to demonstrate that the products from *Pa*DADH-catalyzed oxidation of D-arginine can be taken up by *Pa*LADH and converted to L-arginine, as evidenced by the consumption of NADH/NADPH spectroscopically. *Pa*DADH catalyzes the production of the iminoarginine, which is hydrolyzed to ketoarginine and ammonia. Ammonia would be a tricky molecule to sequester from free solution after it is released from the active site of *Pa*DADH, as it

is a gaseous molecule in its unprotonated form. Hence, forming a protein-protein complex between *Pa*DADH and *Pa*LADH is probably a way to overcome the escape of substrates and maintain the overall metabolic health of *P. aeruginosa* as ammonia is known to be toxic for certain strains of bacteria.[22] A possible channel between PaDADH and PaLADH is likely responsible for transporting ammonia and the oxidized arginine substrate from the active site of *Pa*DADH to *Pa*LADH. Ammonia channels have been determined in Ammonia-transporter (Amt) proteins, Rhesus (Rh) protein family, and the Methylammonium/Ammonium permeases (MEP), all of which are membrane-associated proteins found across various species that facilitate the transport of ammonia, ammonium, and methylated ammonia.[23-27]

While the reaction of *Pa*DADH is irreversible and only proceeds in one direction, the reaction for *Pa*LADH is reversible. The limited substrate specificity and the reversible reaction of *Pa*LADH, compared to that of *Pa*DADH, points to a possible regulatory role of *Pa*LADH in the two-enzyme D-arginine conversion system can catalyze reactions in either direction based on availability and the cytosolic concentrations of L-arginine and ketoarginine. The combined function of *Pa*DADH and *Pa*DADH to convert D-arginine to L-arginine is very important for downstream arginine succinyltranferase (AST) and the arginine transaminase pathways (ATA), which can only utilize L-arginine as a precursor in order to survive in nutrient limiting conditions (Figure 5.4).[12, 28]

It was also validated that *Pa*LADH is specific for arginine as a substrate since it displayed no visible activity with L-lysine or pyruvate, the keto analog of alanine. *Pa*DADH, on the other hand, has a broad substrate specificity and can catalyze the oxidative deamination of most D-amino acids.[14] Similar broad substrate specificity is also observed with another dehydrogenase from *P. aeruginosa*, D-alanine dehydrogenase.[10] While there are no other D-amino acid conversion

systems in *P. aeruginosa* that perhaps form a protein-protein complex in solution to perform their function, there are similar systems that work on the catabolism of other D-amino acids. DadX, an amino acid racemase, and DadA, an alanine dehydrogenase function cooperatively as products of the *dadRAX* operon.[10] DadX catalyzes the reversible conversion of L-ala to D-ala, which can then be taken up by DadA, an FAD-dependent enzyme that catalyzes the oxidative deamination of L-ala to pyruvate and ammonia using an unknown electron acceptor.[10] DadX, DadA, and DadR together are required to maintain reasonable D-ala and L-ala concentrations.[10] The broad substrate specificity of DadA ensures there are multiple redundancies in D-amino acid metabolic pathways in *P. aeruginosa*, ensuring that any free D-amino acids can be metabolized through those pathways. The multiple enzymes with broad substrate specificity in *P. aeruginosa* participating in D-amino acid catabolism highlight the critical role D-amino acids play in PAO1 physiology and pathology.[1, 3-5, 7, 8]

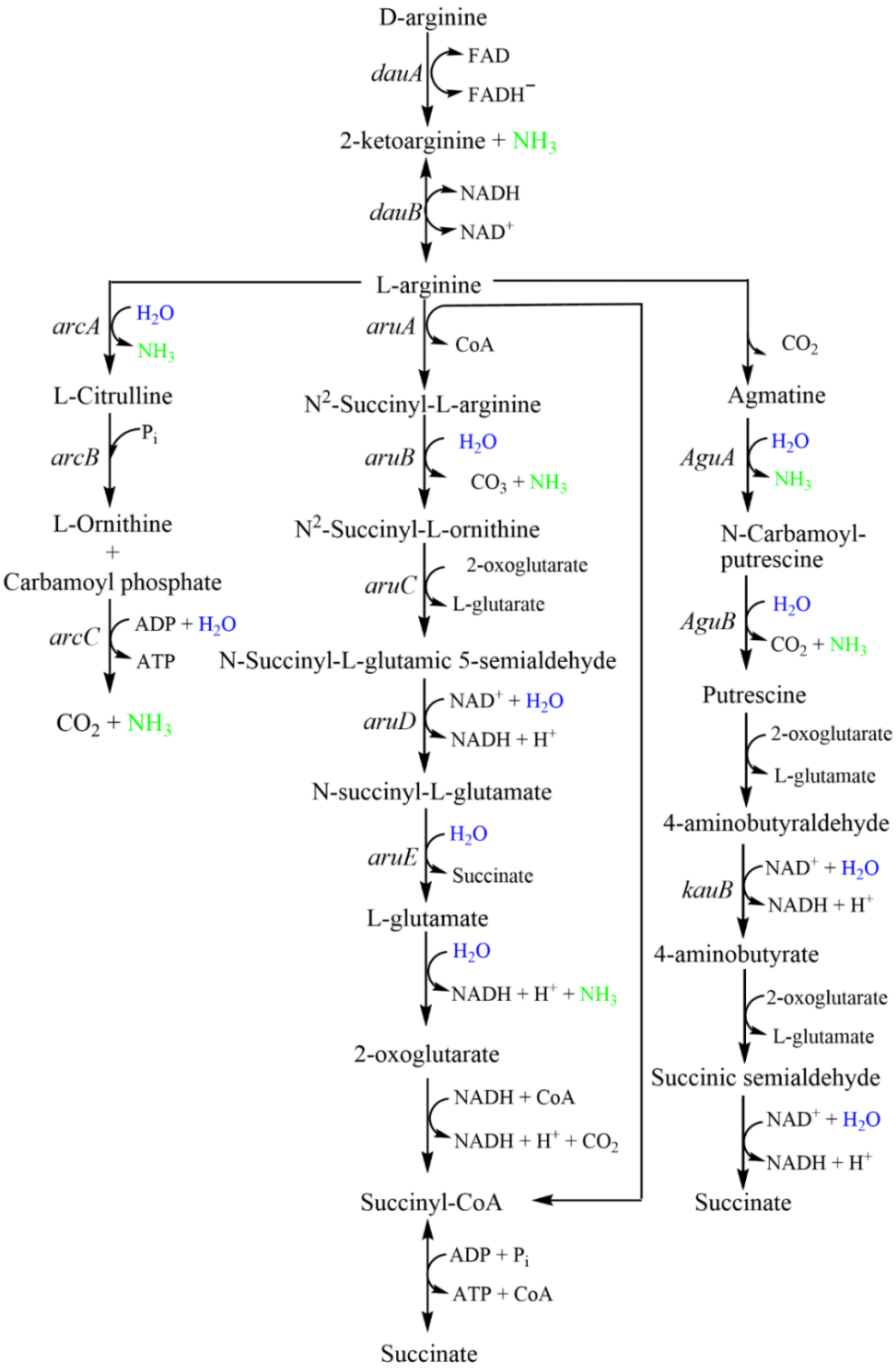

Figure 5.4. Multiple pathways for arginine metabolism in *P. aeruginosa*.[2]

[2] Scheme modified from reference 22 with permission from the Copyright Clearance Center

5.6 REFERENCES

[1] Oliver, K. E., and Silo-Suh, L. (2013) Impact of D-amino acid dehydrogenase on virulence factor production by a Pseudomonas aeruginosa, *Can J Microbiol 59*, 598-603.

[2] Naganuma, T., Iinuma, Y., Nishiwaki, H., Murase, R., Masaki, K., and Nakai, R. (2018) Enhanced Bacterial Growth and Gene Expression of D-Amino Acid Dehydrogenase With D-Glutamate as the Sole Carbon Source, *Front Microbiol 9*, 2097.

[3] Mathee, K., Ciofu, O., Sternberg, C., Lindum, P. W., Campbell, J. I. A., Jensen, P., Johnsen, A. H., Givskov, M., Ohman, D. E., Soren, M., Hoiby, N., and Kharazmi, A. (1999) Mucoid conversion of Pseudomonas aeruginosa by hydrogen peroxide: a mechanism for virulence activation in the cystic fibrosis lung, *Microbiology (Reading) 145 (Pt 6)*, 1349-1357.

[4] Panayidou, S., Georgiades, K., Christofi, T., Tamana, S., Promponas, V. J., and Apidianakis, Y. (2020) Pseudomonas aeruginosa core metabolism exerts a widespread growth-independent control on virulence, *Sci Rep 10*, 9505.

[5] Breidenstein, E. B., de la Fuente-Nunez, C., and Hancock, R. E. (2011) Pseudomonas aeruginosa: all roads lead to resistance, *Trends Microbiol 19*, 419-426.

[6] Palmer, K. L., Mashburn, L. M., Singh, P. K., and Whiteley, M. (2005) Cystic fibrosis sputum supports growth and cues key aspects of Pseudomonas aeruginosa physiology, *J Bacteriol 187*, 5267-5277.

[7] Son, M. S., Matthews, W. J., Jr., Kang, Y., Nguyen, D. T., and Hoang, T. T. (2007) In vivo evidence of Pseudomonas aeruginosa nutrient acquisition and pathogenesis in the lungs of cystic fibrosis patients, *Infect Immun 75*, 5313-5324.

[8] Pedersen, S. S., Hoiby, N., Espersen, F., and Koch, C. (1992) Role of alginate in infection with mucoid Pseudomonas aeruginosa in cystic fibrosis, *Thorax 47*, 6-13.

[9] He, W., Li, G., Yang, C. K., and Lu, C. D. (2014) Functional characterization of the dguRABC locus for D-Glu and d-Gln utilization in Pseudomonas aeruginosa PAO1, *Microbiology (Reading) 160*, 2331-2340.

[10] He, W., Li, C., and Lu, C. D. (2011) Regulation and characterization of the dadRAX locus for D-amino acid catabolism in Pseudomonas aeruginosa PAO1, *J Bacteriol 193*, 2107-2115.

[11] Li, C., Yao, X., and Lu, C. D. (2010) Regulation of the dauBAR operon and characterization of D-amino acid dehydrogenase DauA in arginine and lysine catabolism of Pseudomonas aeruginosa PAO1, *Microbiology (Reading) 156*, 60-71.

[12] Li, C., and Lu, C. D. (2009) Arginine racemization by coupled catabolic and anabolic dehydrogenases, *Proc Natl Acad Sci U S A 106*, 906-911.

[13] Ouedraogo, D., Ball, J., Iyer, A., Reis, R. A. G., Vodovoz, M., and Gadda, G. (2017) Amine oxidation by d-arginine dehydrogenase in Pseudomonas aeruginosa, *Arch Biochem Biophys 632*, 192-201.

[14] Fu, G., Yuan, H., Li, C., Lu, C. D., Gadda, G., and Weber, I. T. (2010) Conformational changes and substrate recognition in Pseudomonas aeruginosa D-arginine dehydrogenase, *Biochemistry 49*, 8535-8545.

[15] Yoshimura, T., and Esak, N. (2003) Amino acid racemases: functions and mechanisms, *J Biosci Bioeng 96*, 103-109.

[16] Baek, M., DiMaio, F., Anishchenko, I., Dauparas, J., Ovchinnikov, S., Lee, G. R., Wang, J., Cong, Q., Kinch, L. N., Schaeffer, R. D., Millan, C., Park, H., Adams, C., Glassman, C. R., DeGiovanni, A., Pereira, J. H., Rodrigues, A. V., van Dijk, A. A., Ebrecht, A. C., Opperman, D. J., Sagmeister, T., Buhlheller, C., Pavkov-Keller, T., Rathinaswamy, M. K.,

Dalwadi, U., Yip, C. K., Burke, J. E., Garcia, K. C., Grishin, N. V., Adams, P. D., Read, R. J., and Baker, D. (2021) Accurate prediction of protein structures and interactions using a three-track neural network, *Science 373*, 871-876.

[17] Yang, J., Anishchenko, I., Park, H., Peng, Z., Ovchinnikov, S., and Baker, D. (2020) Improved protein structure prediction using predicted interresidue orientations, *Proc Natl Acad Sci U S A 117*, 1496-1503.

[18] Hiranuma, N., Park, H., Baek, M., Anishchenko, I., Dauparas, J., and Baker, D. (2021) Improved protein structure refinement guided by deep learning based accuracy estimation, *Nat Commun 12*, 1340.

[19] Kallberg, M., Wang, H., Wang, S., Peng, J., Wang, Z., Lu, H., and Xu, J. (2012) Template-based protein structure modeling using the RaptorX web server, *Nat Protoc 7*, 1511-1522.

[20] Gallagher, D. T., Monbouquette, H. G., Schroder, I., Robinson, H., Holden, M. J., and Smith, N. N. (2004) Structure of alanine dehydrogenase from Archaeoglobus: active site analysis and relation to bacterial cyclodeaminases and mammalian mu crystallin, *J Mol Biol 342*, 119-130.

[21] Kim, D. E., Chivian, D., and Baker, D. (2004) Protein structure prediction and analysis using the Robetta server, *Nucleic Acids Res 32*, W526-531.

[22] Rogul, M., and Carr, S. R. (1972) Variable Ammonia Production Among Smooth and Rough Strains of Pseudomonas pseudomallei: Resemblance to Bacteriocin Production, *Journal of Bacteriology 112*, 372-380.

[23] Ninnemann, O., Jauniaux, J. C., and Frommer, W. B. (1994) Identification of a high affinity NH4+ transporter from plants, *EMBO J 13*, 3464-3471.

[24] Khademi, S., O'Connell, J., 3rd, Remis, J., Robles-Colmenares, Y., Miercke, L. J., and Stroud, R. M. (2004) Mechanism of ammonia transport by Amt/MEP/Rh: structure of AmtB at 1.35 A, *Science 305*, 1587-1594.

[25] Marini, A. M., Vissers, S., Urrestarazu, A., and André, B. (1994) Cloning and expression of the MEP1 gene encoding an ammonium transporter in Saccharomyces cerevisiae, *The EMBO journal 13*, 3456-3463.

[26] Marini, A. M., Soussi-Boudekou, S., Vissers, S., and Andre, B. (1997) A family of ammonium transporters in Saccharomyces cerevisiae, *Mol Cell Biol 17*, 4282-4293.

[27] Marini, A. M., Urrestarazu, A., Beauwens, R., and Andre, B. (1997) The Rh (rhesus) blood group polypeptides are related to NH4+ transporters, *Trends Biochem Sci 22*, 460-461.

[28] Jann, A., Matsumoto, H., and Haas, D. (1988) The fourth arginine catabolic pathway of Pseudomonas aeruginosa, *J Gen Microbiol 134*, 1043-1053.

6 GENERAL DISCUSSION AND CONCLUSIONS

Pseudomonas aeruginosa (PAO1) can utilize D-arginine as a sole carbon and nitrogen source and survive. The coupled-enzyme system consists of D-arginine dehydrogenase (*Pa*DADH) and L-arginine dehydrogenase (*Pa*LADH). *Pa*DADH catalyzes the oxidation of D-arginine into 2-ketoarginine and ammonia, and *Pa*LADH uses NADH as a co-substrate to convert 2-ketoarginine and ammonia to L-arginine. The conversion of D-arginine to L-arginine by the coupled enzyme system enables P. *aeruginosa* to survive solely on D-arginine as a nitrogen and carbon source.

A tyrosine 249 to phenylalanine variant (*Pa*DADH-Y249F) of *Pa*DADH was purified as a mixture of populations containing two cofactors, one protein population with the unmodified, yellow-colored FAD(Y249F-y) and one with a green-colored modified FAD (Y249F-g). Through various spectroscopic techniques, the green modified FAD was identified as 6-OH-FAD (Y249F-g). Crystal structures of Y249F-g and Y249F-y enzymes were determined at 1.55 Å and 1.33 Å resolutions, respectively. A closer look at the structures of Y249F-g and Y249F-y showed no significant differences compared with the wild-type enzyme's overall fold and structure. Alternate conformations for some active site residues and the flavin cofactor were observed in Y249F-y. Molecular Dynamics simulations revealed that Y249F-y exists in two conformational substates: A and B. There was an increase in the spin density at the C6 position of the flavin, as evidenced by the QM/MM in conformation B with an alternate conformation of some residues, unlike that seen in the wild-type enzyme. The study shows the vital role of the active site residues in modulating fluctuations between different conformational substates, fine-tuning cofactor versatility, the absence of which can ultimately lead to a deleterious cofactor modification as observed in *Pa*DADH-Y249F.

The structure of *Pa*DADH-Y249F expressed and crystallized in the presence of D-arginine was determined at a resolution of 1.29 Å. Upon analysis of the structure of *Pa*DADH-Y249F, ambiguous electron density was noticed around the C6 and the N5 positions of the isoalloxazine. Accurate mass analysis revealed that the two modified flavins were both N5-(4-guanidino-oxobutyl)-FAD and 6-OH-FAD. The presence of two modified flavin cofactors in a single crystal is highly unusual and speaks to the versatility of the reduced flavin, which is a precursor to the modification reactions for both the N5-(4-guanidino-oxobutyl)-FAD and 6-OH-FAD.

*Pa*LADH was purified and was characterized kinetically to follow a ternary-complex mechanism, as expected for an enzyme that does not use bound cofactors to catalyze a hydride transfer reaction. A coupled-enzyme assay was established and determined that the products from *Pa*DADH can be channeled into *Pa*LADH, as evidenced by NADH consumption in the coupled-enzyme assay. We had hypothesized that *Pa*LADH and *Pa*DADH might form a protein complex for converting D-arginine to L-arginine. The protein complex formation was probed using analytical ultracentrifugation and size-exclusion chromatography, suggesting that *Pa*LADH and *Pa*DADH form a complex in a 1:1 stoichiometry. Forming a protein complex is beneficial since one of the products from the hydrolysis of iminoarginine is ammonia, which is hard to sequester from the free solution once it leaves the enzyme's active site.

In conclusion, these studies have provided insight into the kinetic mechanism of *Pa*LADH, which plays a role in the coupled-enzyme D-arginine conversion system that helps *P. aeruginosa* to survive in nutrient limiting conditions. The insight gained from this unusual two-enzyme D-amino acid metabolic systems among similar systems from *P. aeruginosa* will help identify and isolate virulence and survival factors for this opportunistic pathogen. These studies have also

provided insight into how seemingly benign modifications to the active site by site-directed mutagenesis can significantly affect protein dynamics and cofactor reactivity. Proteins function through concerted movements to achieve catalytically relevant conformational ensembles by optimal placement of critical residues. While most of the focus is on active site residues that participate directly in catalysis, attention must also be diverted towards residues that do not have a discernible function but can function as conformational switches and enhance or diminish enzyme activity.